NASA Technical Paper 1119

Effect of Winglets on a First-Generation Jet Transport Wing

IV - Stability Characteristics for a Full-Span Model at Mach 0.30

Robert R. Meyer, Jr.

FEBRUARY 1978

NASA

NASA Technical Paper 1119

Effect of Winglets on a First-Generation Jet Transport Wing

IV - Stability Characteristics for a Full-Span Model at Mach 0.30

Robert R. Meyer, Jr.
Dryden Flight Research Center
Edwards, California

National Aeronautics
and Space Administration

**Scientific and Technical
Information Office**

1978

SUMMARY

An investigation was made at a Mach number of 0.30 to determine the effect of upper winglets on the static longitudinal and lateral-directional aerodynamic characteristics of a 0.035-scale full-span model of a first-generation jet transport. Results are presented which indicate that at typical take-off and landing lift coefficients and flap settings, upper winglets decrease the drag coefficient. The winglets slightly increase longitudinal stability, indicating that trim drag could be slightly increased for a given center-of-gravity location. Effectiveness of horizontal-tail deflection is essentially unaffected by winglets. The addition of the winglets produces increases in positive effective dihedral and the directional stability. Winglets notably increase aileron effectiveness.

INTRODUCTION

Winglets, described in reference 1, are intended to provide substantially greater reductions in drag due to lift at subsonic speeds than those obtained with simple wing-tip extensions which produce bending moments at the wing-fuselage juncture essentially equal to those produced by the winglets (refs. 1 to 3). The National Aeronautics and Space Administration (NASA) has been conducting extensive experimental investigations on the effects of winglets for representative jet transport wings at high subsonic Mach numbers. For example, the winglets developed in reference 3 for a first-generation jet transport wing lowered the induced drag near design lift coefficients by about 20 percent with a resulting increase in wing lift-drag ratio of about 9 percent at the design Mach number of 0.78. These improvements were more than twice as great as those achieved with a simple wing-tip extension with essentially equal wing bending moments at the wing-fuselage juncture.

As a result of these indicated gains in performance, NASA and the U.S. Air Force (USAF) have initiated a joint flight research and demonstration program to examine the application of winglets to the USAF KC-135A aircraft. The flight research program is proposed to obtain results at full-scale Reynolds numbers and to provide a basis for a USAF decision to retrofit the KC-135 fleet with winglets. In support of the proposed flight research program, extensive wind-tunnel investigations have been conducted on semispan and full-span models of the KC-135A aircraft. Performance, loads, stability and control, and buffet data have been obtained over the aircraft operational envelope.

This report, which is one of a series, presents force and moment data obtained on a full-span model of the KC-135A; semispan model tests are described in reference 3. Earlier investigations (refs. 3 to 5) have determined that the advantages associated with the lower winglet on the KC-135A are considered marginal. Therefore, for simplification, the lower winglet has been dropped in the design for the KC-135A application. The present investigation was conducted to

determine the effects of upper winglets, which had been optimized for cruise conditions (refs. 3 to 5), on the longitudinal and lateral-directional aerodynamic characteristics in landing and take-off configurations. Results are presented for several configurations: the basic wing without winglets, with upper winglets on both wing tips, and with an upper winglet on one wing tip only, for several aileron, flap, and horizontal-tail deflections and with the horizontal tail removed.

The tests were conducted in the Langley 8-foot transonic pressure tunnel. The wind-tunnel free-stream Mach number was 0.30 at a constant dynamic pressure of 11.97 kPa (250 lb/ft^2). The angle-of-attack range varied from approximately -6° to 16° at fixed sideslip angles of 0° and 5°. The Reynolds number was held at approximately 12.30 × 10^6 per meter (3.75 × 10^6 per foot).

SYMBOLS

The results presented in this report are referred to the stability-axis system for the longitudinal aerodynamic characteristics and to the body-axis system for the lateral-directional aerodynamic characteristics. Force and moment data have been reduced to conventional coefficient form based on the geometry of the base-line wing planform. Moments are referenced to the quarter-chord point of the mean aerodynamic chord of the base-line wing (fig. 2). All dimensional values are given in both the International System of Units (SI) and U.S. Customary Units; however, all measurements and calculations were made in U.S. Customary Units. (See ref. 6.) Sign convention is shown in figure 1.

Coefficients and symbols used herein are defined as follows:

b wing span, 138.7 cm (54.6 in.)

C_D drag coefficient, Drag/$q_\infty S$

C_L lift coefficient, Lift/$q_\infty S$

C_l rolling-moment coefficient, Rolling moment/$q_\infty Sb$

C_{l_β} rate of change of rolling-moment coefficient with sideslip angle (effective-dihedral parameter), $\Delta C_l/\Delta\beta$, per degree

$C_{l_{\delta_a}}$ rate of change of rolling-moment coefficient with differential aileron deflection, $\Delta C_l/\Delta\delta_a$, per degree

C_m pitching-moment coefficient, Pitching moment/$q_\infty S\bar{c}$

$C_{m_{\delta_h}}$ rate of change of pitching-moment coefficient with horizontal-tail deflection, $\Delta C_m/\Delta\delta_h$, per degree

C_n yawing-moment coefficient, Yawing moment/$q_\infty Sb$

C_{n_β} rate of change of yawing-moment coefficient with sideslip angle (directional-stability parameter), $\Delta C_n/\Delta\beta$, per degree

C_Y side-force coefficient, Side force/$q_\infty S$

C_{Y_β} rate of change of side-force coefficient with sideslip angle (side-force parameter), $\Delta C_Y/\Delta\beta$, per degree

c local chord, cm (in.)

$\bar{c}$ mean aerodynamic chord of base-line reference wing panel, 21.03 cm (8.28 in.)

c_t tip chord of basic wing, cm (in.)

q_∞ free-stream dynamic pressure, Pa (psf)

S base-line wing planform reference area, 0.270 m^2 (2.91 ft^2)

x chordwise distance from leading edge, positive aft, cm (in.)

z vertical coordinate of airfoil, positive upward, cm (in.)

α angle of attack, deg

β angle of sideslip, deg

Δ incremental values

δ_a differential aileron deflection, $\delta_{a,R} - \delta_{a,L}$, deg

$\delta_{a,R}$ right aileron deflection, positive for trailing edge down, deg

$\delta_{a,L}$ left aileron deflection, positive for trailing edge down, deg

δ_f flap deflection, positive for trailing edge down, deg

δ_h horizontal-tail deflection, positive for trailing edge down, deg

APPARATUS AND PROCEDURES

Test Facility

This investigation was conducted in the Langley 8-foot transonic pressure tunnel, a continuous-flow, single-return tunnel with a slotted rectangular test section. The longitudinal slots in the floor and ceiling of the test section reduce tunnel wall interference and allow relatively large models to be tested through the subsonic speed range. Controls are available to permit independent variation of Mach number, stagnation pressure, temperature, and dew point. A more detailed description of the wind tunnel is found in reference 7.

Model Description

A sting-mounted, full-span, 0.035-scale model of a KC-135A transport aircraft was used in this study. Drawings of the model are shown in figure 2 and photographs of the model are shown in figure 3.

Fuselage.- The fuselage contours closely simulated the full-scale fuselage shape, with the exception of the aft fuselage area. An enlargement of this area was necessitated by the sting mounting apparatus.

Wing.- The basic wing of the KC-135A model has 7° dihedral, 2° of incidence at the root chord, and no geometric twist. The trailing edge of the wing near the root breaks from the basic trapezoidal planform, as shown in figure 2. The basic trapezoidal planform of the wing has a sweep at the quarter-chord of 35°, an aspect ratio of 7.00, and a taper ratio of 0.35. The reference geometry parameters S, b, and $\bar{c}$ used for all data analysis are based on the trapezoidal planform of the basic wing extended to the fuselage center line.

A typical wing airfoil section is shown in figure 4. The wing thickness ratio varies nonlinearly from 15 percent at the wing-fuselage juncture to 9 percent at the trailing-edge break and then remains constant to the wing tip.

Winglets.- A detailed drawing of the upper winglet used in this investigation is given in figure 2(b). The winglet employed an 8-percent-thick general aviation airfoil. The airfoil section is shown in figure 2(b), and the coordinates are presented in table I.

The winglet has a span equal to the wing-tip chord, a root chord equal to 65 percent of the wing-tip chord, a leading-edge sweep of 38°, a taper ratio of 0.32, and an aspect ratio of 2.33. The planform area of each winglet is 1.6 percent of the trapezoidal planform of the basic wing. The winglet is canted outboard 15° from vertical (75° dihedral) and toed out 4° (leading edge outboard) relative to the fuselage center line. The upper winglet is untwisted and therefore has constant negative geometric incidence across its span. The "upper surface" of the winglet is the inboard surface. To smooth the transition from the wing to the winglet, fillets were added to the inside corners at these junctures and the outside corners were rounded.

Flaps and ailerons.- Fixed-position trailing-edge flaps and outboard ailerons simulating the full-scale configuration were incorporated in the model. Flap deflections could be set at 0°, 30°, and 50°. The ailerons could be set at 0°, ±10°, and ±20°.

Tail.- The horizontal tail could be set at fixed deflections of 0°, -4°, and -10° and was removed for some of the tests. The vertical tail was fixed at a deflection of 0°.

Nacelles.- Flow-through nacelles were used with an inlet diameter of 2.90 cm (1.14 in.) and an exit diameter of 2.08 cm (0.82 in.). The inlet diameter was maintained back to approximately 0.66 of the nacelle length and then tapered linearly to the exit.

Test Conditions

Measurements were taken at a Mach number of 0.30 for an angle-of-attack range from -6° to 16° and nominal sideslip angles of 0° and 5°. Measurements were made without winglets, with a winglet on one wing tip, and with winglets on both wing tips. The Reynolds number varied slightly from 12.14×10^6 per meter (3.70×10^6 per foot) to 12.57×10^6 per meter (3.83×10^6 per foot) and the dynamic pressure was held constant at 11.97 kPa (250 lb/ft^2). The stagnation temperature varied between 305 K (90° F) and 322 K (120° F); this variation was the reason for the small variation in Reynolds number at the test Mach number. The tunnel air was dried until the dew point was sufficiently low to prevent condensation effects.

Boundary-Layer Transition

Boundary-layer transition strips were placed on the fuselage, pylons, and nacelles and on both surfaces of the wings, winglets, horizontal tail, and vertical tail. These strips consisted of bands, 0.16 cm (0.06 in.) wide, of carborundum grains set in a plastic adhesive. The carborundum grains and the strip width were sized for the test Mach number on the basis of reference 8. The transition strips were applied at conventional locations on all surfaces except the winglet lower surfaces on which they were located by the method of reference 9 in an attempt to simulate a full-scale trailing-edge boundary-layer displacement thickness at a Reynolds number based on the mean aerodynamic chord of 40×10^6.

On the fuselage, No. 220 grains were applied 3.81 cm (1.50 in.) aft of the nose. No. 220 grain transition strips were applied at 0.05 of the chord on the upper and lower surfaces of the wings, horizontal tail, and vertical tail. Transition strips on the winglets were No. 240 grains applied at 0.05 of the chord on the upper surface and No. 220 grains applied at 0.35 of the chord on the lower surface. The pylons and nacelles had No. 240 grain transition strips placed 0.64 cm (0.25 in.) from the leading edges

Measurements

Force and moment data were obtained by use of a six-component electrical strain-gage balance housed within the fuselage cavity Angle of attack was measured by an accelerometer that was also housed within the fuselage. Static pressures were measured in the model sting cavity and at the model base by using differential-pressure transducers referenced to free-stream static pressures.

Corrections

The angle of attack of the model was corrected for flow angularity in the tunnel test section. This correction was obtained from upright and inverted tests of the base-line wing configuration. The lift, drag, and pitching-moment coefficients have been adjusted to correspond to the condition of free-stream static pressure in the model sting cavity.

PRESENTATION OF RESULTS

The results of this investigation are presented in the following figures:

DISCUSSION

The purpose of the following discussion is to examine the effect of winglets, which have been optimized for cruise conditions, on the low-speed stability characteristics of the KC-135A aircraft.

Longitudinal Aerodynamic Characteristics

Effect of winglets for several flap deflections.- Results showing the effect of winglets for several flap and aileron deflections, and with and without the horizontal tail are presented in figures 5 to 12. Winglets generally increase the lift-curve slope. This is attributed to the effective increase in aspect ratio due to the addition of winglets. The lift-drag curves show benefits with winglets on, particularly near $C_L = 1.0$ for $\delta_f = 30^\circ$, which is representative of take-off conditions, and near $C_L = 1.2$ for $\delta_f = 50^\circ$, which is representative of landing conditions. Somewhat larger gains in lift-drag ratio are indicated in reference 3 for a semispan model which was tested at higher Reynolds numbers. The winglets increase the negative slope of C_m versus C_L ($\Delta C_m/\Delta C_L$). This increase represents a slight increase in longitudinal stability which indicates that a slight increase in trim drag for a given center-of-gravity location could be possible.

Effect of winglets for several horizontal-tail deflections.- Figure 13 shows the effect of winglets on longitudinal aerodynamic characteristics for several horizontal-tail deflections. Figure 14, which summarizes these results, shows that the horizontal-tail effectiveness is not noticeably affected by the presence of winglets.

Lateral-Directional Aerodynamic Characteristics

Effect of winglets for several aileron deflections.- Figure 15 presents lateral-directional data for nonsymmetric aileron deflections, as well as for a winglet on one wing tip only. The data for both winglets on show that negative deflection of the left aileron (up aileron) is more effective in roll control than positive deflection of the right aileron (down aileron). It is interesting to note that for $\delta_f = 50^\circ$ and $\beta = 0^\circ$, a constant deflection of the down aileron gives essentially a constant level of rolling-moment coefficient with lift coefficient, whereas the rolling-moment coefficient for constant deflection of the up aileron varies with lift coefficient up to C_L of about 0.75, and above $C_L = 0.9$, it remains essentially constant with lift coefficient. It is also interesting that at lift coefficients from about 0.55 to 0.9, the sum of the roll produced by individual aileron deflections is slightly greater than the roll produced by deflecting both ailerons simultaneously (that is, C_l for $\delta_{a,L} = -20^\circ$ and $\delta_{a,R} = 0^\circ$ plus C_l for $\delta_{a,L} = 0^\circ$ and $\delta_{a,R} = 20^\circ$ is greater than C_l for $\delta_a = 40^\circ$). Above lift coefficients of about 0.9 until flow begins to separate, the sum of the roll produced by individual aileron deflections essentially equals the roll produced by deflecting both ailerons simultaneously.

Figure 15 also presents the effect of aileron deflection on side force (C_Y) due to the presence of winglets. The up aileron tends to decrease side force by unloading the winglet, whereas the down aileron tends to increase side force by loading the winglet. These results would indicate an increase in side force due to differential aileron deflection with the addition of winglets.

As a matter of interest from a stability and control point of view as well as a loads point of view, lateral-directional aerodynamic data for a winglet on one wing tip only are presented in figure 15.

Figures 16 to 19 present the basic lateral-directional aerodynamic characteristics for several aileron deflections at two flap deflections and sideslip angles, and these data are further analyzed in figures 20 to 29.

Effect of winglets on lateral-directional stability derivatives.- Figures 20 to 22 present lateral-directional stability derivatives for $\delta_f = 30^\circ$ and show that adding winglets increased positive effective dihedral $\left(-C_{l_\beta}\right)$. This noted increase in effective dihedral is a probable result of the effects of winglets on the outboard wing loadings as sideslip increases. The data show that the addition of winglets increases C_{n_β} and increases the negative level of C_{Y_β}.

Figures 23 to 25, for a flap deflection of 50°, show that the addition of winglets increases positive effective dihedral $\left(-C_{l_\beta}\right)$. The effects of the winglets on C_{n_β} and C_{Y_β} for $\delta_f = 50^\circ$ are not as consistent as they are for $\delta_f = 30^\circ$; in fact, at some specific lift coefficients, the effect of winglets is to lower slightly the level of C_{n_β} and $-C_{Y_\beta}$ below that of the basic configuration.

Effect of winglets on aileron effectiveness.- A summary of aileron effectiveness with and without winglets (presented in figs. 26 to 29) shows notable increase in aileron effectiveness $(-\Delta C_l/\Delta\delta_a)$ due to the addition of winglets. The noted increase in aileron effectiveness is probably a result of increased aileron loading due to the presence of the winglets. The increase in aileron effectiveness due to winglets does not seem to be affected by flap deflection or sideslip. However, at very high lift coefficients, where flow separation probably exists at the wing tip, the addition of winglets does not increase aileron effectiveness.

SUMMARY OF RESULTS

An investigation was made at a Mach number of 0.30 to determine the static longitudinal and lateral-directional aerodynamic characteristics of a 0.035-scale model of a first-generation jet transport (U.S. Air Force KC-135A), with and without upper winglets. The following results were obtained:

1. At typical take-off and landing lift coefficients and flap settings, winglets decrease the drag coefficient.

2. Winglets slightly increase longitudinal stability (more negative slope of the curve of pitching-moment coefficient versus lift coefficient). This indicates that the trim drag could be increased slightly for a given center-of-gravity location. However, effectiveness of horizontal-tail deflection is not noticeably affected by winglets.

3. Noticeable effects of winglets occur in the lateral-directional aerodynamic characteristics, particularly an increase in effective dihedral and a small increase in directional stability.

4. Winglets notably increase aileron effectiveness.

National Aeronautics and Space Administration
Langley Research Center
Hampton, VA 23665
December 20, 1977

REFERENCES

1. Whitcomb, Richard T.: A Design Approach and Selected Wind-Tunnel Results at High Subsonic Speed for Wing-Tip Mounted Winglets. NASA TN D-8260, 1976.

2. Flechner, Stuart G.; Jacobs, Peter F.; and Whitcomb, Richard T.: A High Subsonic Speed Wind-Tunnel Investigation of Winglets on a Representative Second-Generation Jet Transport Wing. NASA TN D-8264, 1976.

3. Jacobs, Peter F.; Flechner, Stuart G.; and Montoya, Lawrence C.: Effect of Winglets on a First-Generation Jet Transport Wing. I - Longitudinal Aerodynamic Characteristics of a Semispan Model at Subsonic Speeds. NASA TN D-8473, 1977.

4. Montoya, Lawrence C.; Flechner, Stuart G.; and Jacobs, Peter F.: Effect of Winglets on a First-Generation Jet Transport Wing. II - Pressure and Spanwise Load Distributions for a Semispan Model at High Subsonic Speeds. NASA TN D-8474, 1977.

5. Montoya, Lawrence C.; Jacobs, Peter F.; and Flechner, Stuart G.: Effect of Winglets on a First-Generation Jet Transport Wing. III - Pressure and Spanwise Load Distributions for a Semispan Model at Mach 0.30. NASA TN D-8478, 1977.

6. Mechtly, E. A.: The International System of Units - Physical Constants and Conversion Factors (Second Revision). NASA SP-7012, 1973.

7. Schaefer, William T., Jr.: Characteristics of Major Active Wind Tunnels at the Langley Research Center. NASA TM X-1130, 1965.

8. Braslow, Albert L.; and Knox, Eugene C.: Simplified Method for Determination of Critical Height of Distributed Roughness Particles for Boundary-Layer Transition at Mach Numbers From 0 to 5. NACA TN 4363, 1958.

9. Blackwell, James A., Jr.: Preliminary Study of Effects of Reynolds Number and Boundary-Layer Transition Location on Shock-Induced Separation. NASA TN D-5003, 1969.

TABLE I.- AIRFOIL COORDINATES FOR WINGLETS

x/c	z/c for -	
	Upper surface	Lower surface
0	0	0
.0020	.0077	-.0032
.0050	.0119	-.0041
.0125	.0179	-.0060
.0250	.0249	-.0077
.0375	.0296	-.0090
.0500	.0333	-.0100
.0750	.0389	-.0118
.1000	.0433	-.0132
.1250	.0469	-.0144
.1500	.0499	-.0154
.1750	.0525	-.0161
.2000	.0547	-.0167
.2500	.0581	-.0175
.3000	.0605	-.0176
.3500	.0621	-.0174
.4000	.0628	-.0168
.4500	.0627	-.0158
.5000	.0618	-.0144
.5500	.0599	-.0122
.5750	.0587	-.0106
.6000	.0572	-.0090
.6250	.0554	-.0071
.6500	.0533	-.0052
.6750	.0508	-.0033
.7000	.0481	-.0015
.7250	.0451	.0004
.7500	.0419	.0020
.7750	.0384	.0036
.8000	.0349	.0049
.8250	.0311	.0060
.8500	.0270	.0065
.8750	.0228	.0064
.9000	.0184	.0059
.9250	.0138	.0045
.9500	.0089	.0021
.9750	.0038	-.0013
1.0000	-.0020	-.0067

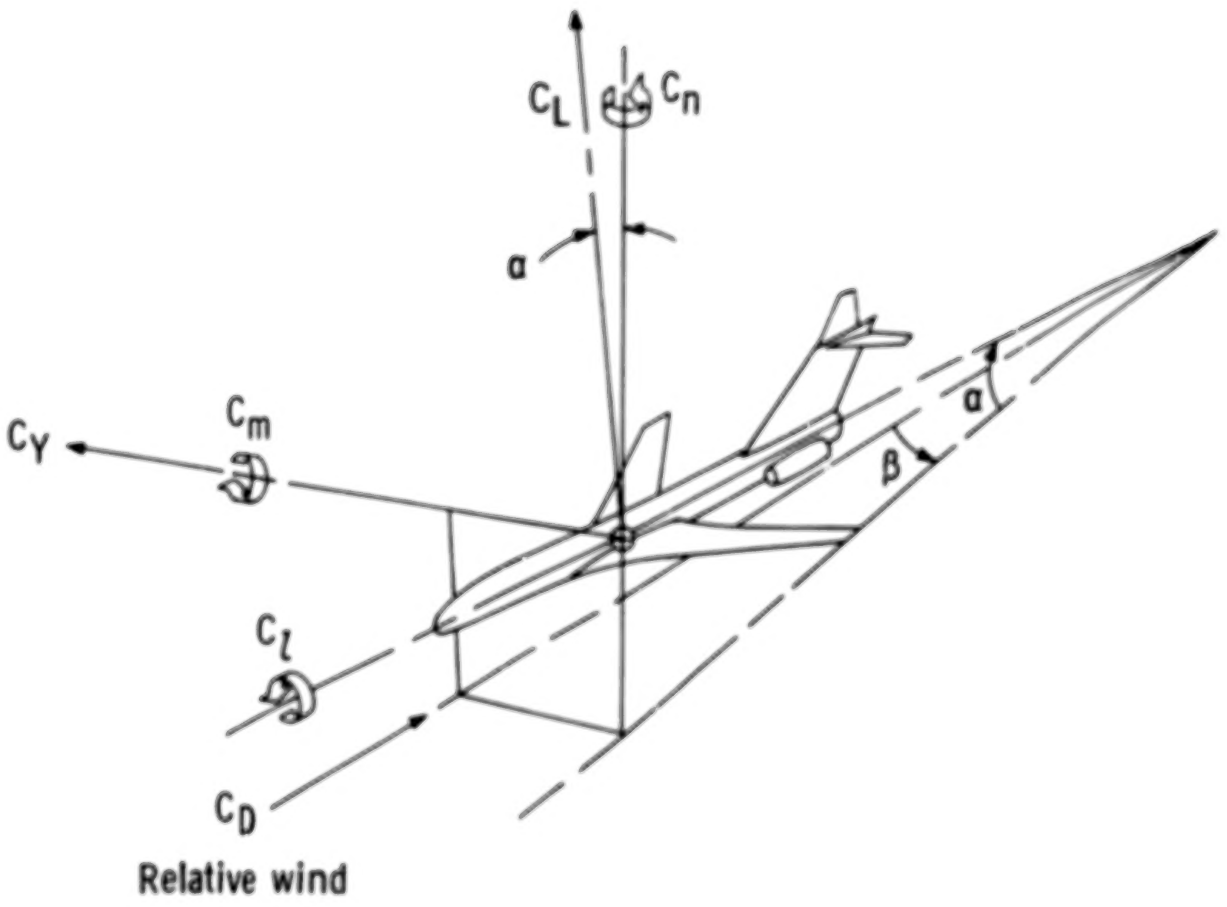

Figure 1.- Axes system. Positive values of forces, moments, and angles are indicated by arrows. Origin of stability axes has been displaced from moment reference center for clarity.

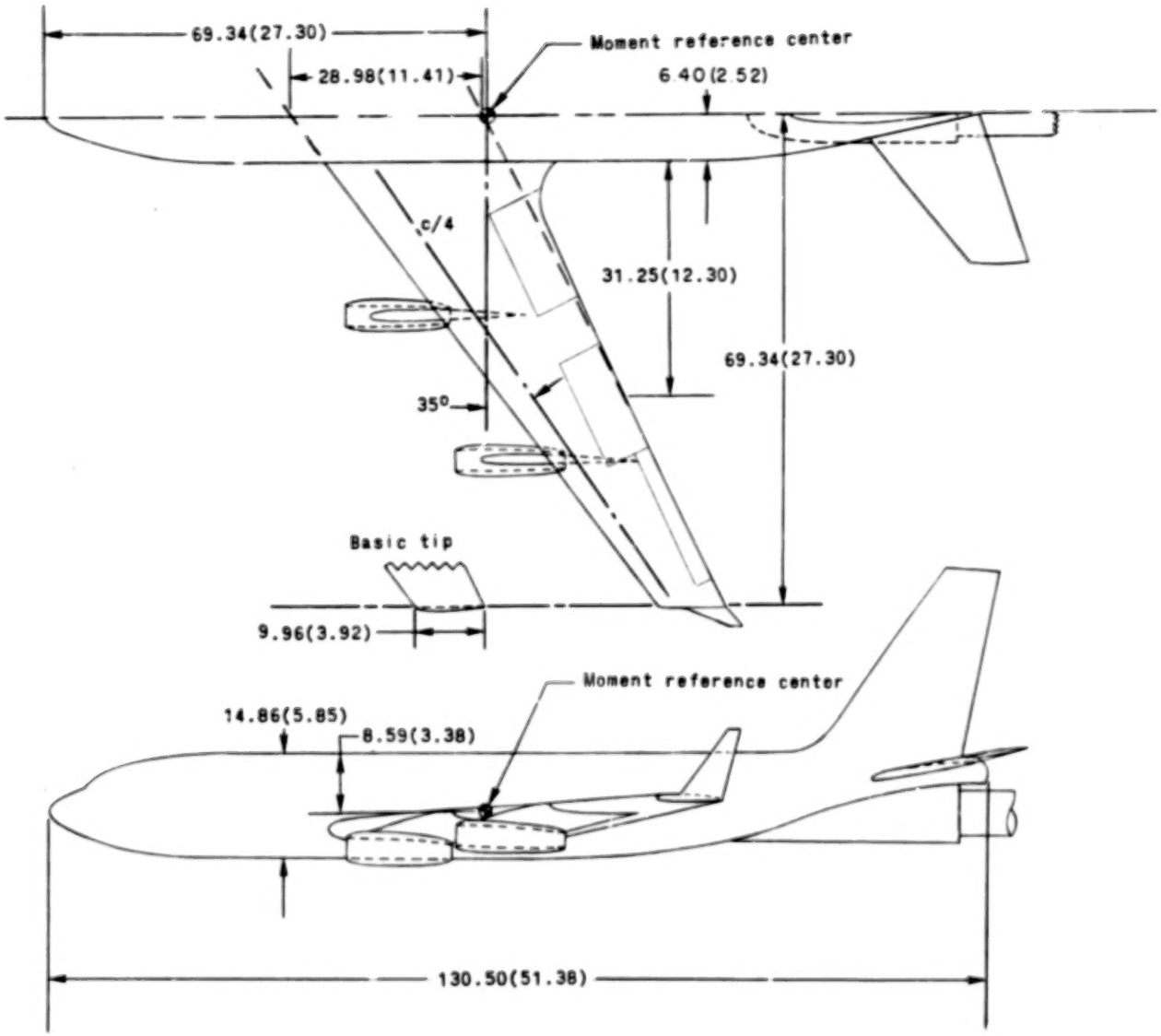

(a) General arrangement.

Figure 2.- Drawing of 0.035 scale, full-span KC-135A model. Dimensions are in centimeters (inches).

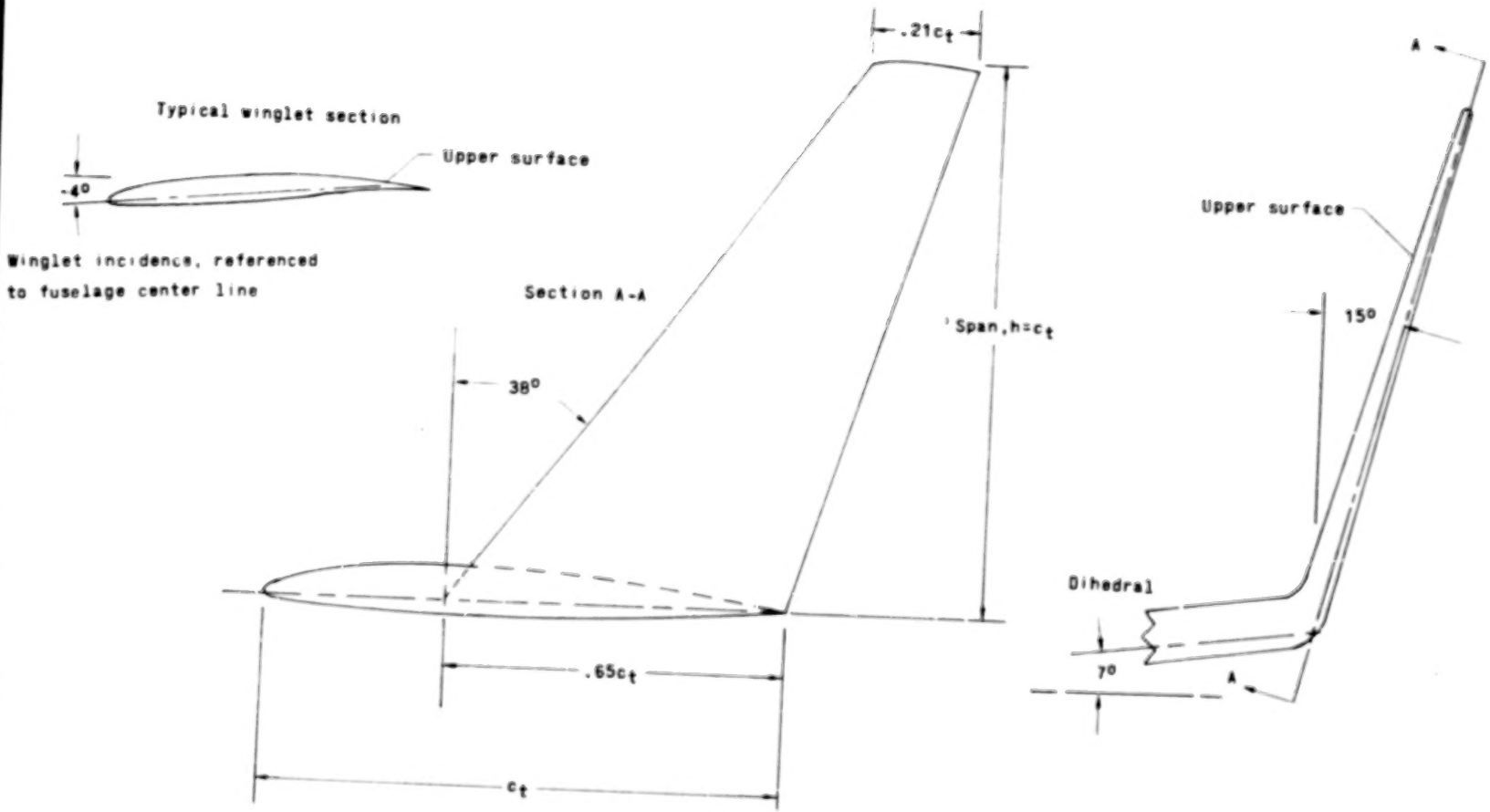

(b) Winglet details.

Figure 2.- Continued.

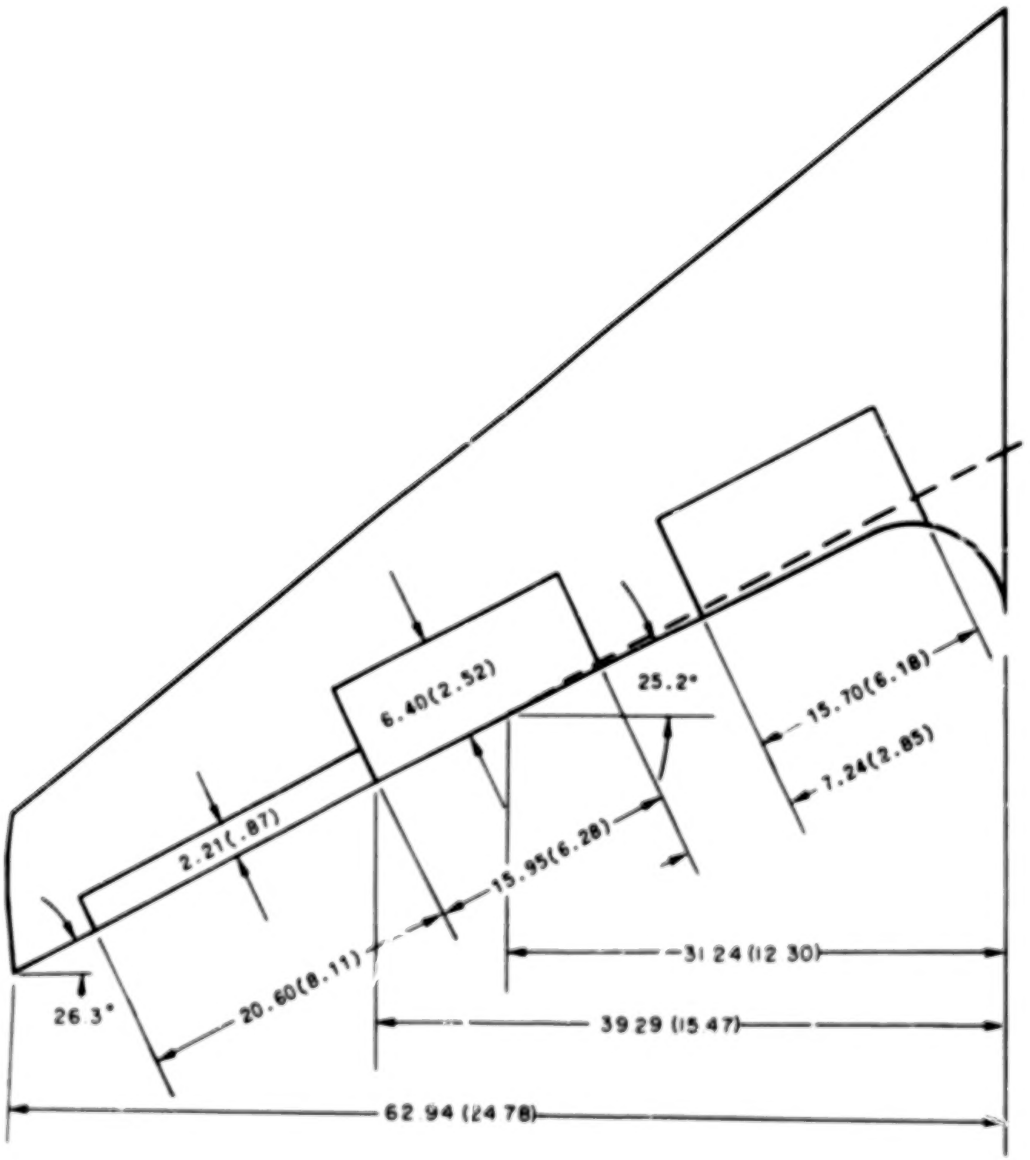

(c) Flap and aileron detail.

Figure 2.- Concluded.

(a) General arrangement.

L-76-5691

Figure 3.- Photographs of KC-135A full-span model with winglets.

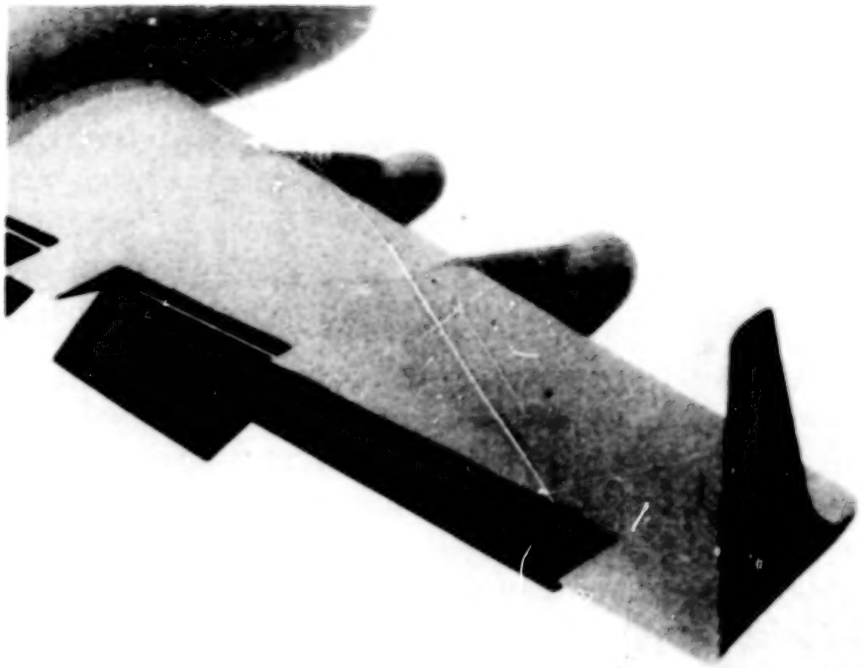

L-76-5692

(b) Winglet, aileron, and flap.

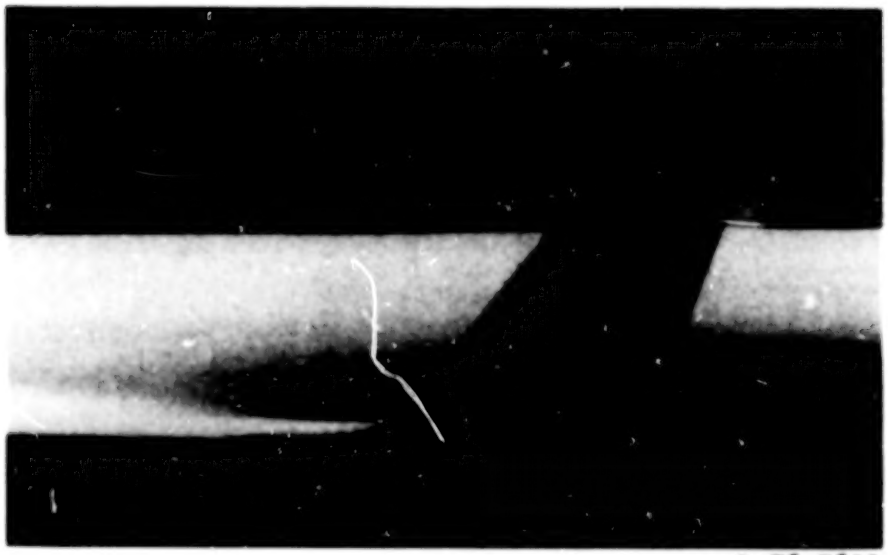

L-76-5690

(c) Winglet.

Figure 3.- Concluded.

Figure 4.- Typical outboard wing airfoil section.

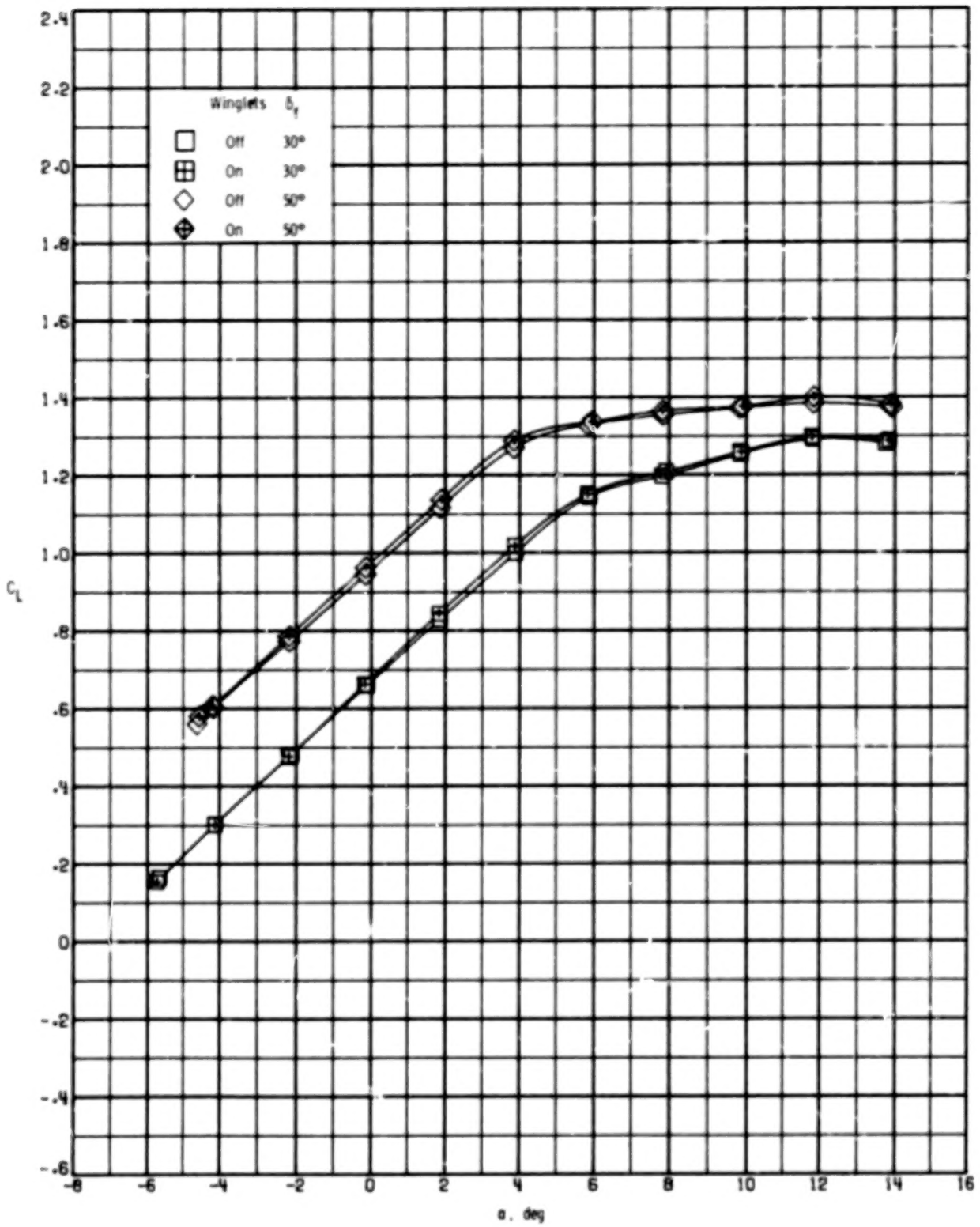

Figure 5.- Effect of winglets on longitudinal aerodynamic characteristics for two flap deflections. $\delta_h = -10^o$; $\delta_{a,L} = 0^o$; $\delta_{a,R} = 0^o$; $\beta = 0^o$.

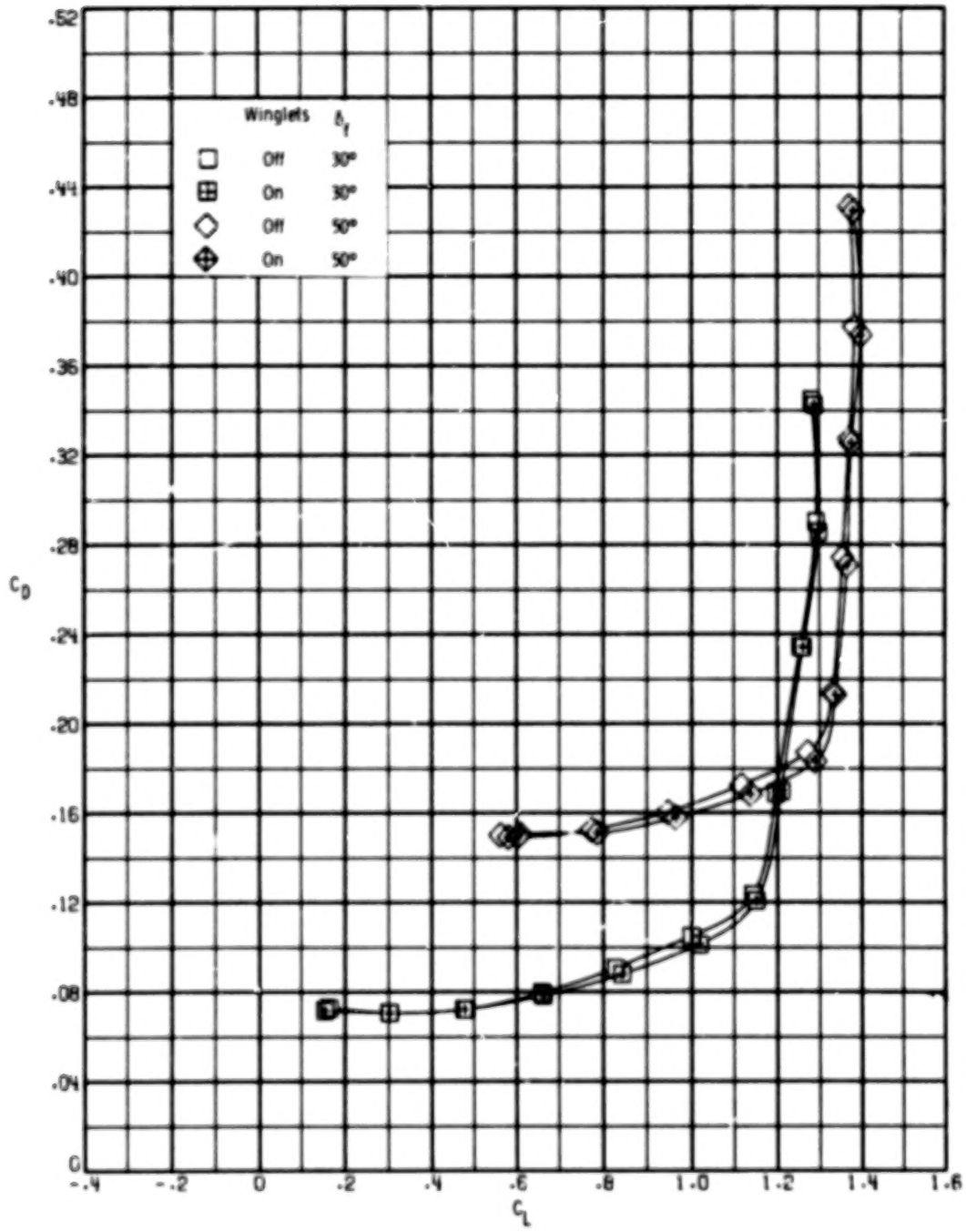

Figure 5.- Continued.

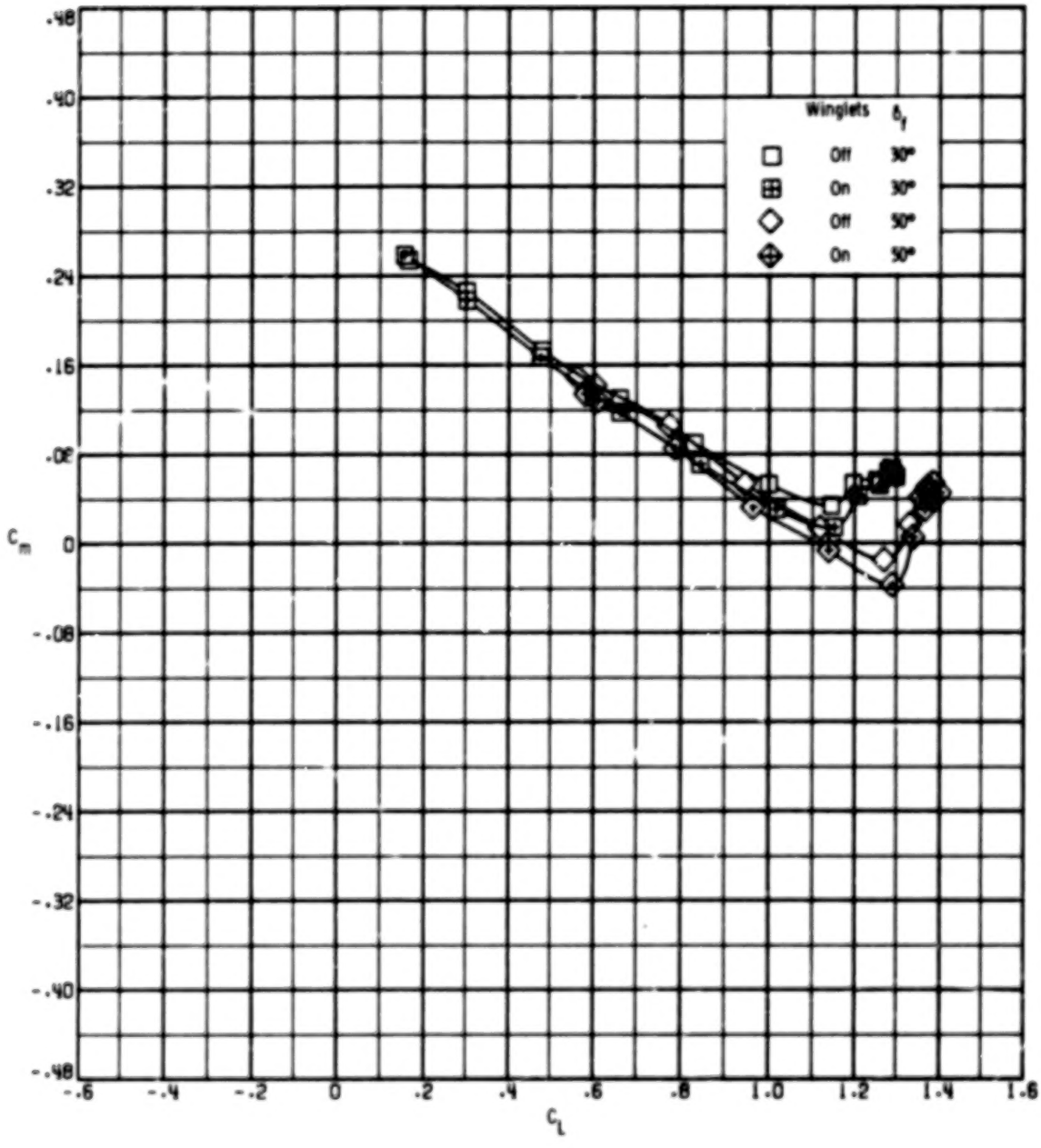

Figure 5.- Concluded.

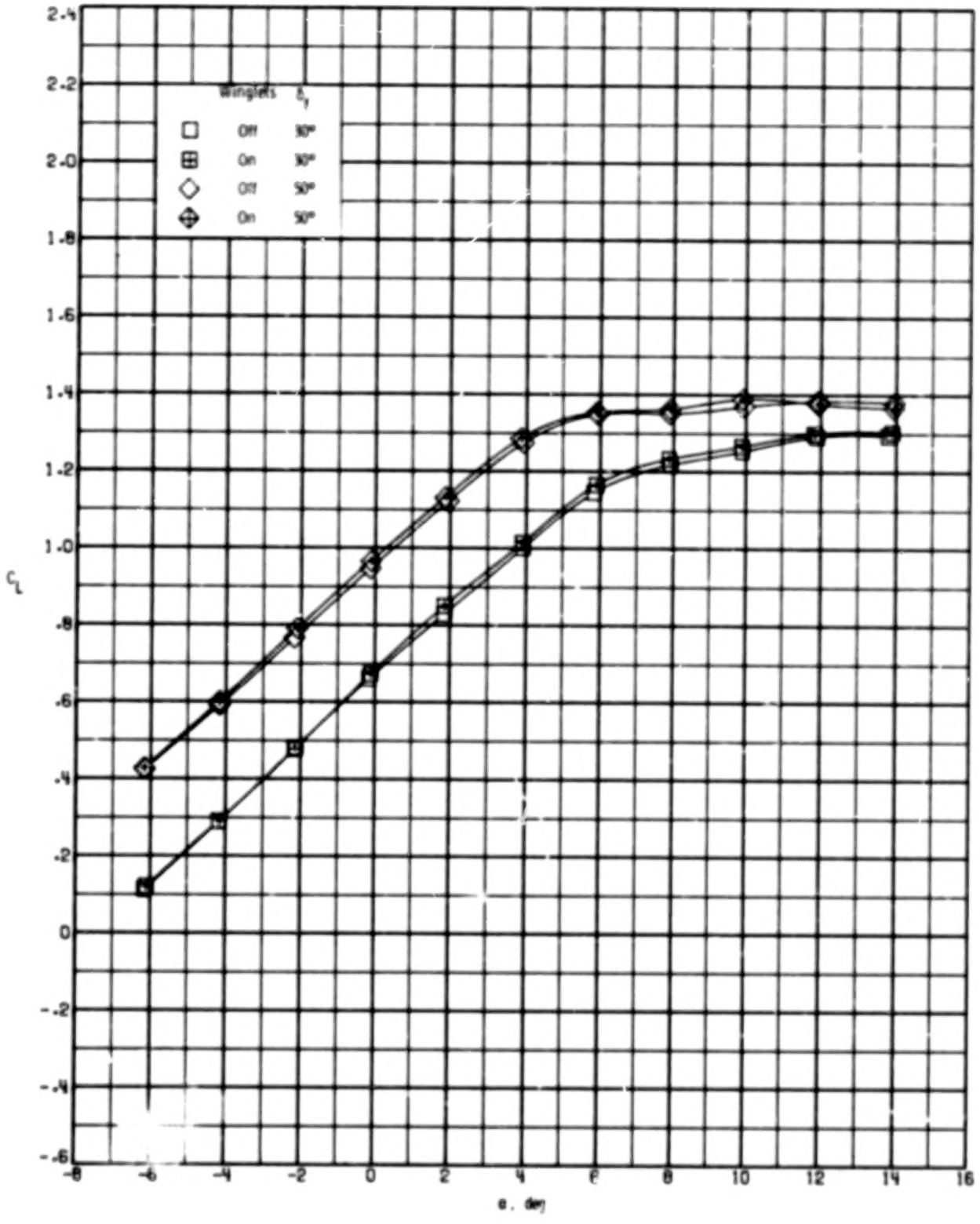

Figure 6.- Effect of winglets on longitudinal aerodynamic characteristics for two flap deflections. $\delta_h = -10^\circ$; $\delta_{a,L} = 0^\circ$; $\delta_{a,R} = 0^\circ$; $\beta = 5^\circ$.

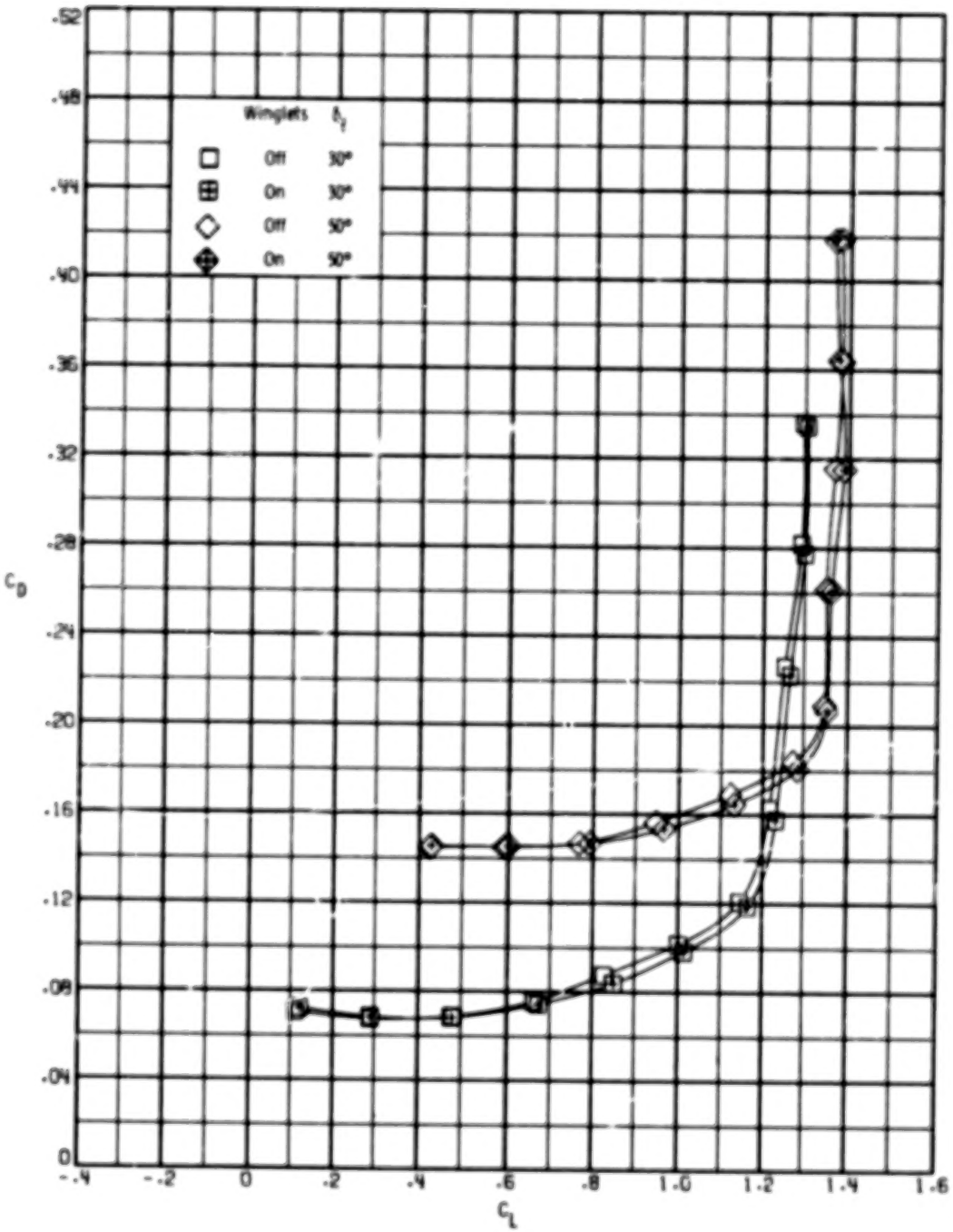

Figure 6.- Continued.

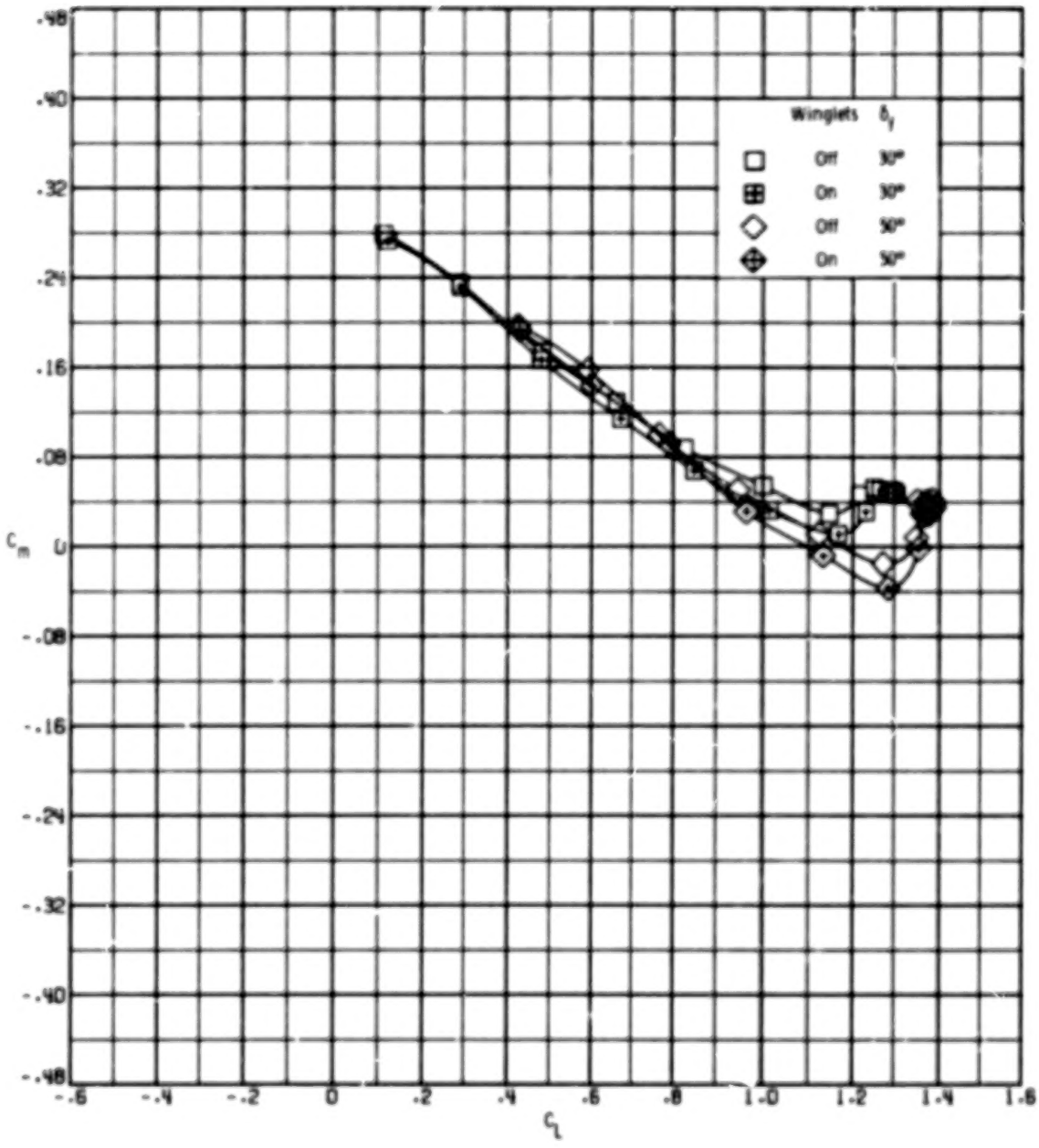

Figure 6.- Concluded.

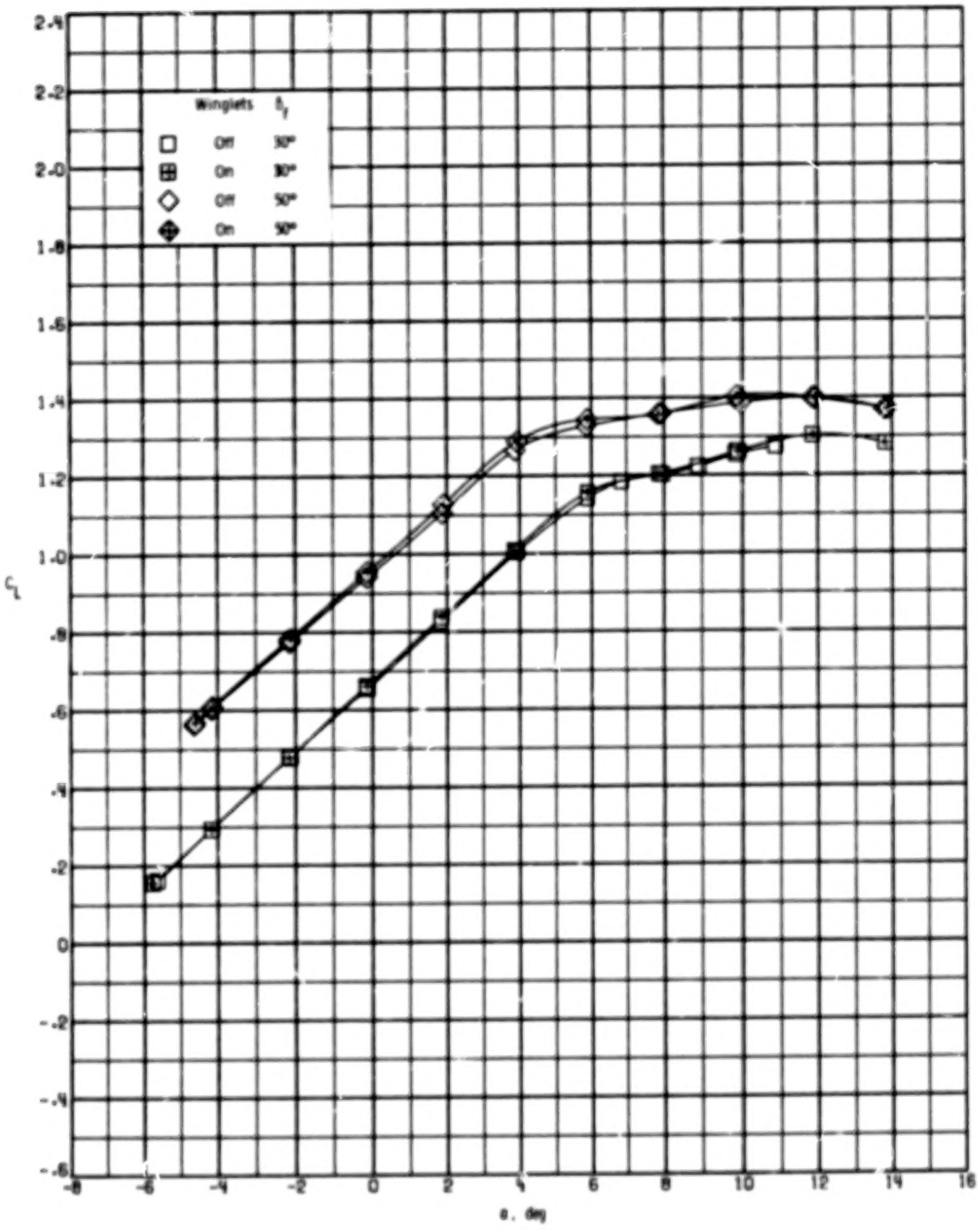

Figure 7.- Effect of winglets on longitudinal aerodynamic characteristics for two flap deflections. $\delta_h = -10^o$; $\delta_{a,L} = -10^o$; $\delta_{a,R} = 10^o$; $\beta = 0^o$.

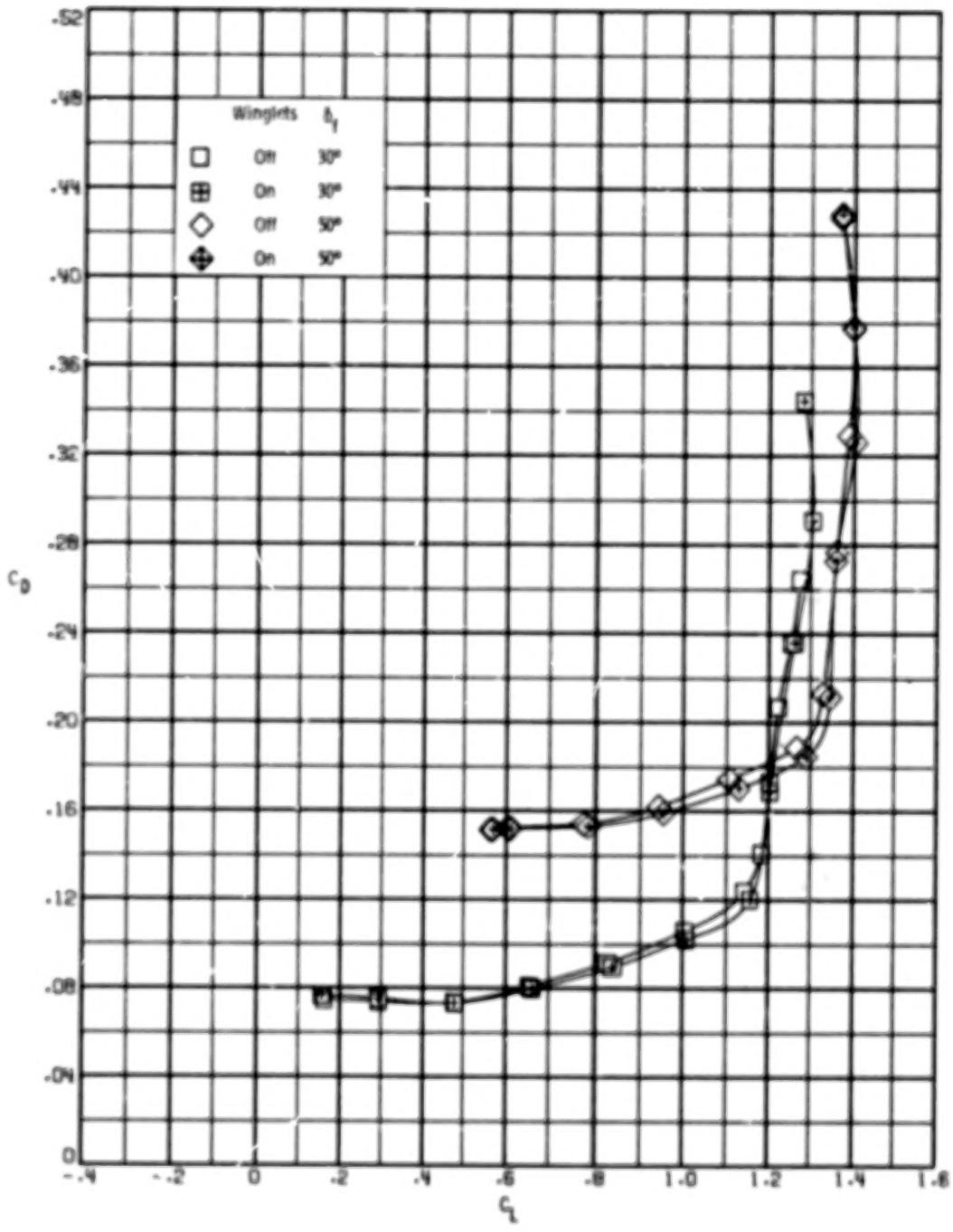

Figure 7.- Continued.

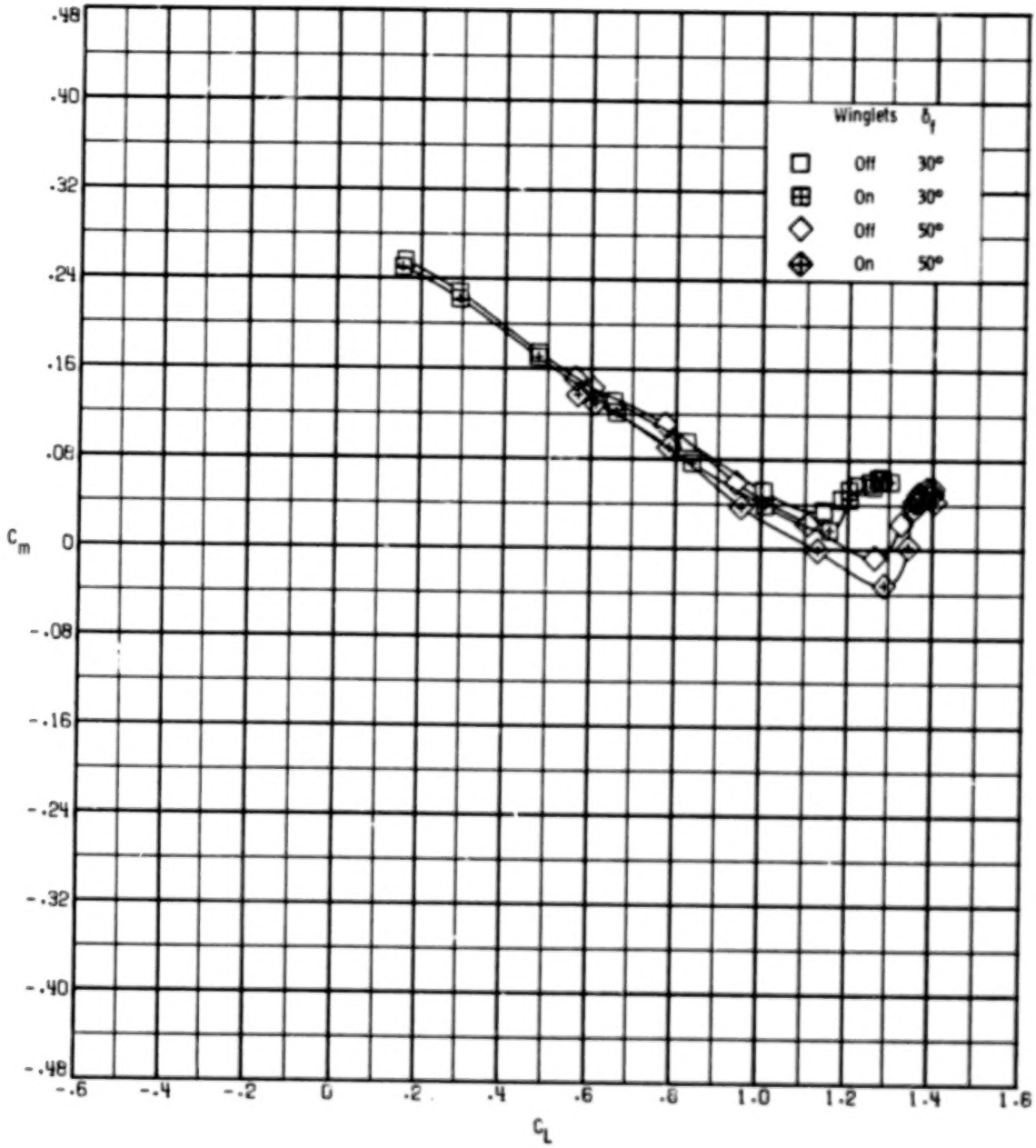

Figure 7.- Concluded.

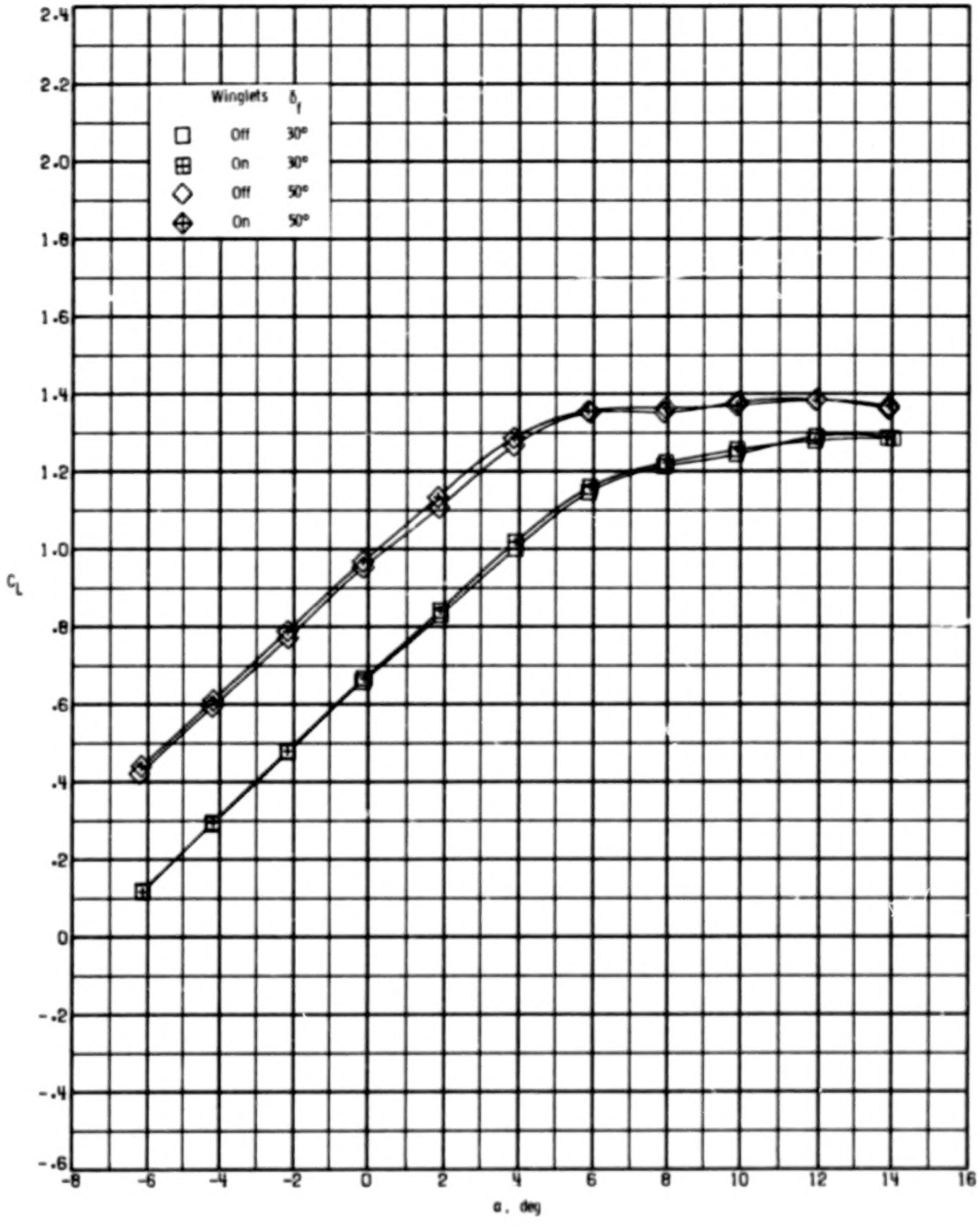

Figure 8.- Effect of winglets on longitudinal aerodynamic characteristics for two flap deflections. $\delta_h = -10^o$; $\delta_{a,L} = -10^o$; $\delta_{a,R} = 10^o$; $\beta = 5^o$.

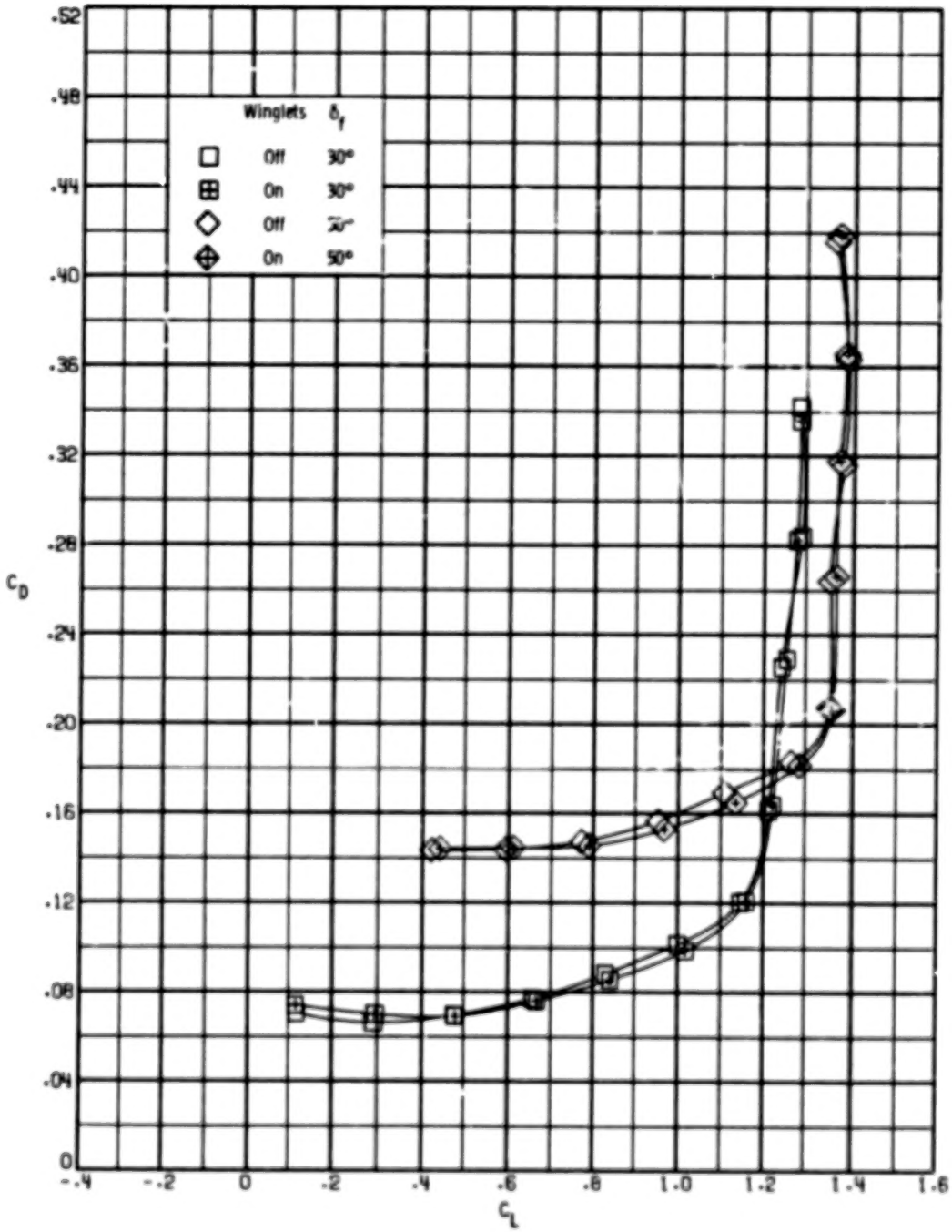

Figure 8.- Continued.

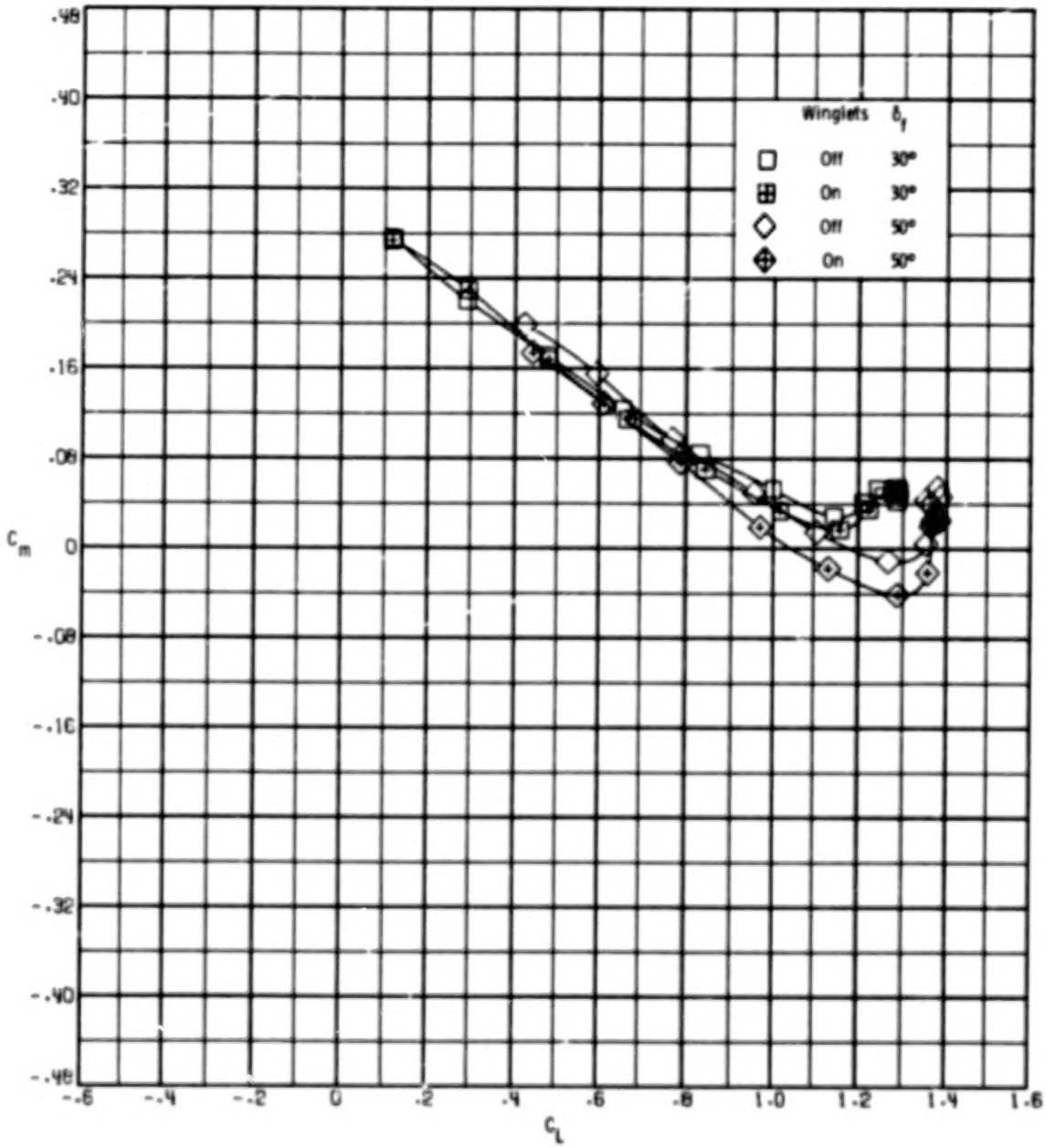

Figure 8.- Concluded.

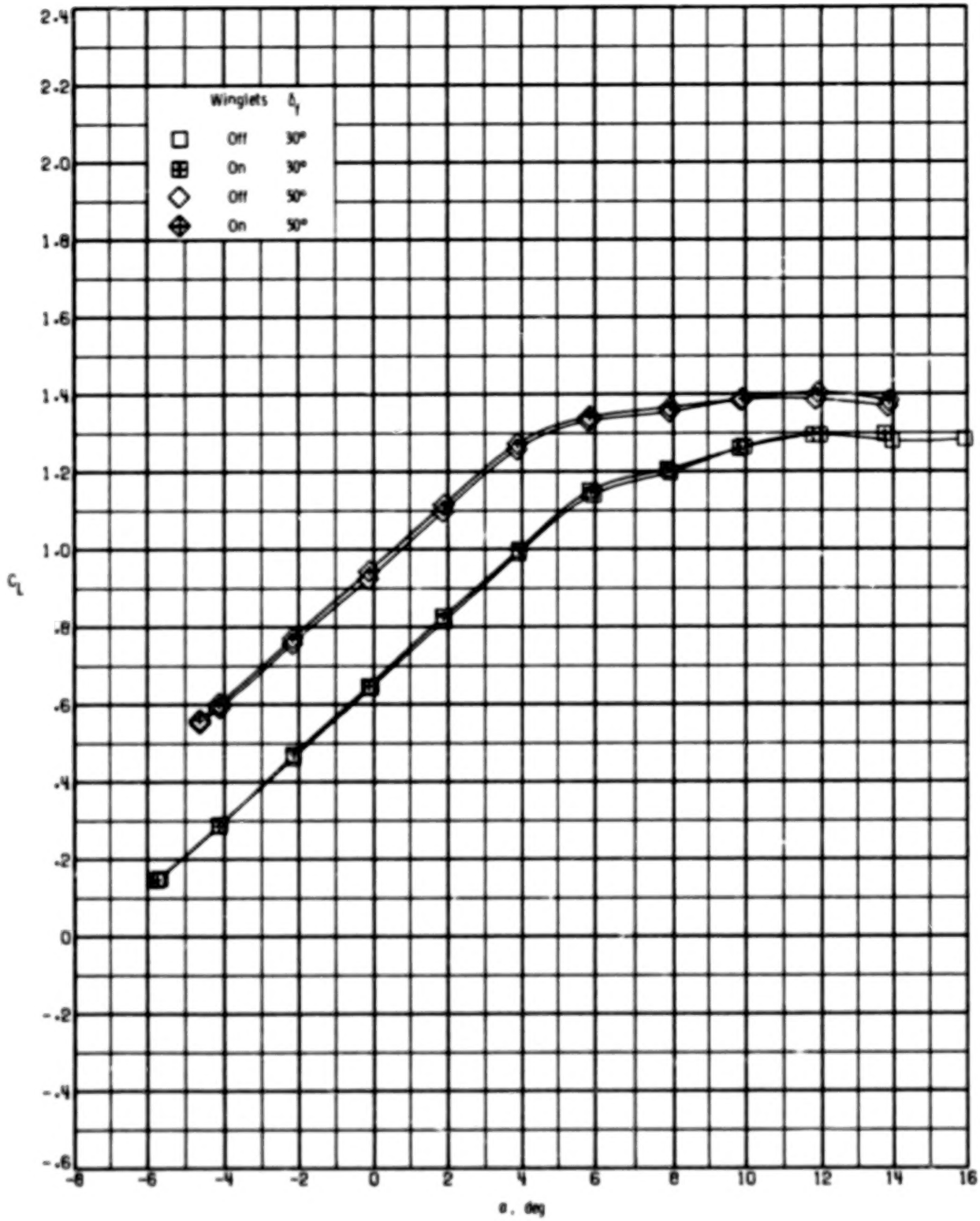

Figure 9.- Effect of winglets on longitudinal aerodynamic characteristics for two flap deflections. $\delta_h = -10°$; $\delta_{a,L} = -20°$; $\delta_{a,R} = 20°$; $\beta = 0°$.

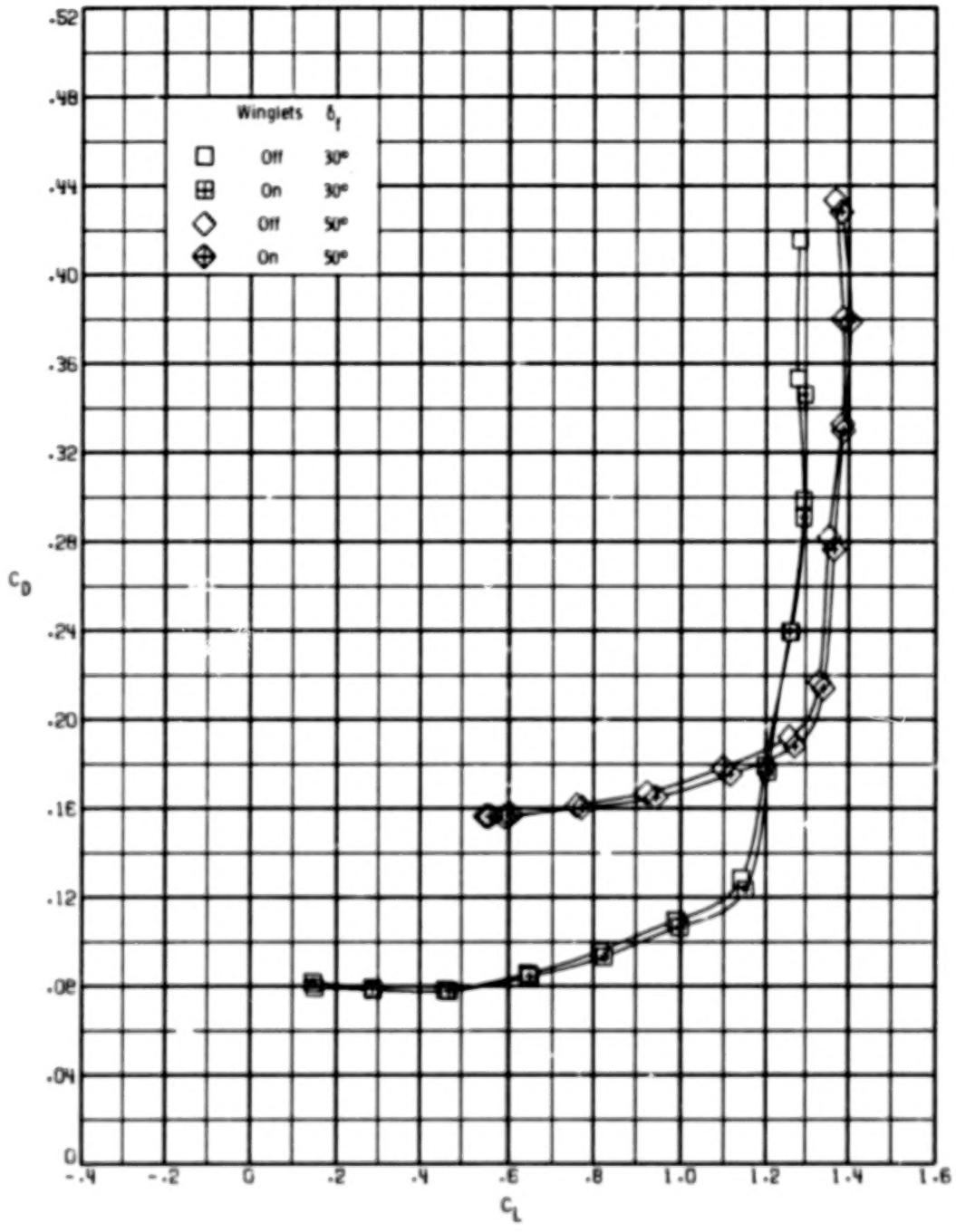

Figure 9.- Continued.

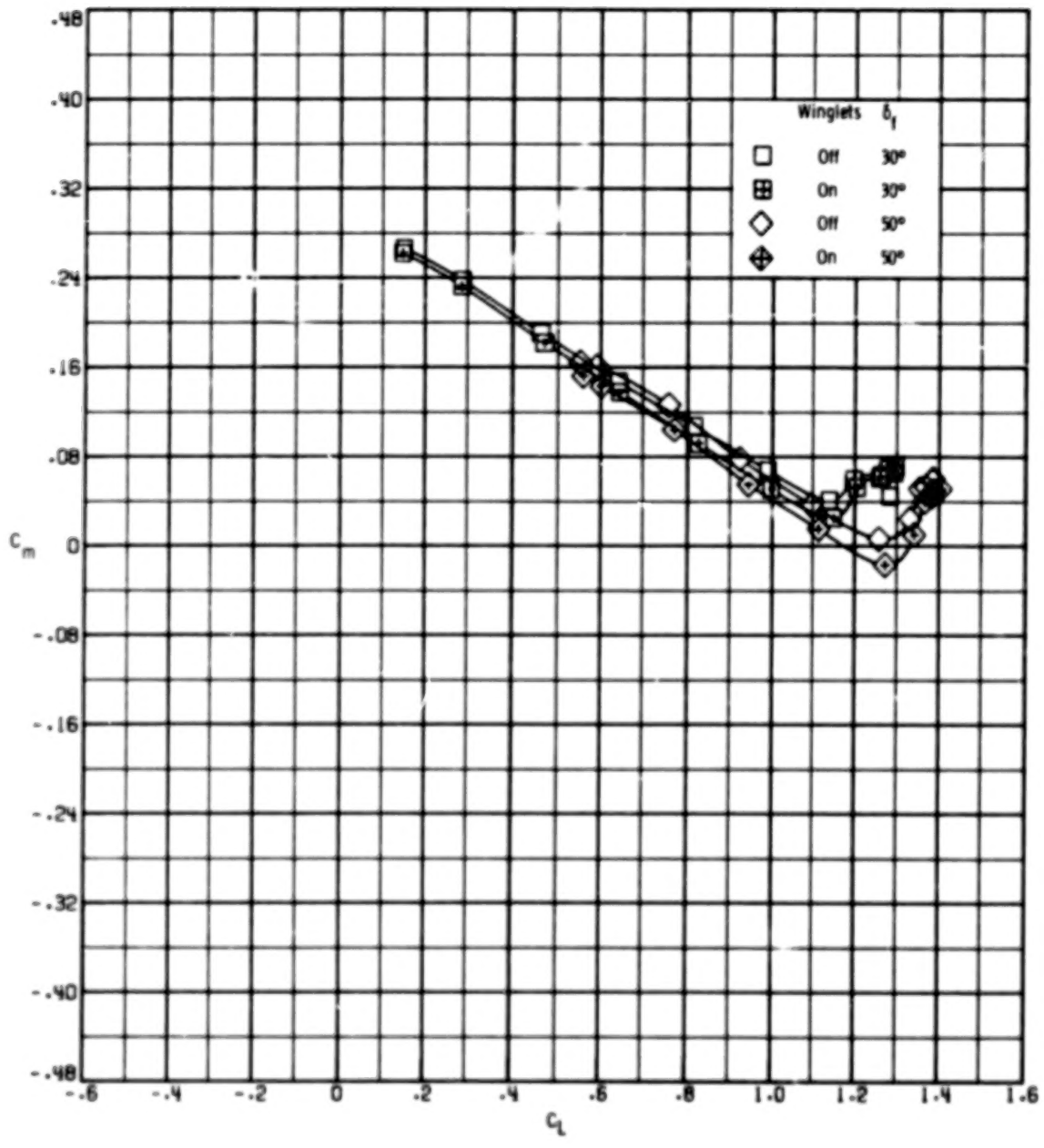

Figure 9.- Concluded.

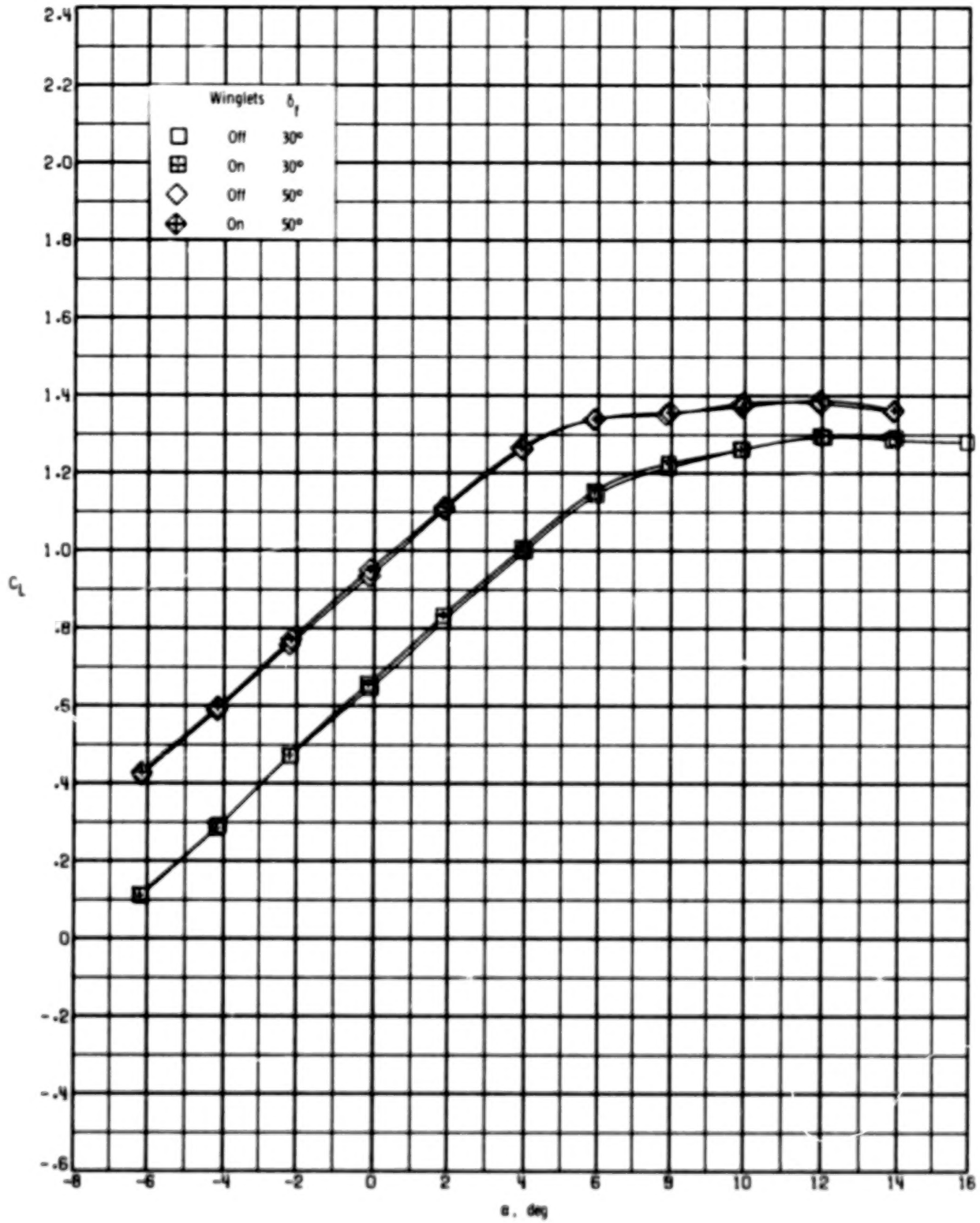

Figure 10.- Effect of winglets on longitudinal aerodynamic characteristics for two flap deflections. $\delta_h = -10^o$; $\delta_{a,L} = -20^o$; $\delta_{a,R} = 20^o$; $\beta = 5^o$.

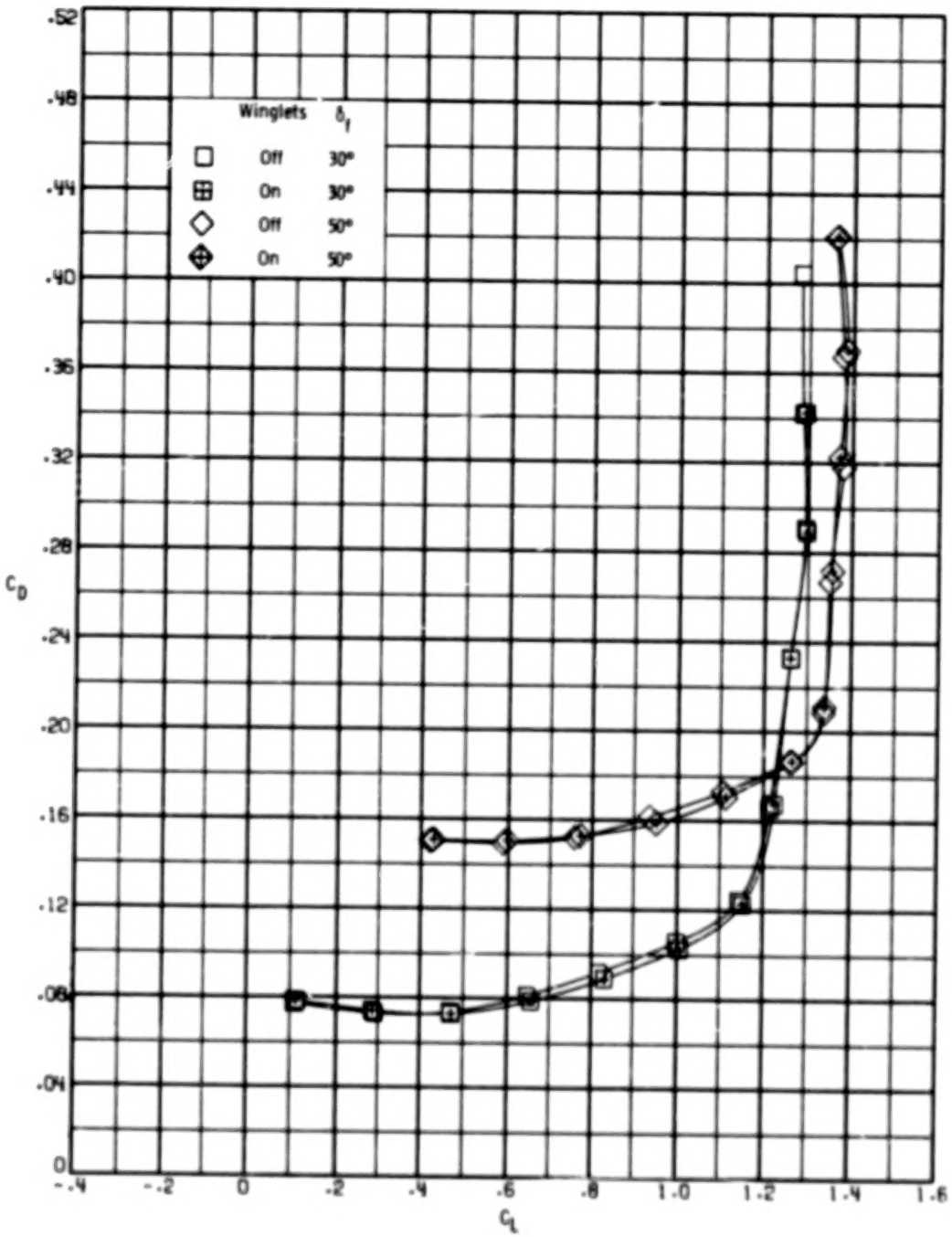

Figure 10.- Continued.

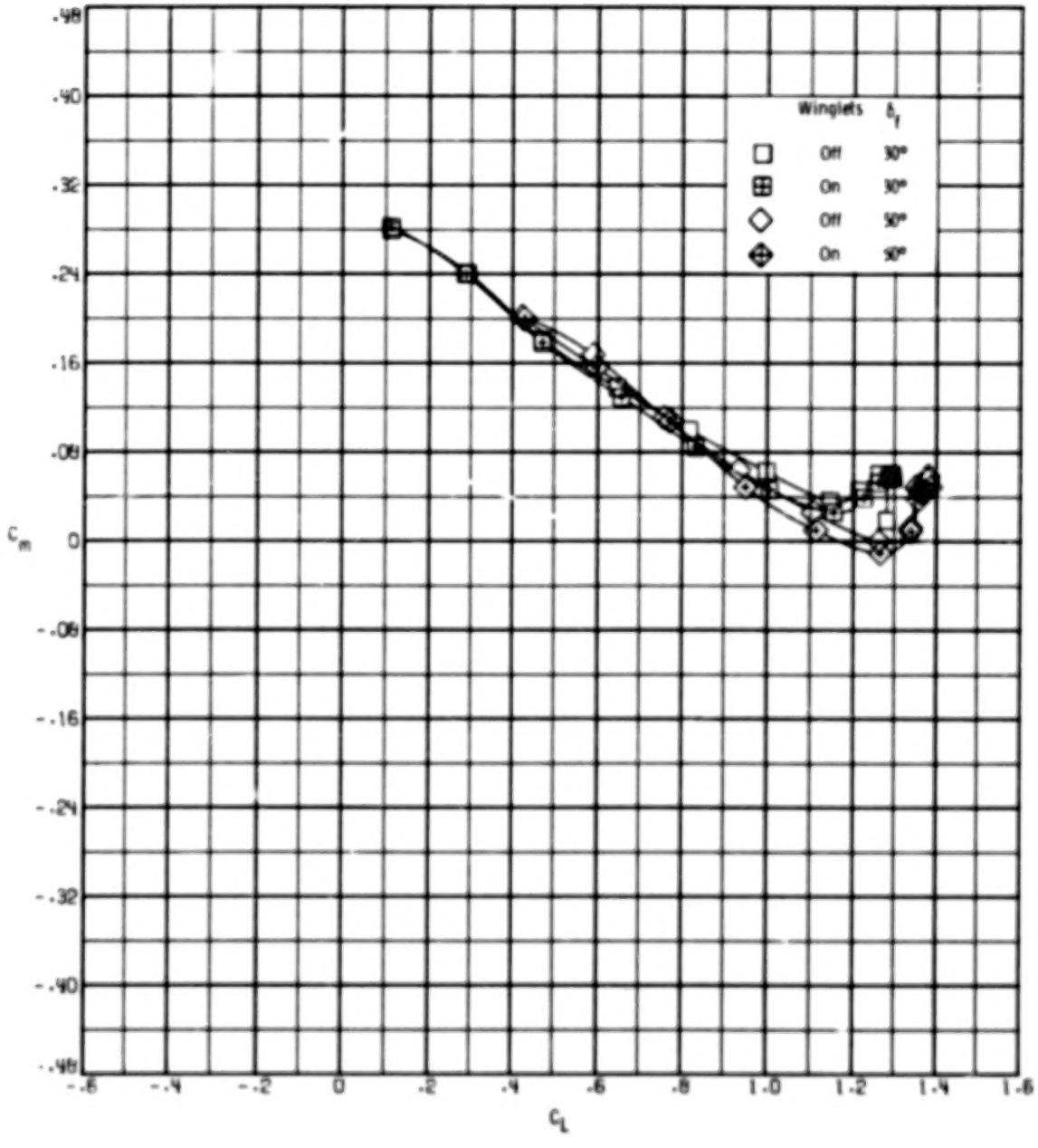

Figure 10.- Concluded.

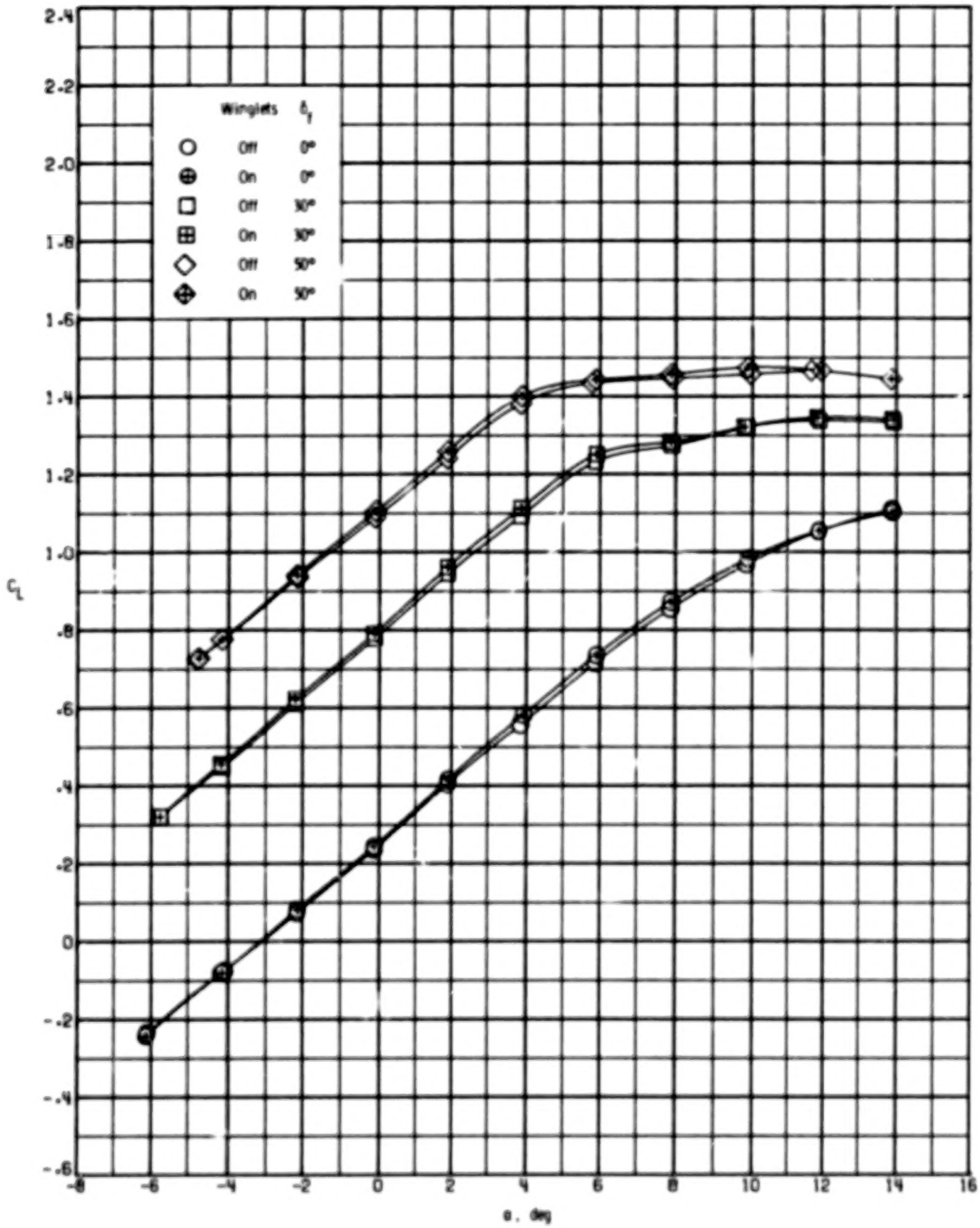

Figure 11.- Effect of winglets on longitudinal aerodynamic characteristics for three flap deflections with horizontal tail removed. $\delta_{a,L} = 0°$; $\delta_{a,R} = 0°$; $\beta = 0°$.

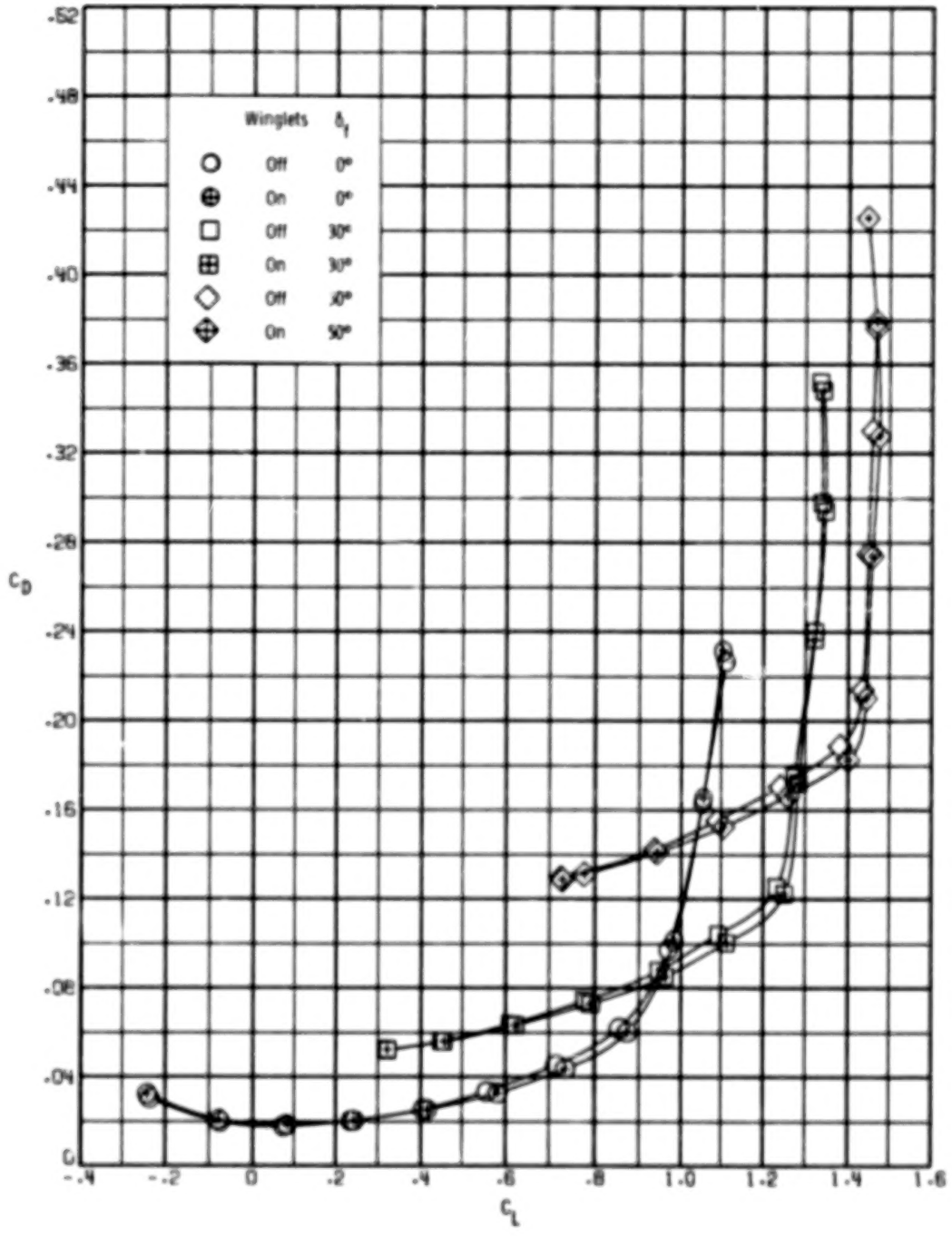

Figure 11.- Continued.

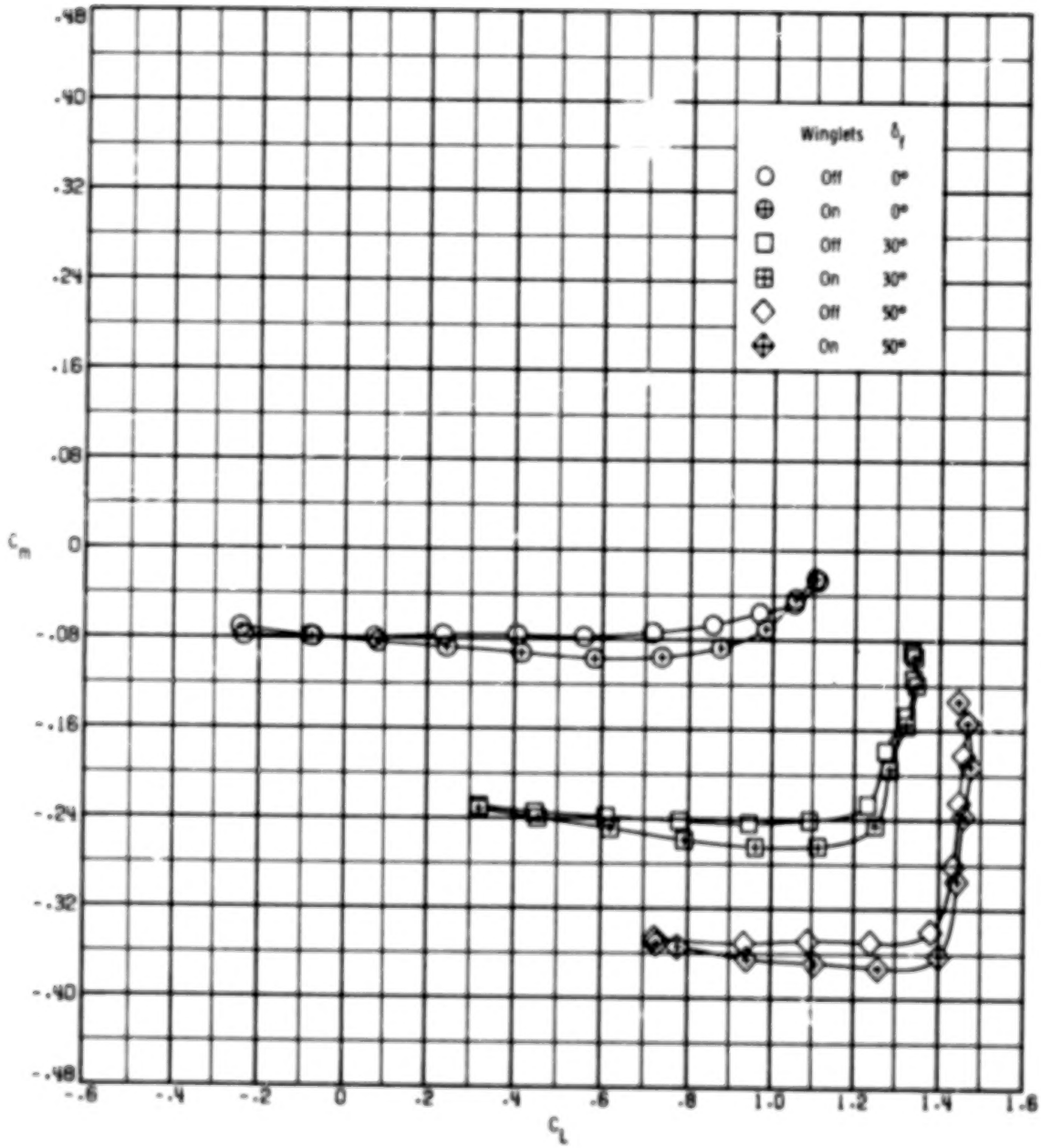

Figure 11.- Concluded.

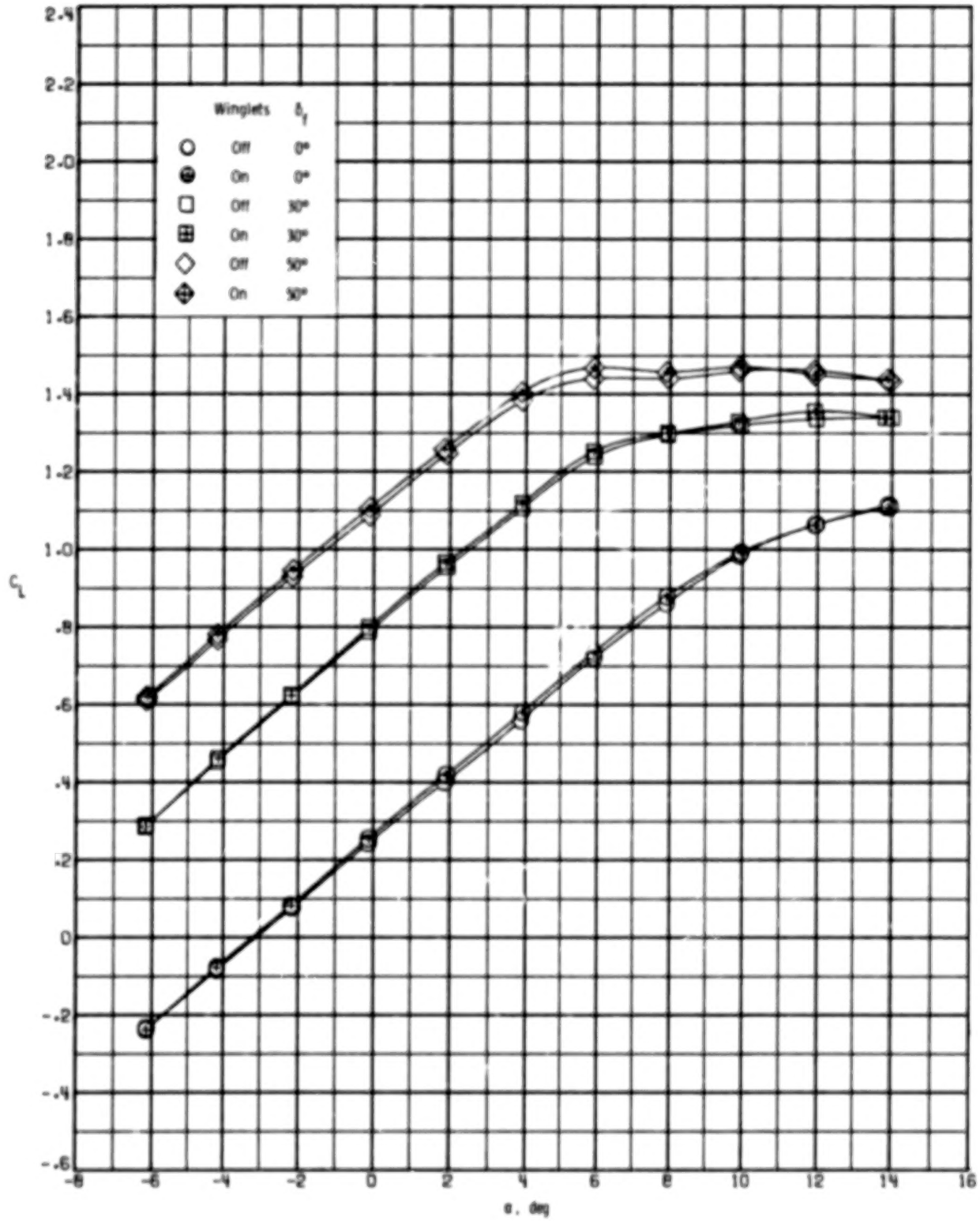

Figure 12.- Effect of winglets on longitudinal aerodynamic characteristics for three flap deflections with horizontal tail removed. $\delta_{a,L} = 0^\circ$; $\delta_{a,R} = 0^\circ$; $\beta = 5^\circ$.

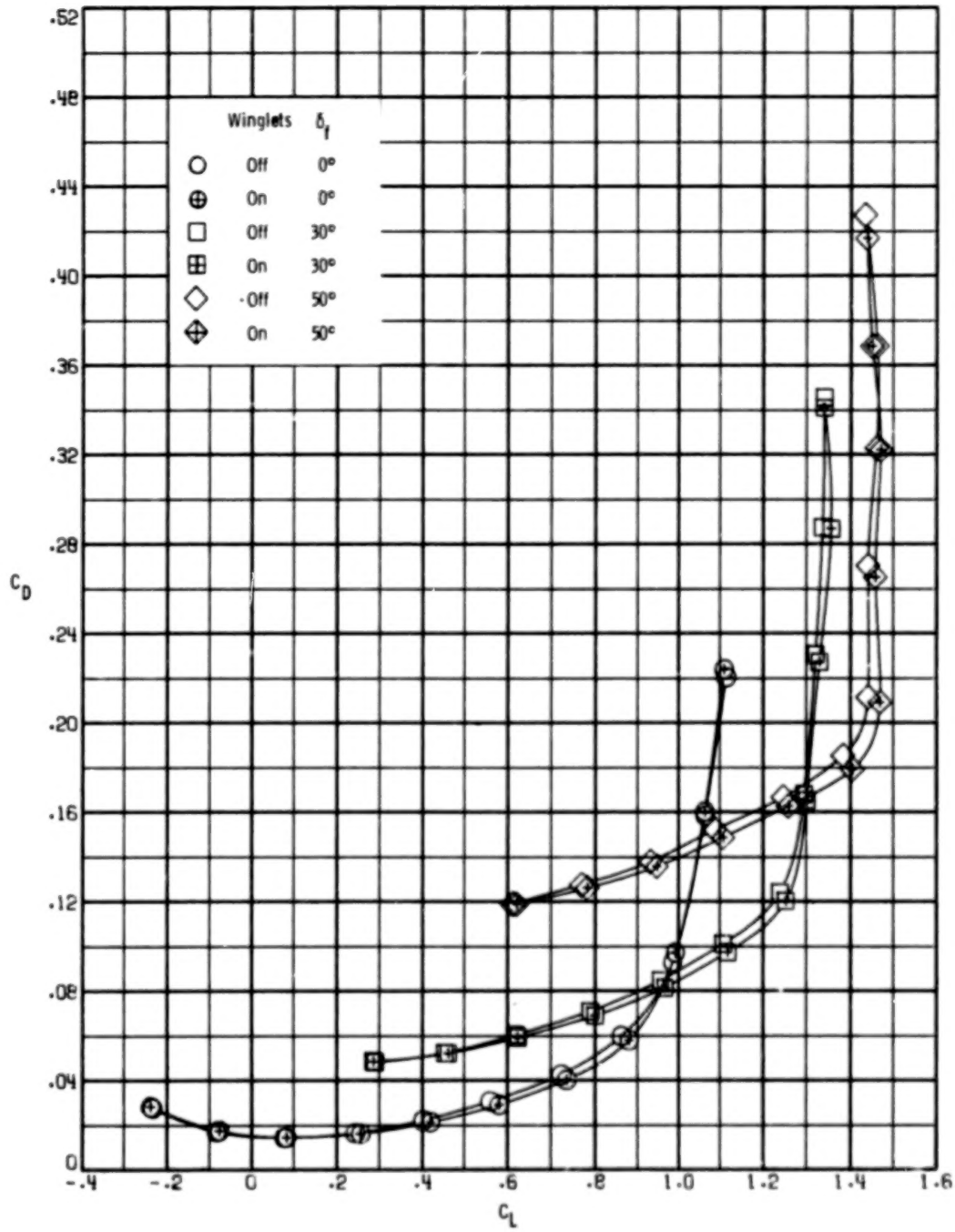

Figure 12.- Continued.

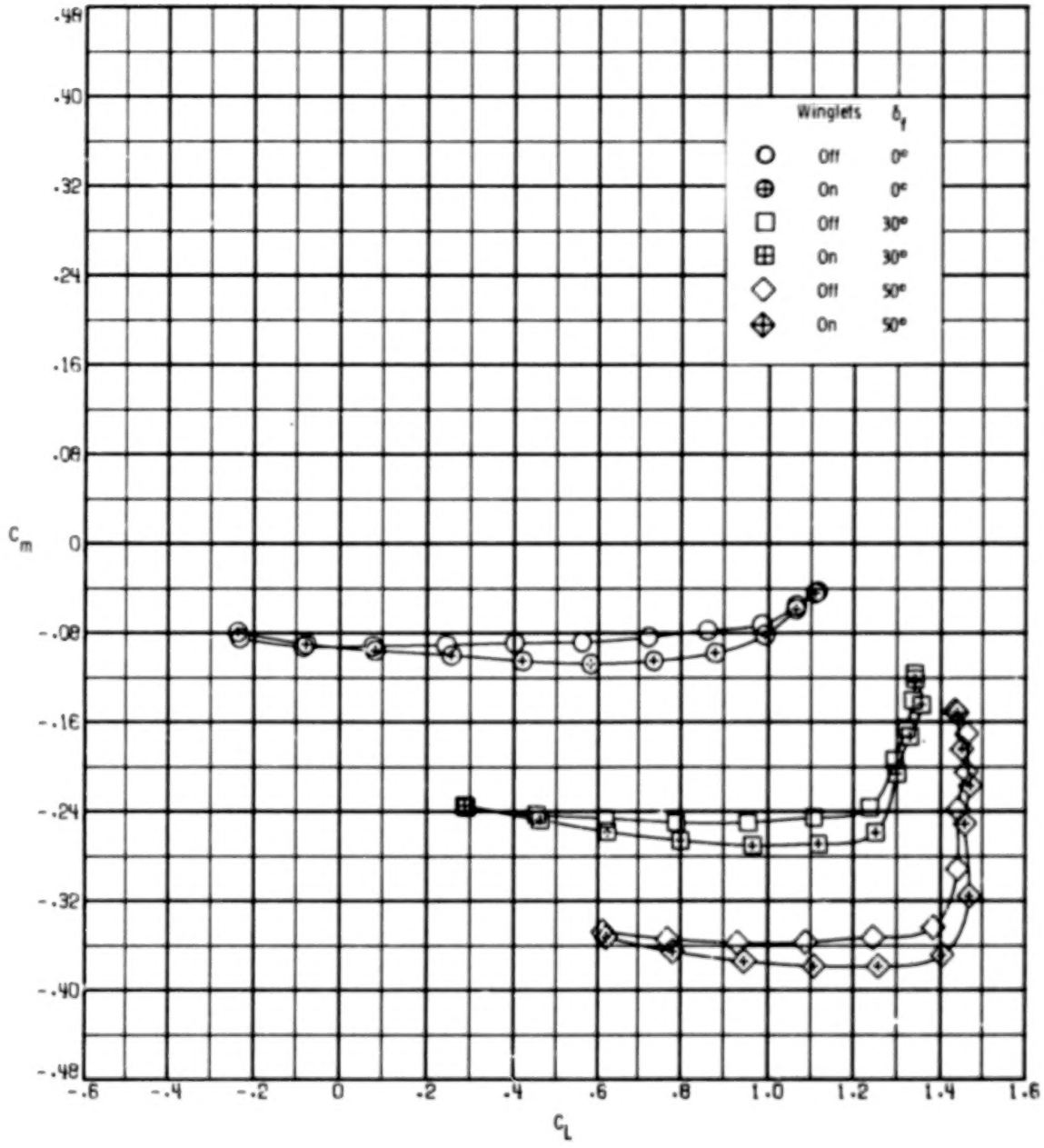

Figure 12.- Concluded.

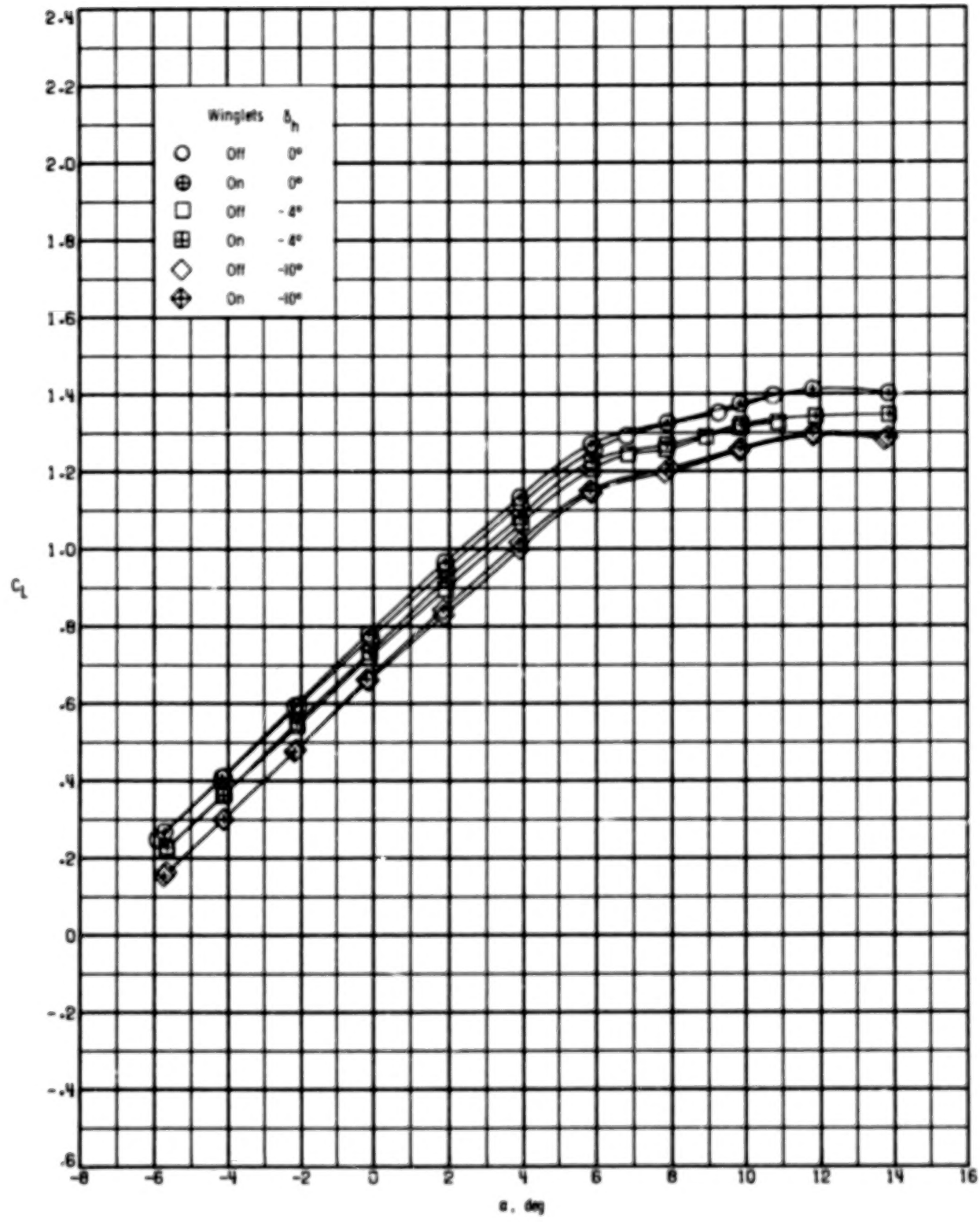

Figure 13.- Effect of winglets on longitudinal aerodynamics characteristics for three horizontal-tail deflections. $\delta_f = 30°$; $\delta_{a,L} = 0°$; $\delta_{a,R} = 0°$; $\beta = 0°$.

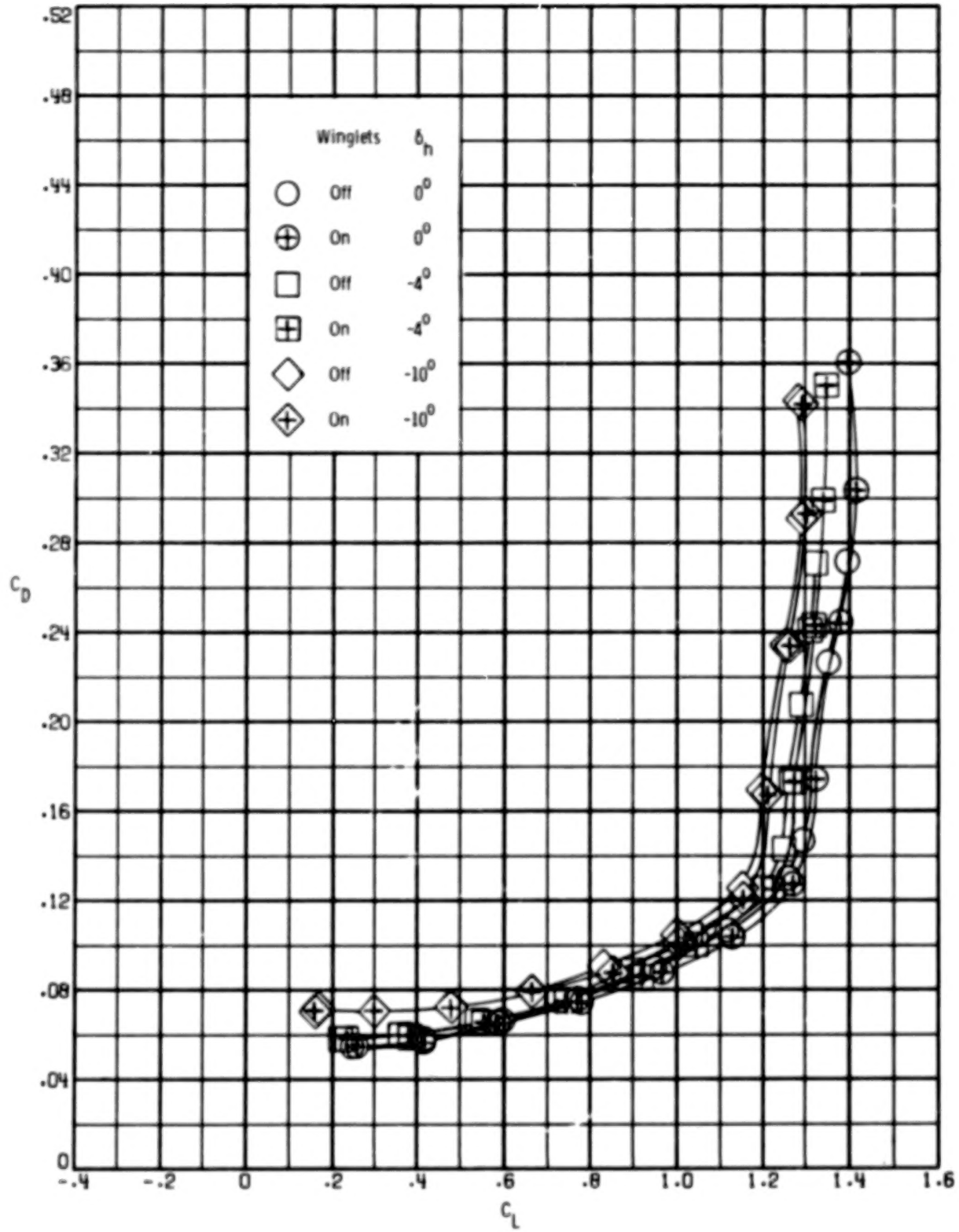

Figure 13.- Continued.

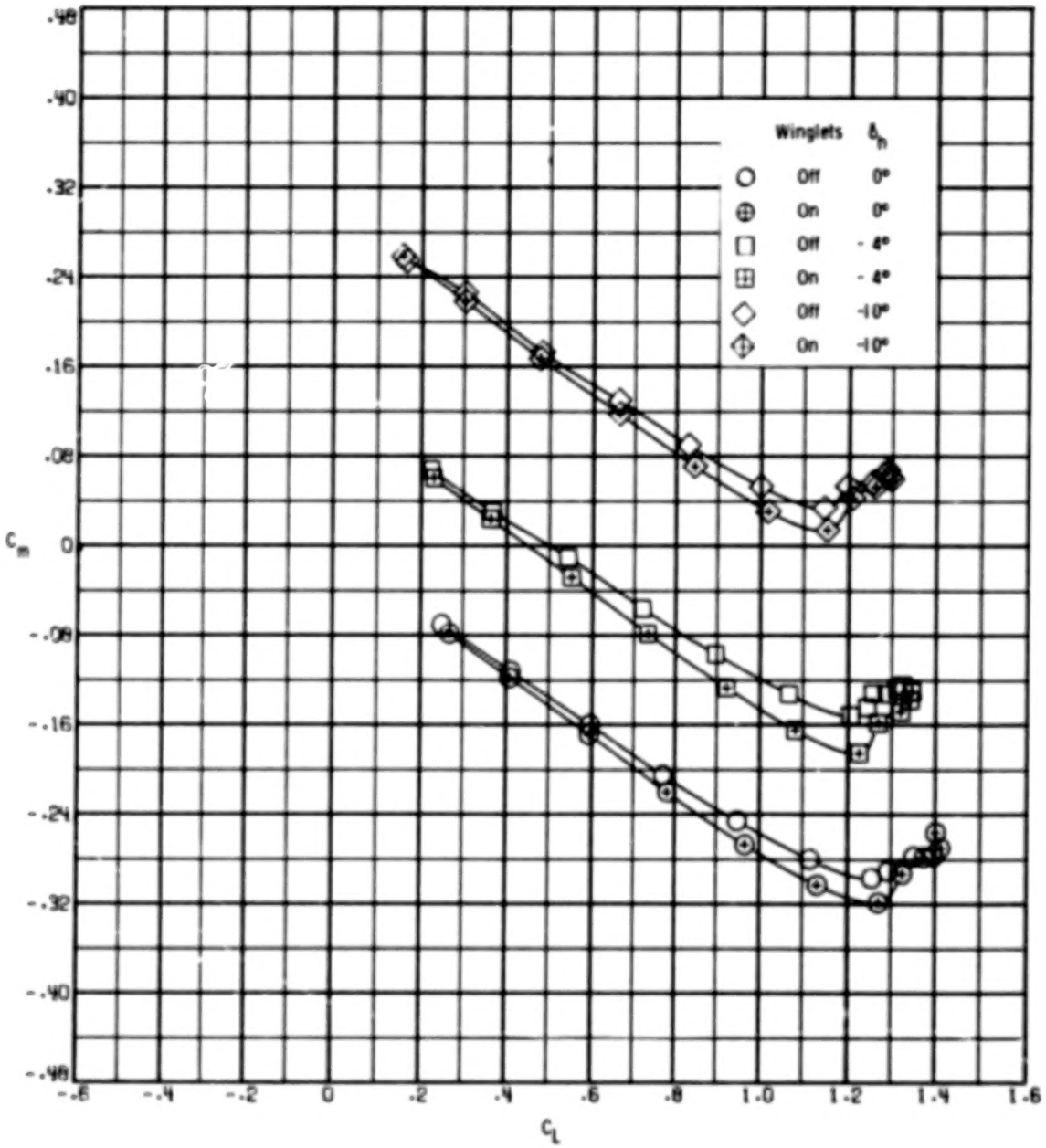

Figure 13.- Concluded.

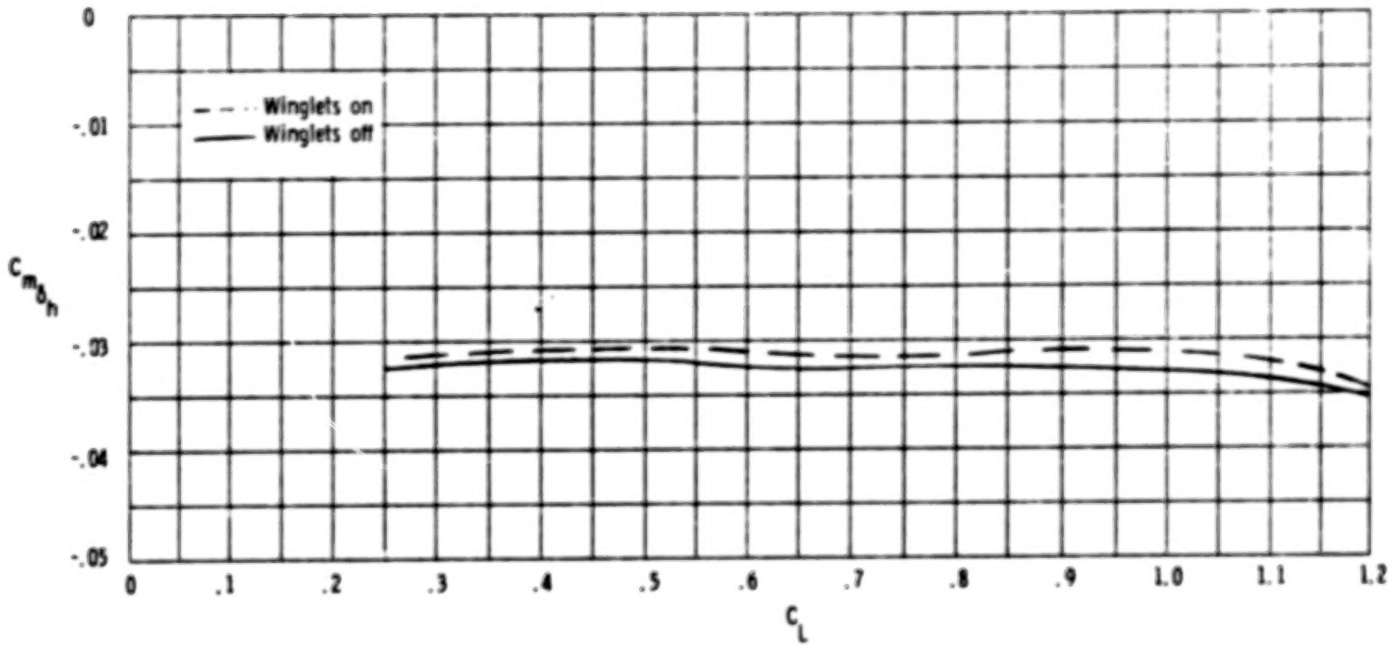

Figure 14.- Effect of winglets on horizontal-tail effectiveness. $\delta_f = 30°$; $\delta_{a,L} = 0°$; $\delta_{a,R} = 0°$; $\beta = 0°$.

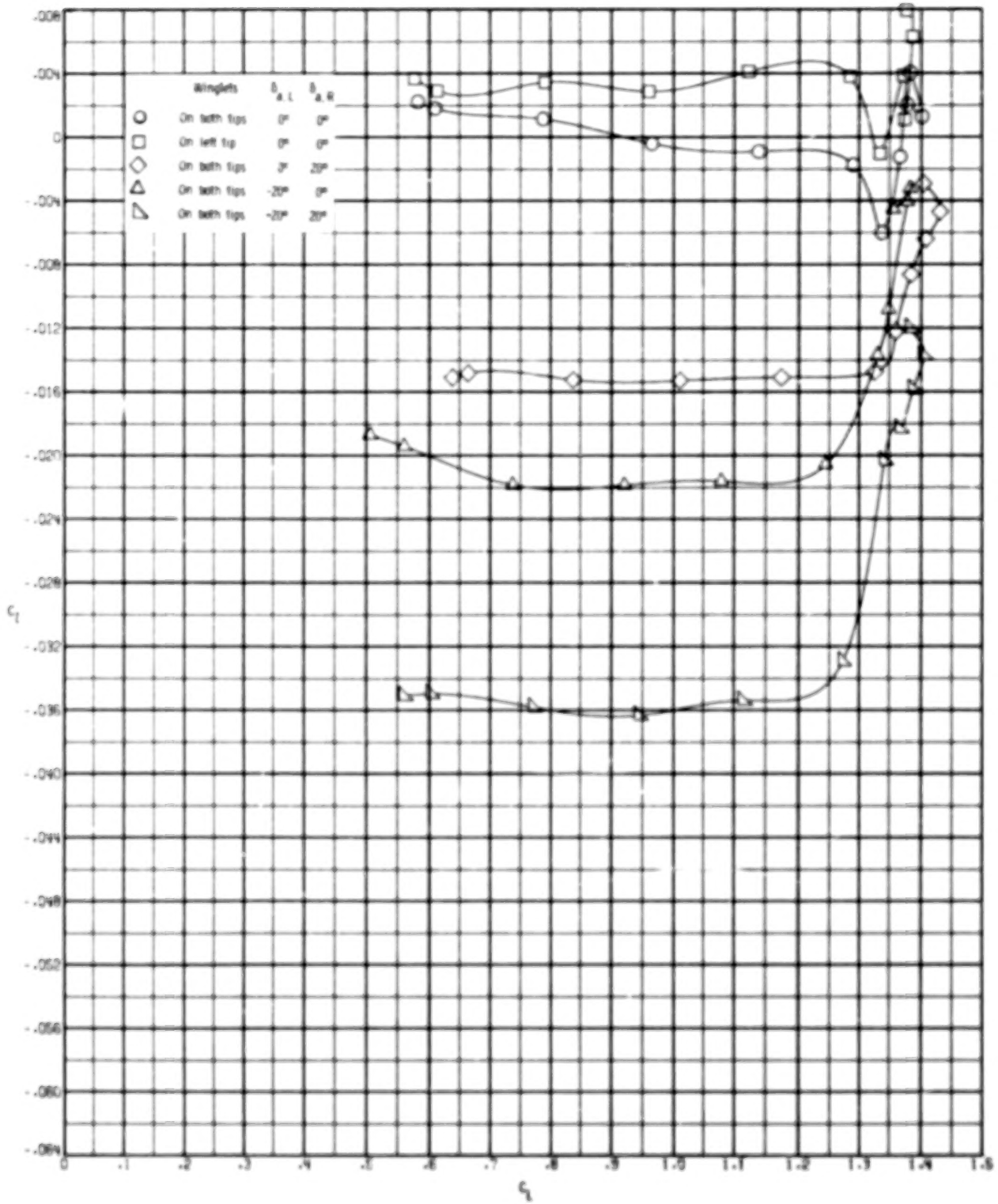

Figure 15.- Effect of winglets on lateral-directional aerodynamic characteristics for winglets on both wings with nonsymmetric aileron deflection and for a winglet on one wing only. $\delta_h = -10^\circ$; $\delta_f = 50^\circ$; $\beta = 0^\circ$.

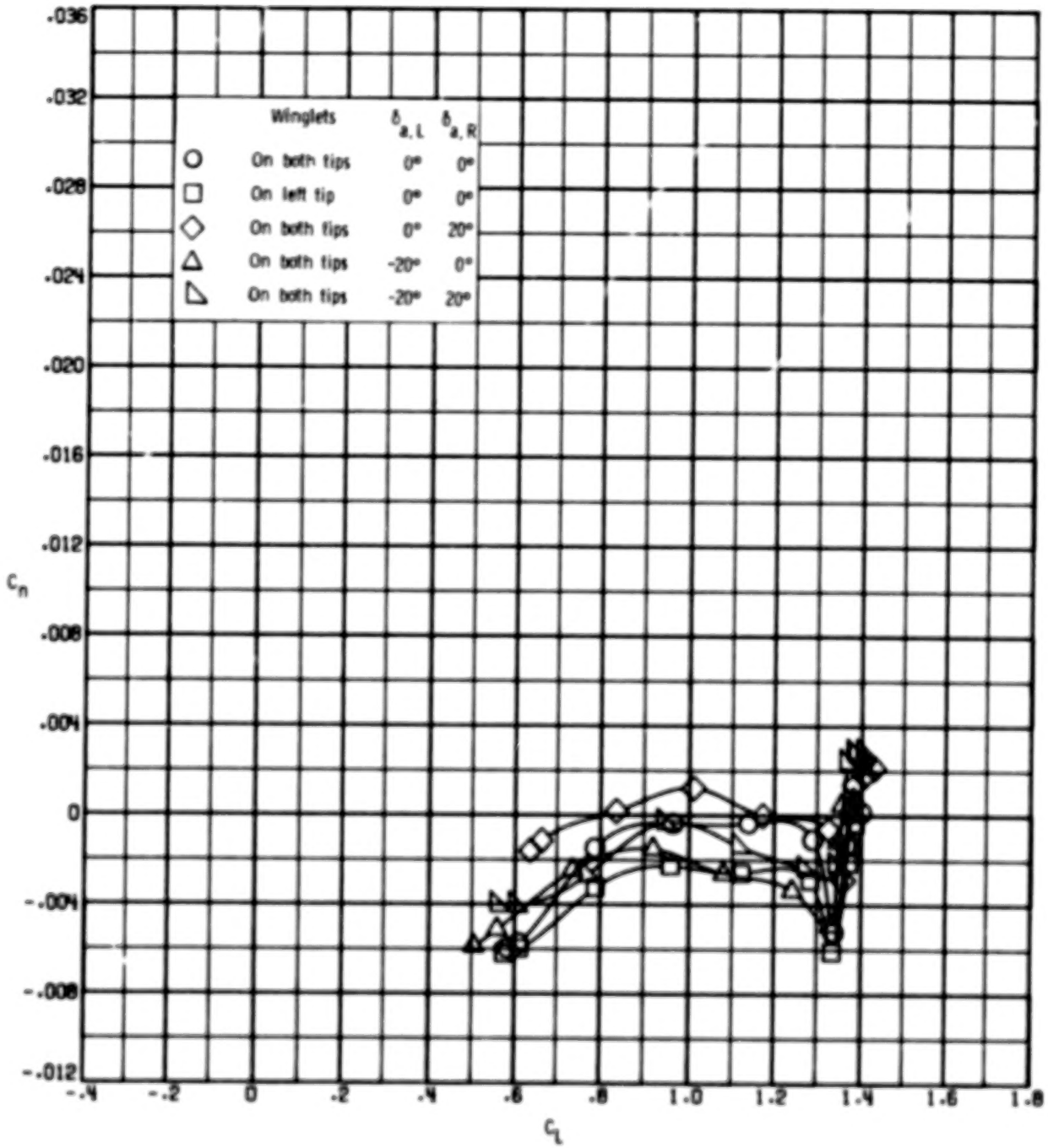

Figure 15.- Continued.

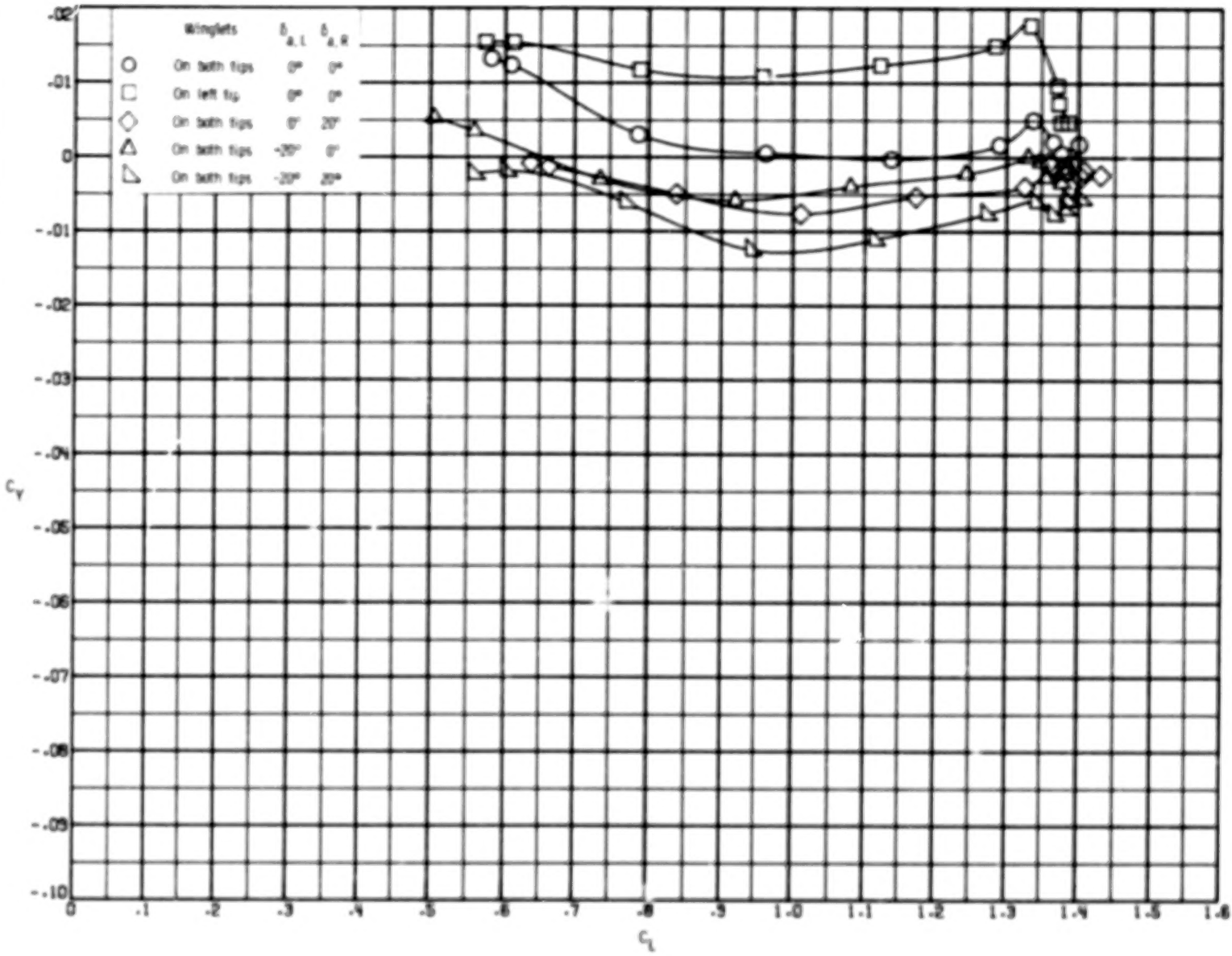

Figure 15.- Concluded.

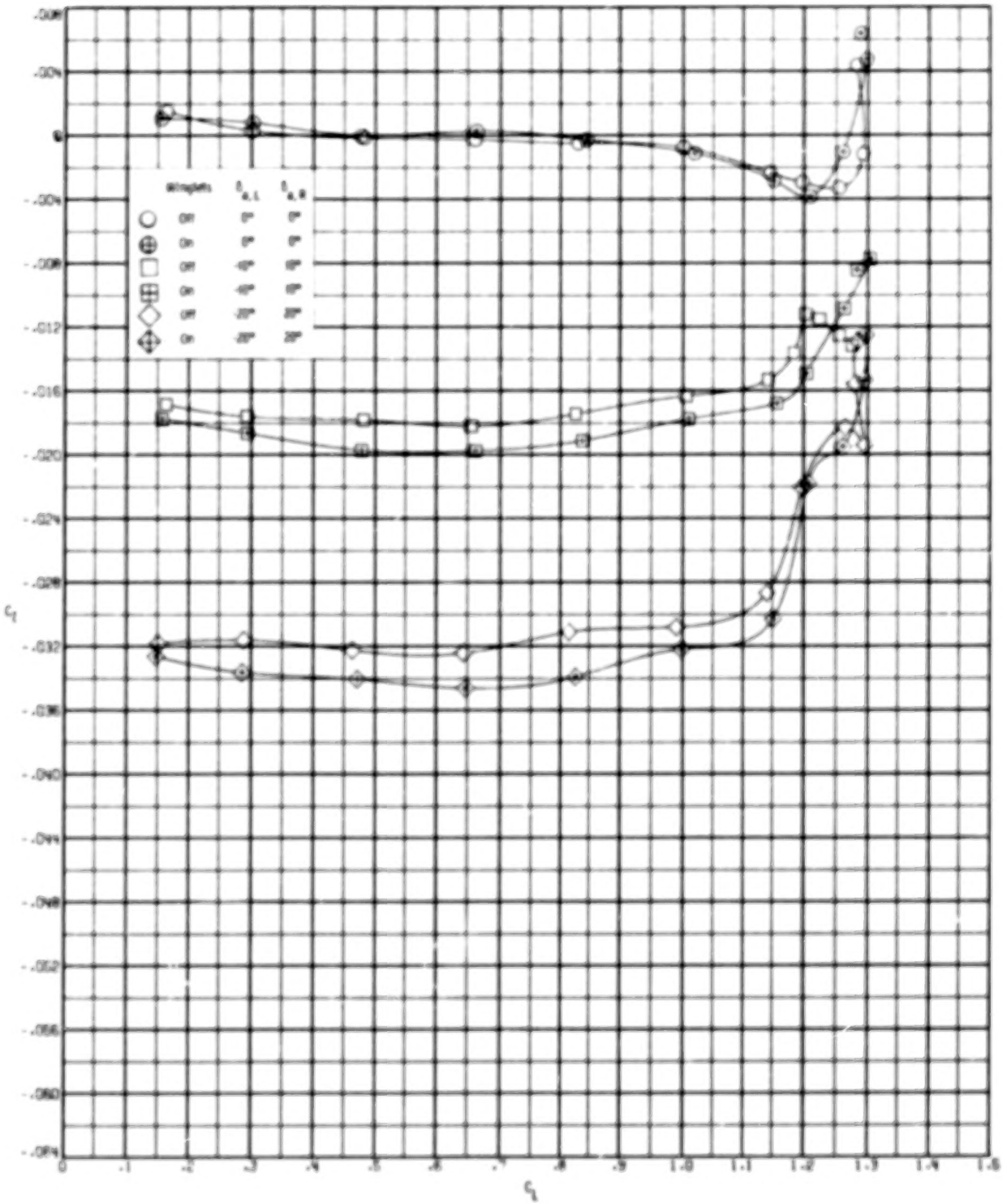

Figure 16.- Effect of winglets on lateral-directional aerodynamic characteristics for three aileron deflections. $\delta_h = -10°$; $\delta_f = 30°$; $\beta = 0°$.

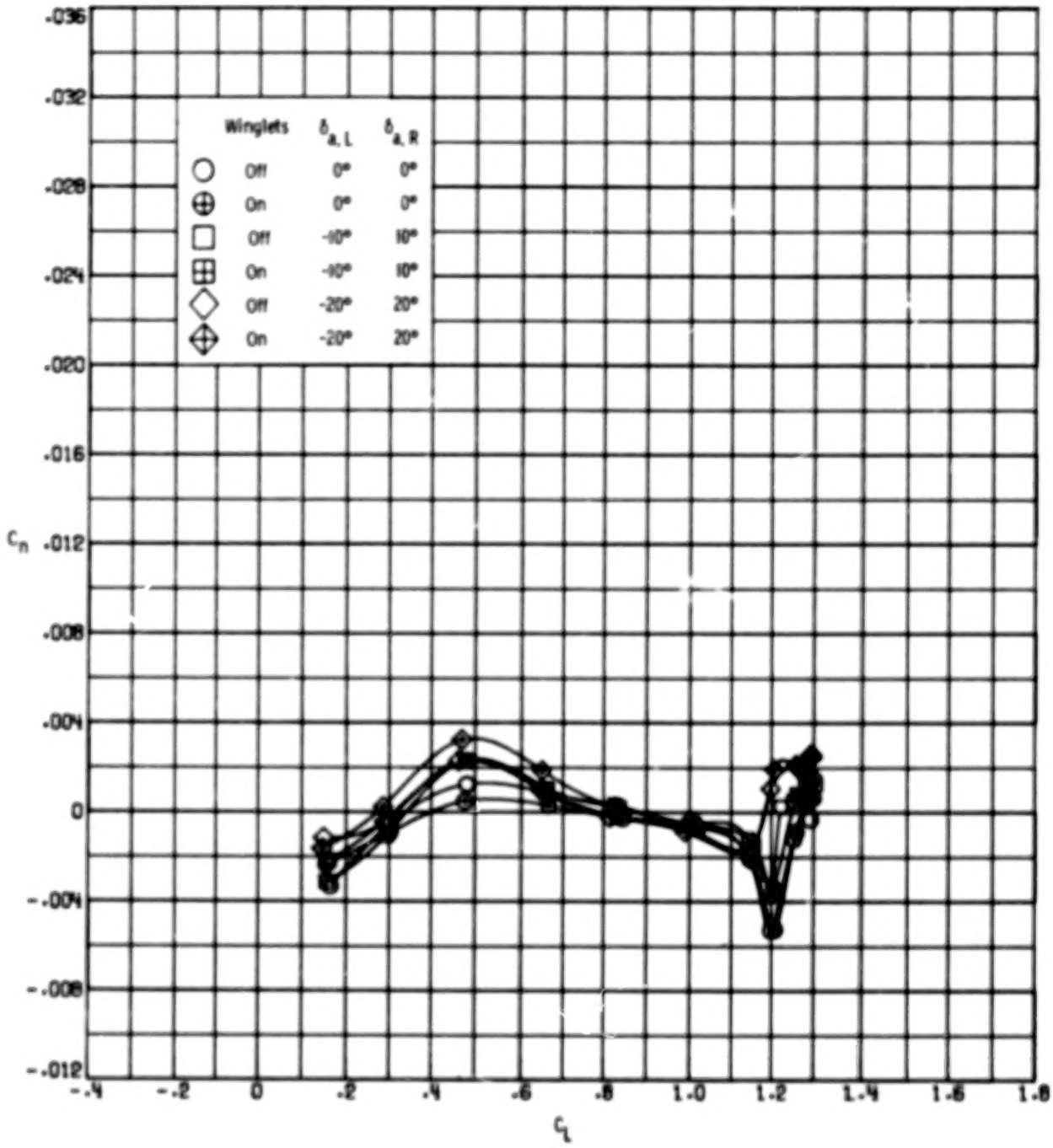

Figure 16.- Continued.

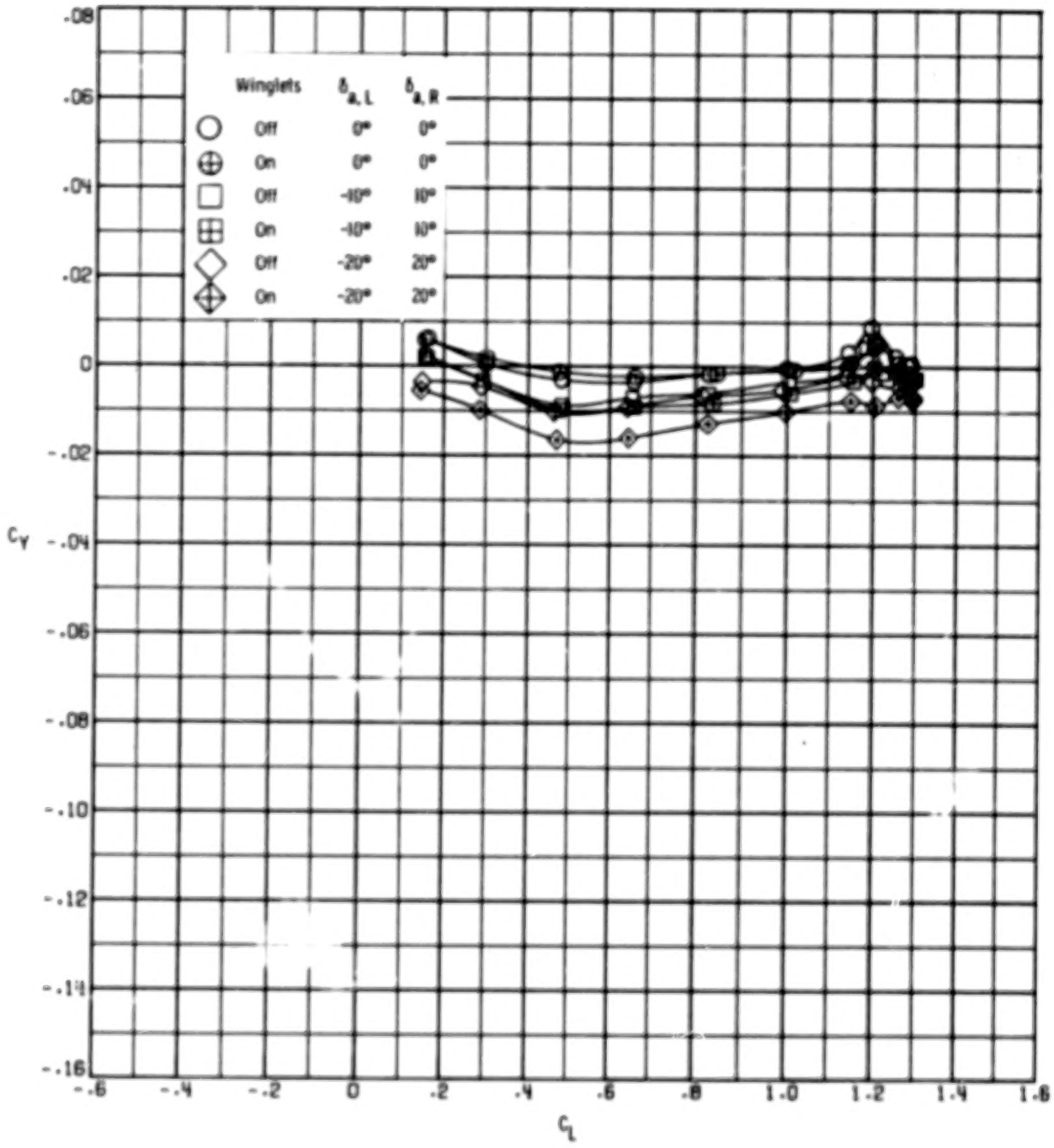

Figure 16.- Concluded.

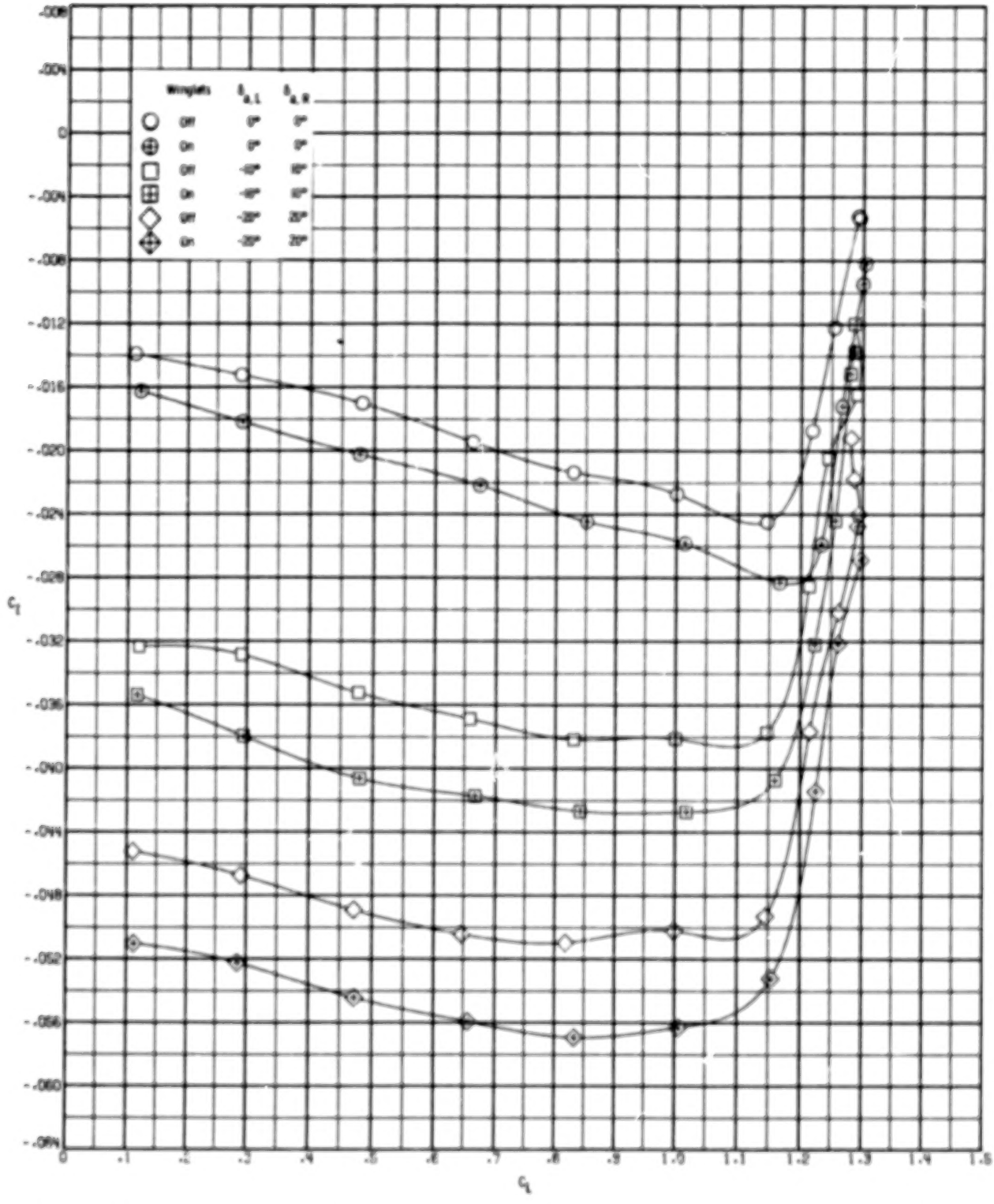

Figure 17.- Effect of winglets on lateral-directional aerodynamic characteristics for three aileron deflections. $\delta_h = -10^\circ$; $\delta_f = 30^\circ$; $\beta = 5^\circ$.

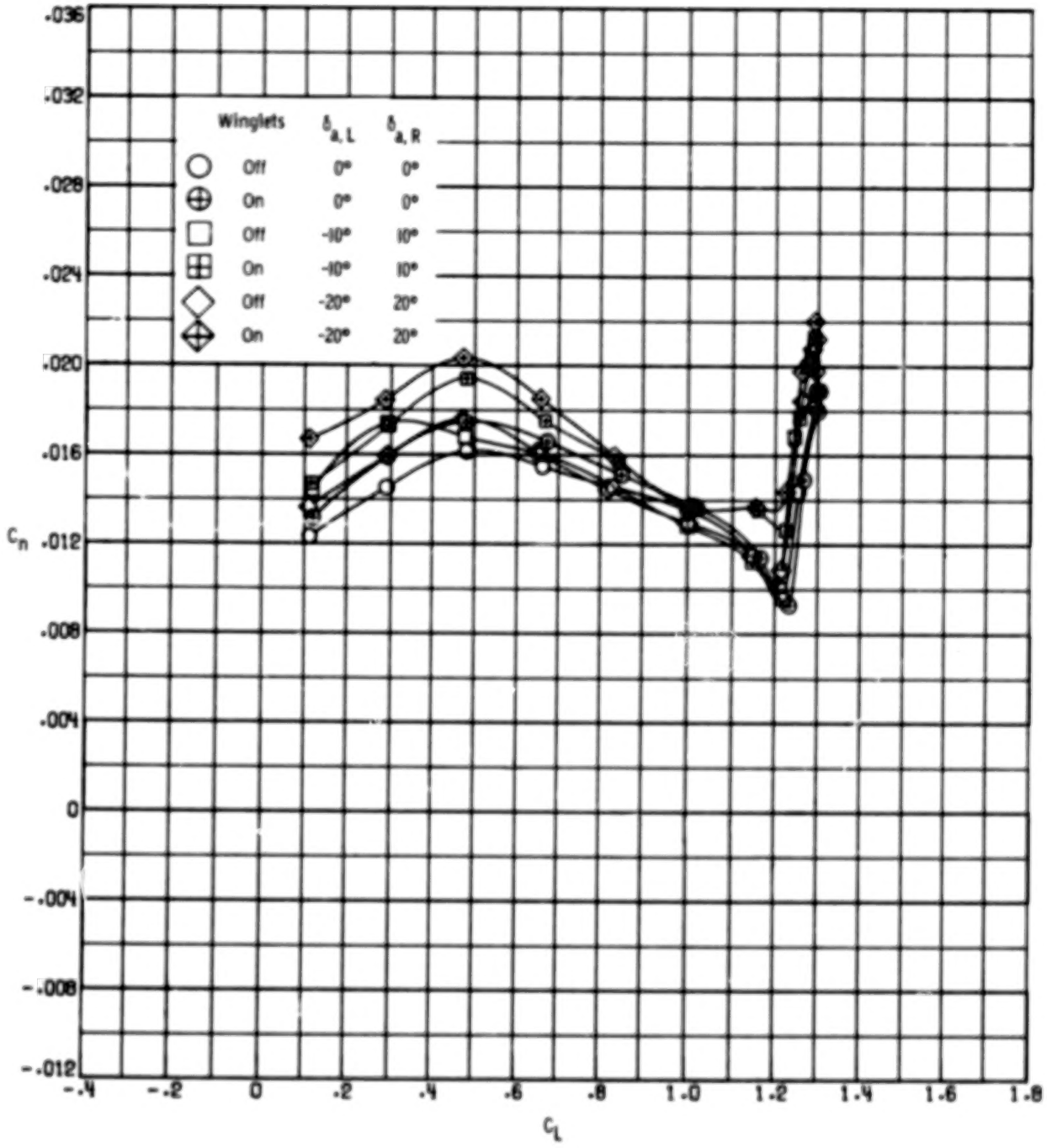

Figure 17.- Continued.

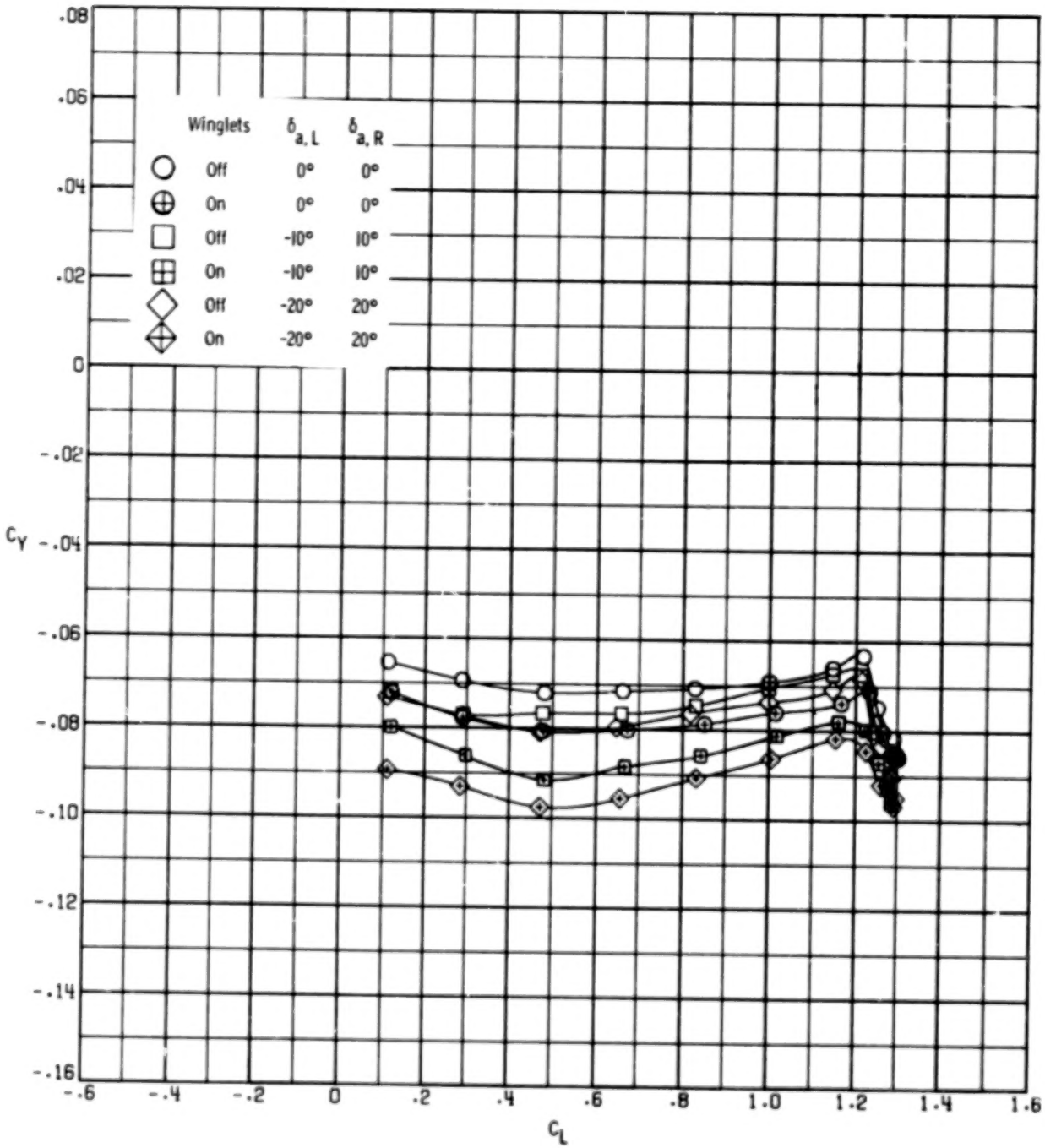

Figure 17.- Concluded.

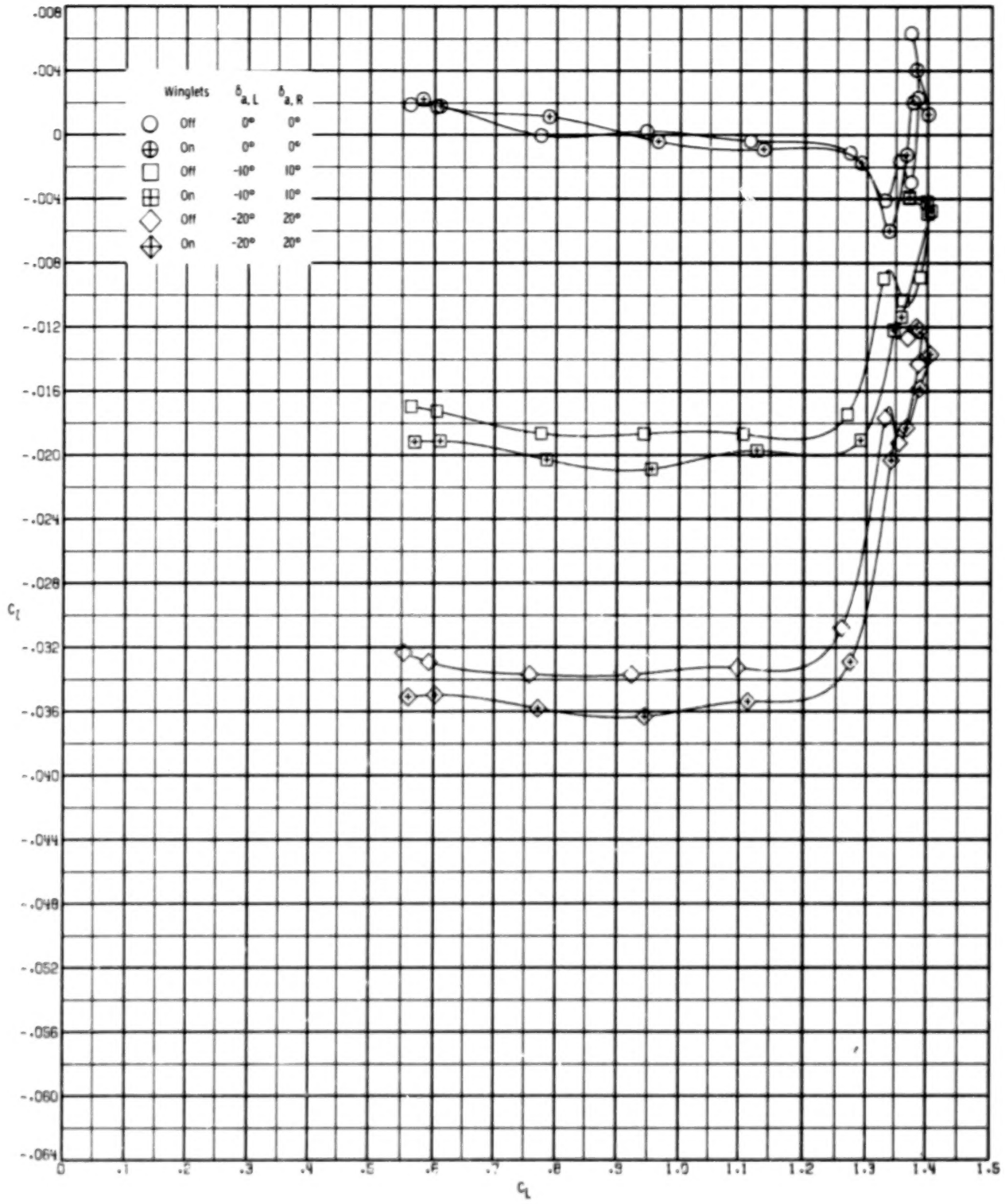

Figure 18.- Effect of winglets on lateral-directional aerodynamic characteristics for three aileron deflections. $\delta_h = -10^o$; $\delta_f = 50^o$; $\beta = 0^o$.

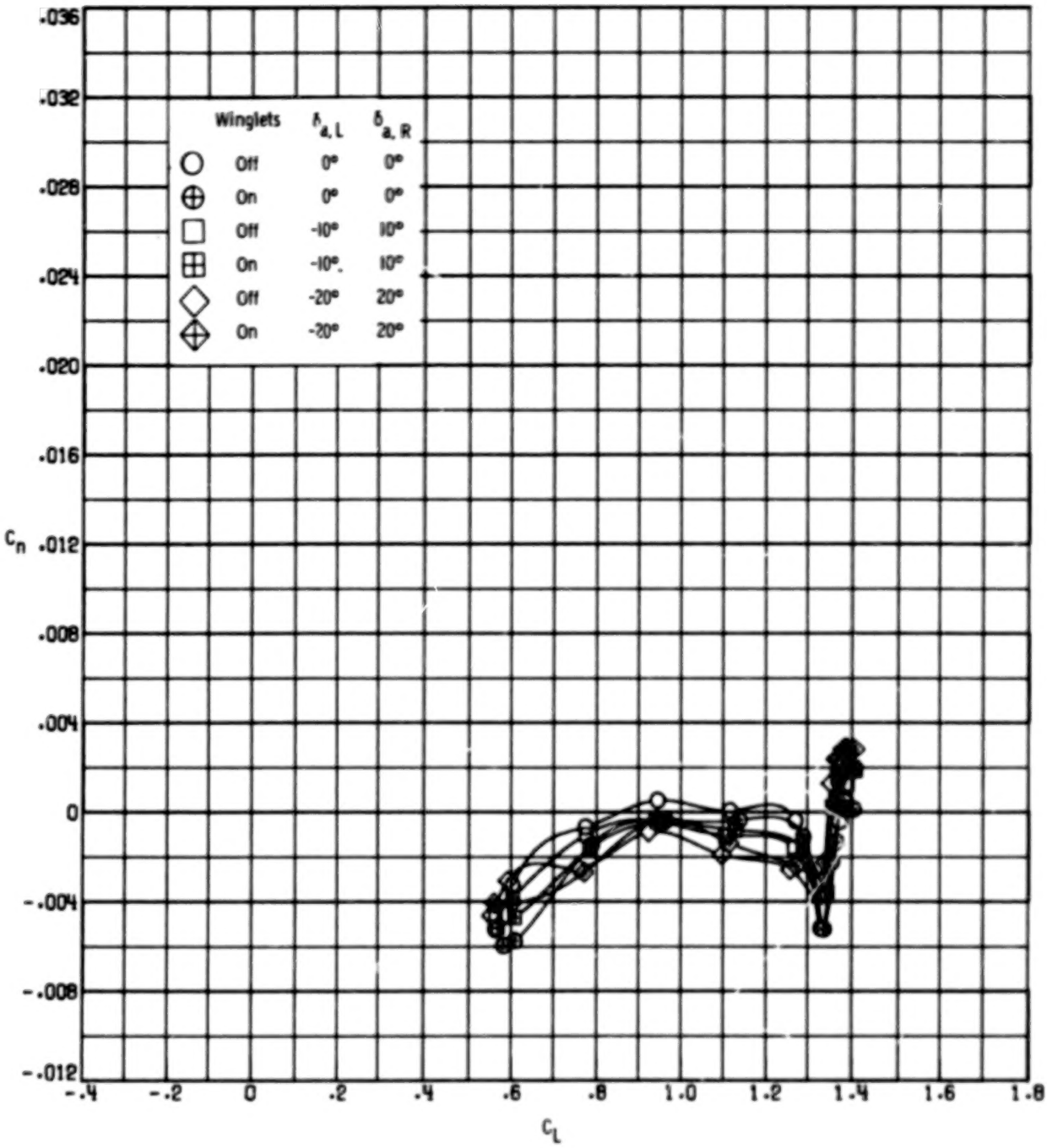

Figure 18.- Continued.

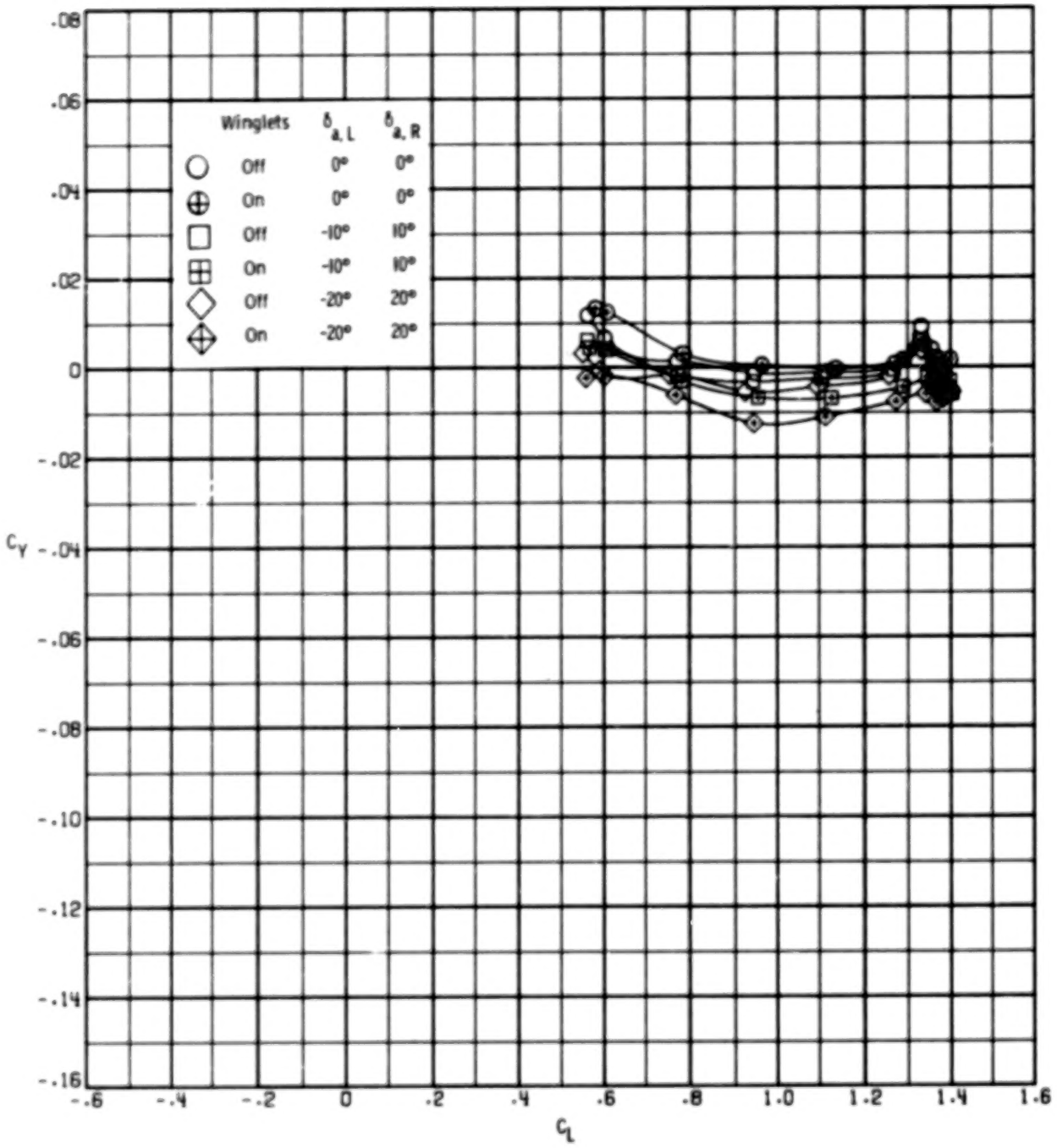

Figure 18.- Concluded.

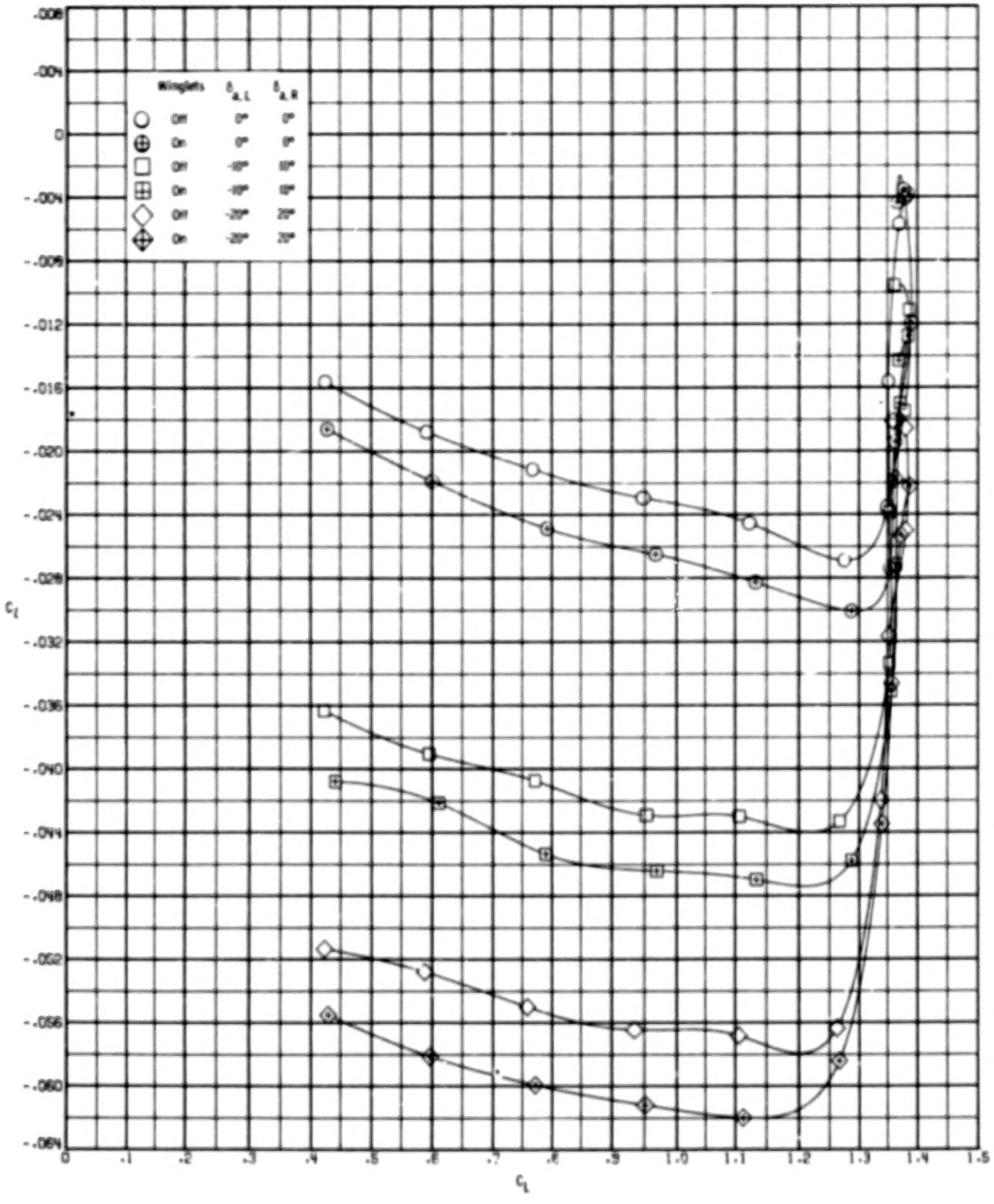

Figure 19.- Effect of winglets on lateral-directional aerodynamic characteristics for three aileron deflections. $\delta_h = -10^o$; $\delta_f = 50^o$; $\beta = 5^o$.

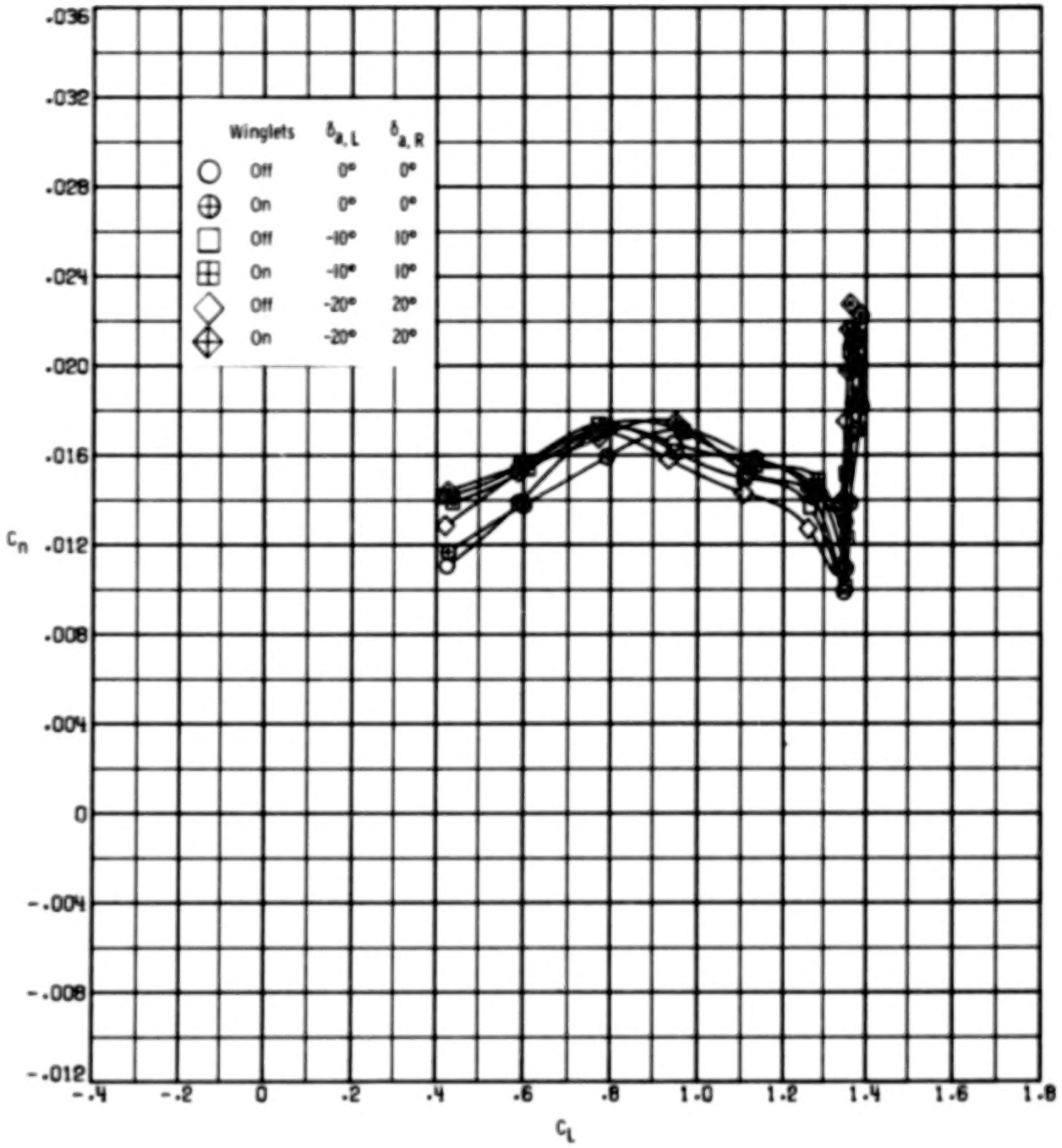

Figure 19.- Continued.

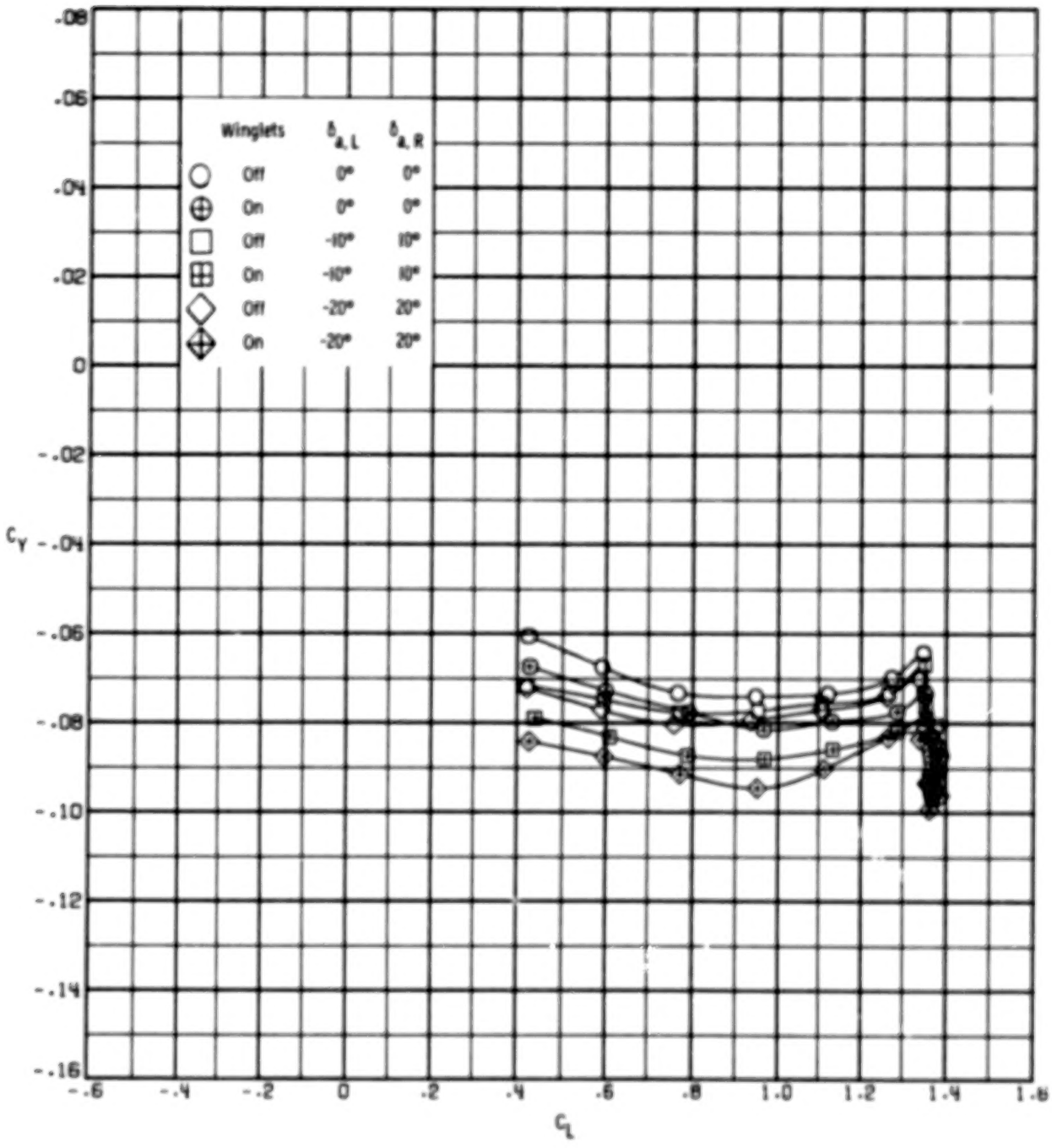

Figure 19.- Concluded.

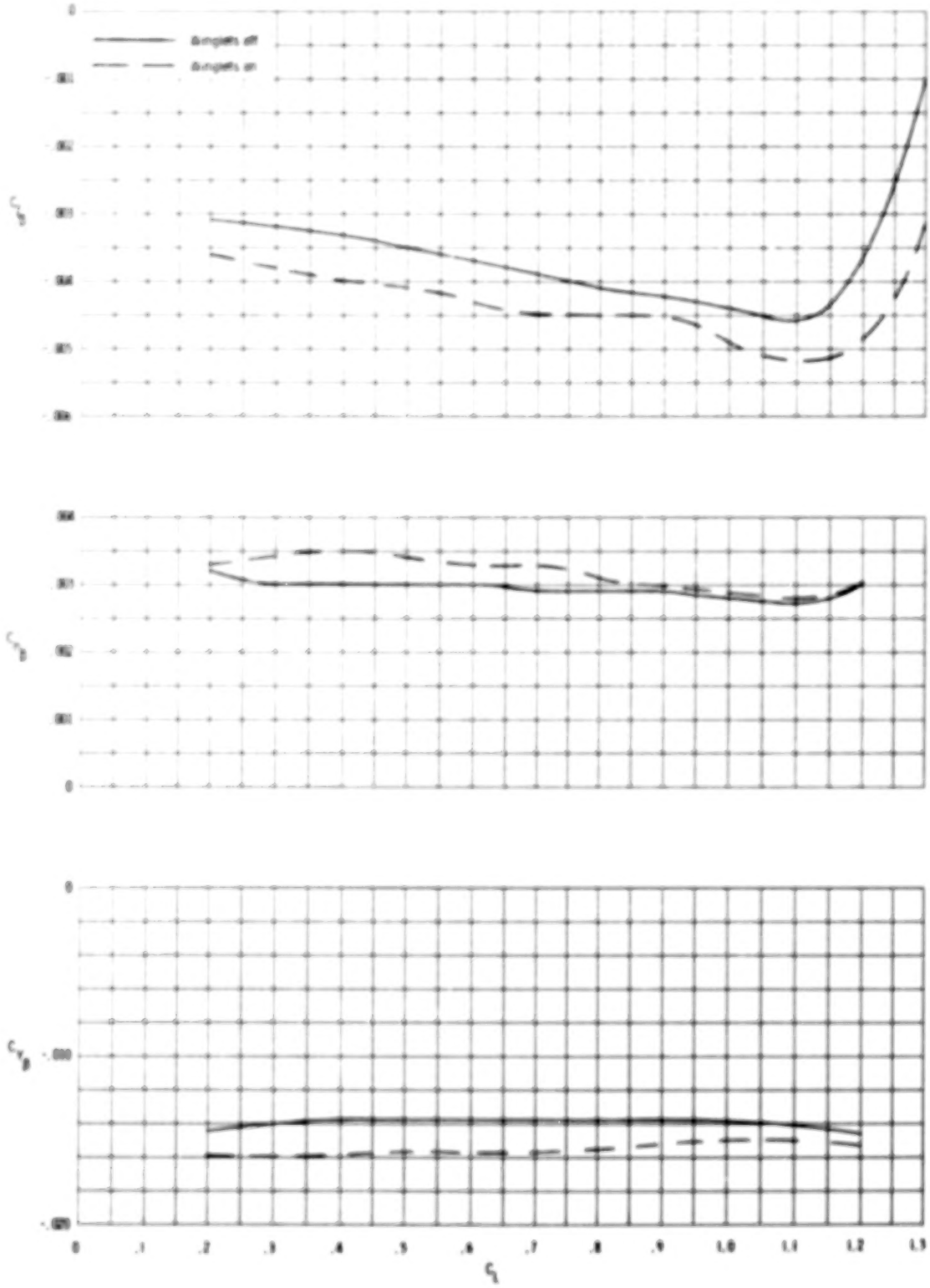

Figure 20.- Effect of winglets on lateral-directional stability derivatives. $\delta_h = -10^o$; $\delta_f = 30^o$; $\delta_{a,L} = 0^o$; $\delta_{a,R} = 0^o$.

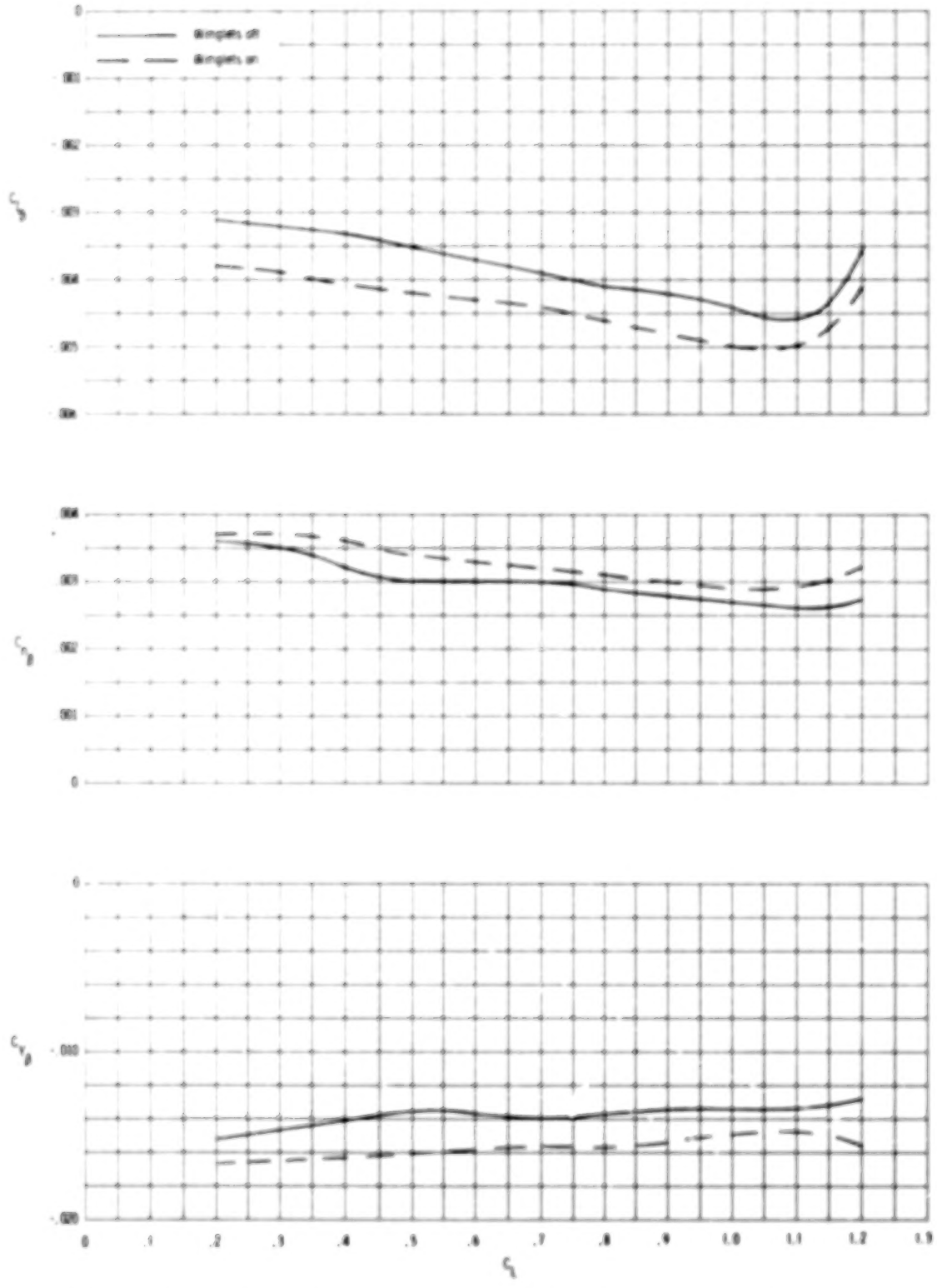

Figure 21.- Effect of winglets on lateral-directional stability derivatives. $\delta_h = -10^o$; $\delta_f = 30^o$; $\delta_{a,L} = -10^o$; $\delta_{a,R} = 10^o$.

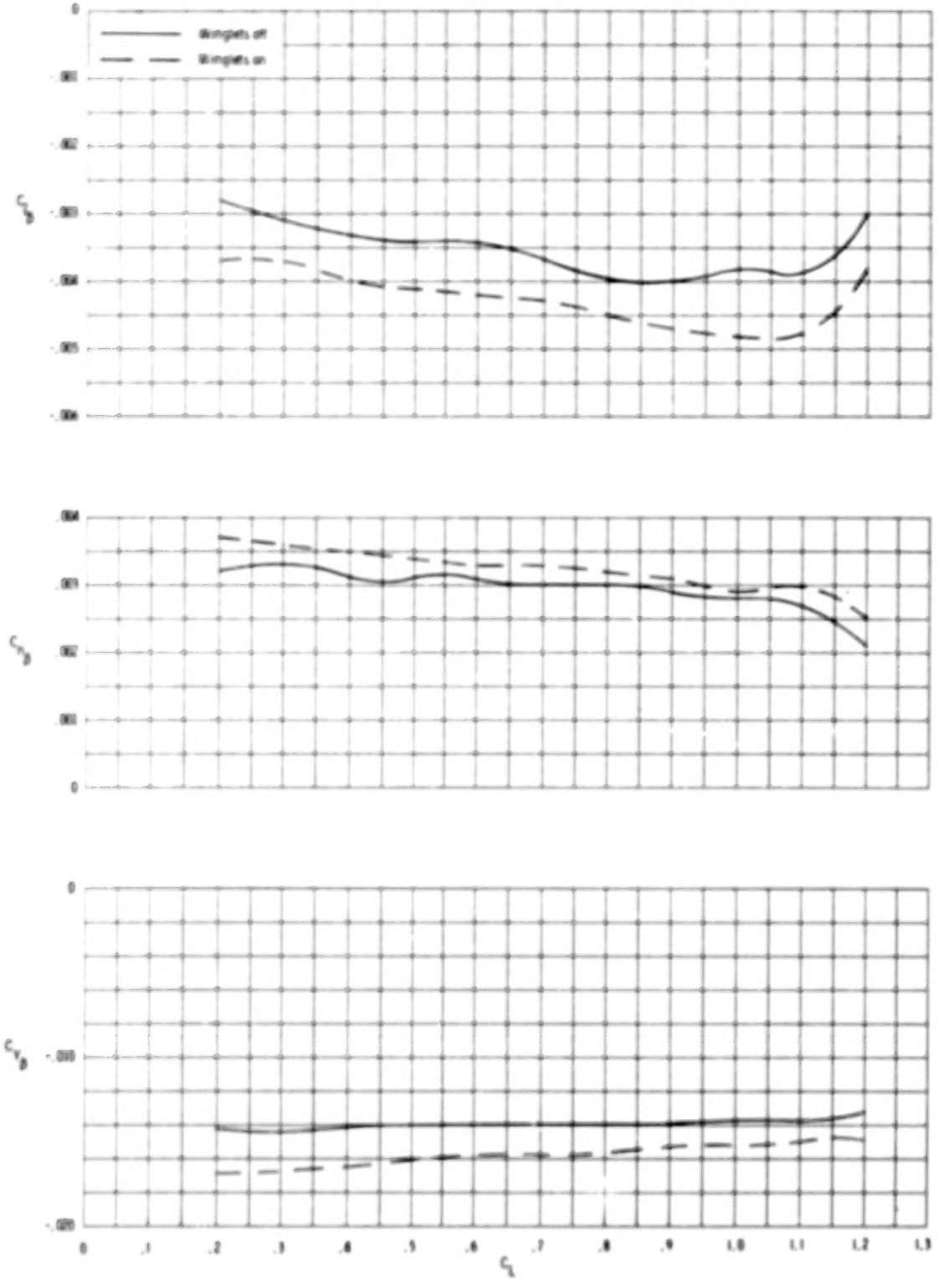

Figure 22.- Effect of winglets on lateral-directional stability derivatives. $\delta_h = -10^\circ$; $\delta_f = 30^\circ$; $\delta_{a,L} = -20^\circ$; $\delta_{a,R} = 20^\circ$.

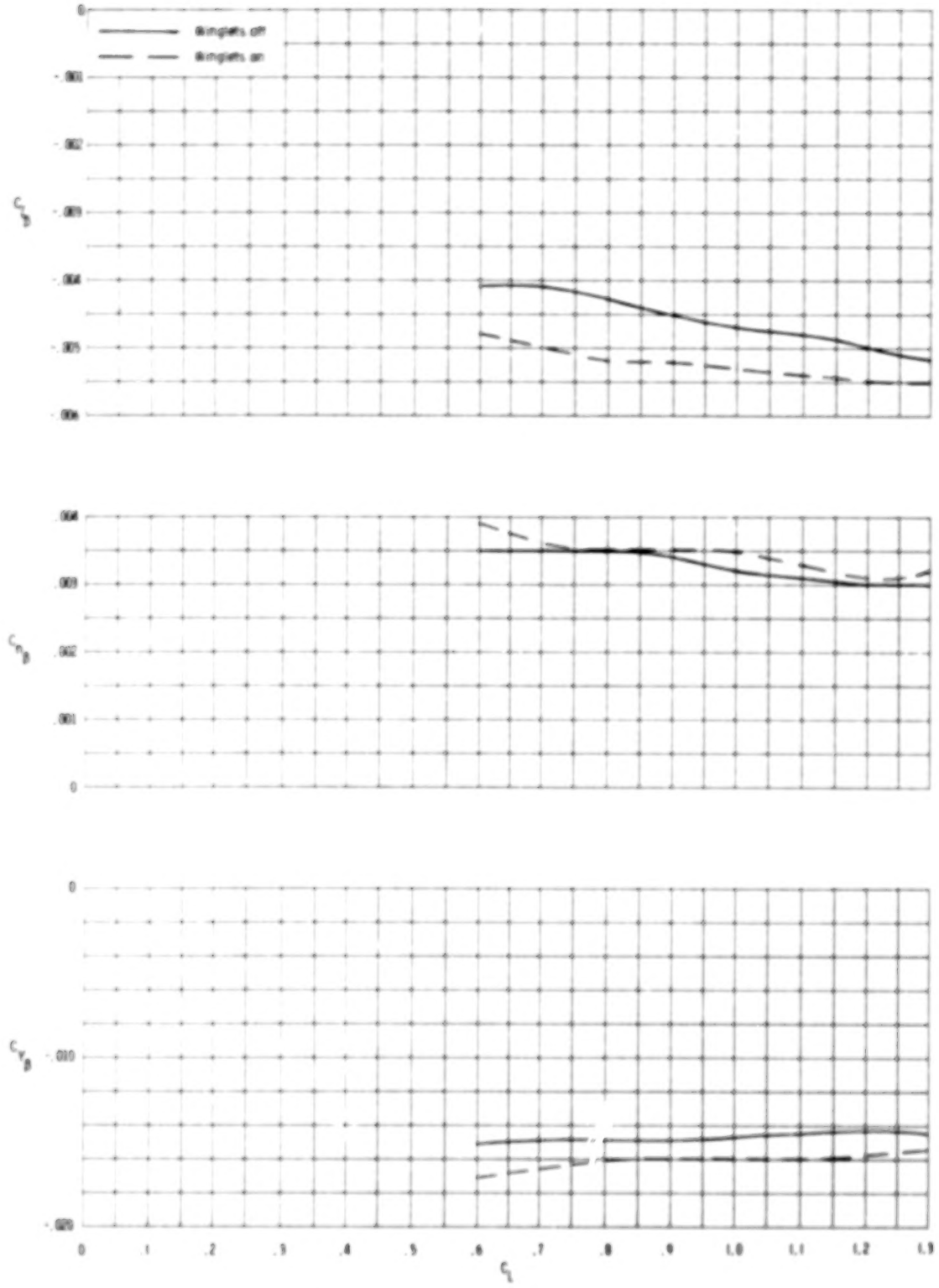

Figure 23.- Effect of winglets on lateral-directional stability derivatives. $\delta_h = -10^\circ$; $\delta_f = 50^\circ$; $\delta_{a,L} = 0^\circ$; $\delta_{a,R} = 0^\circ$.

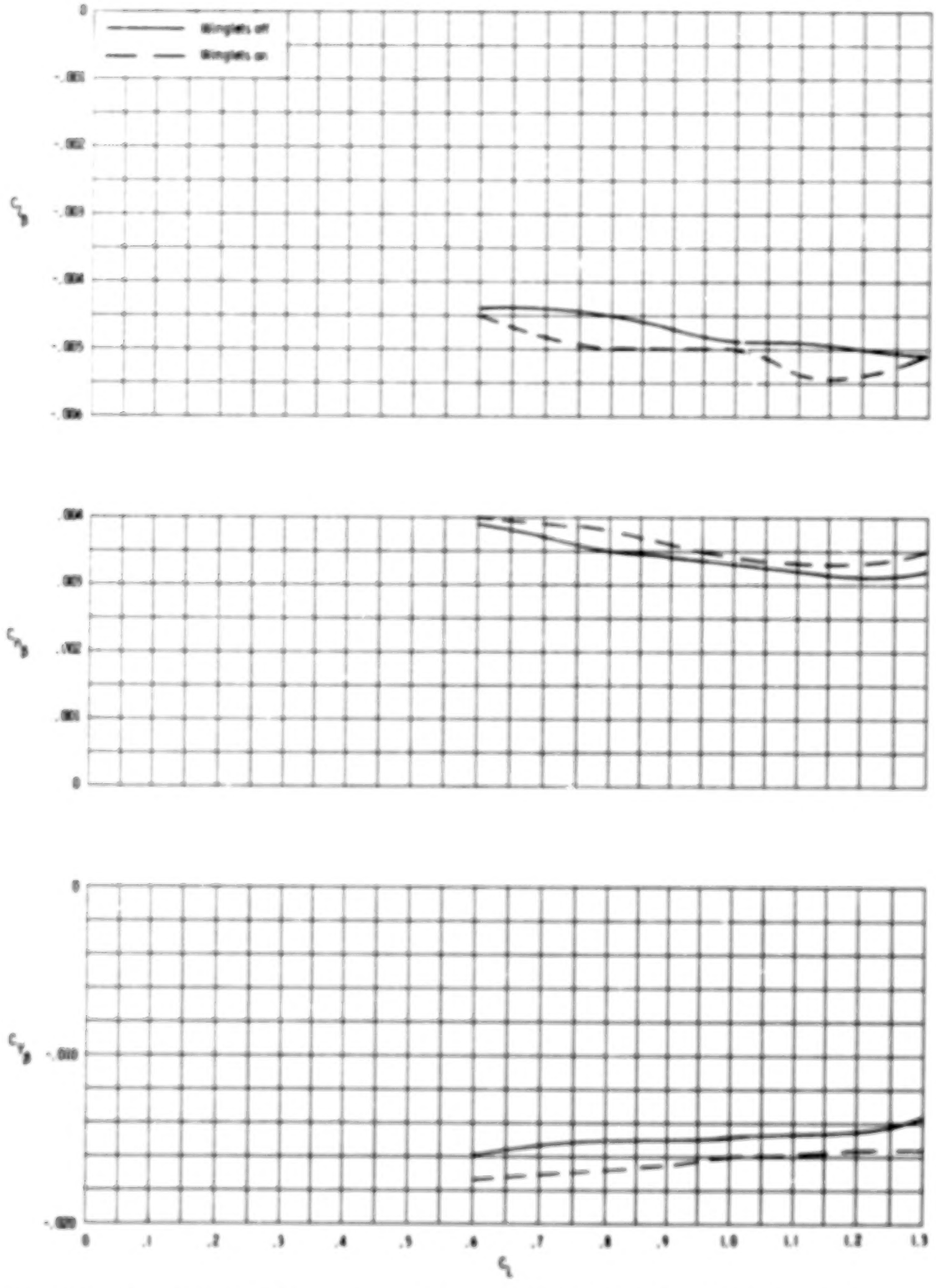

Figure 24.- Effect of winglets on lateral-directional stability derivatives. $\delta_h = -10°$; $\delta_f = 50°$; $\delta_{a,L} = -10°$; $\delta_{a,R} = 10°$.

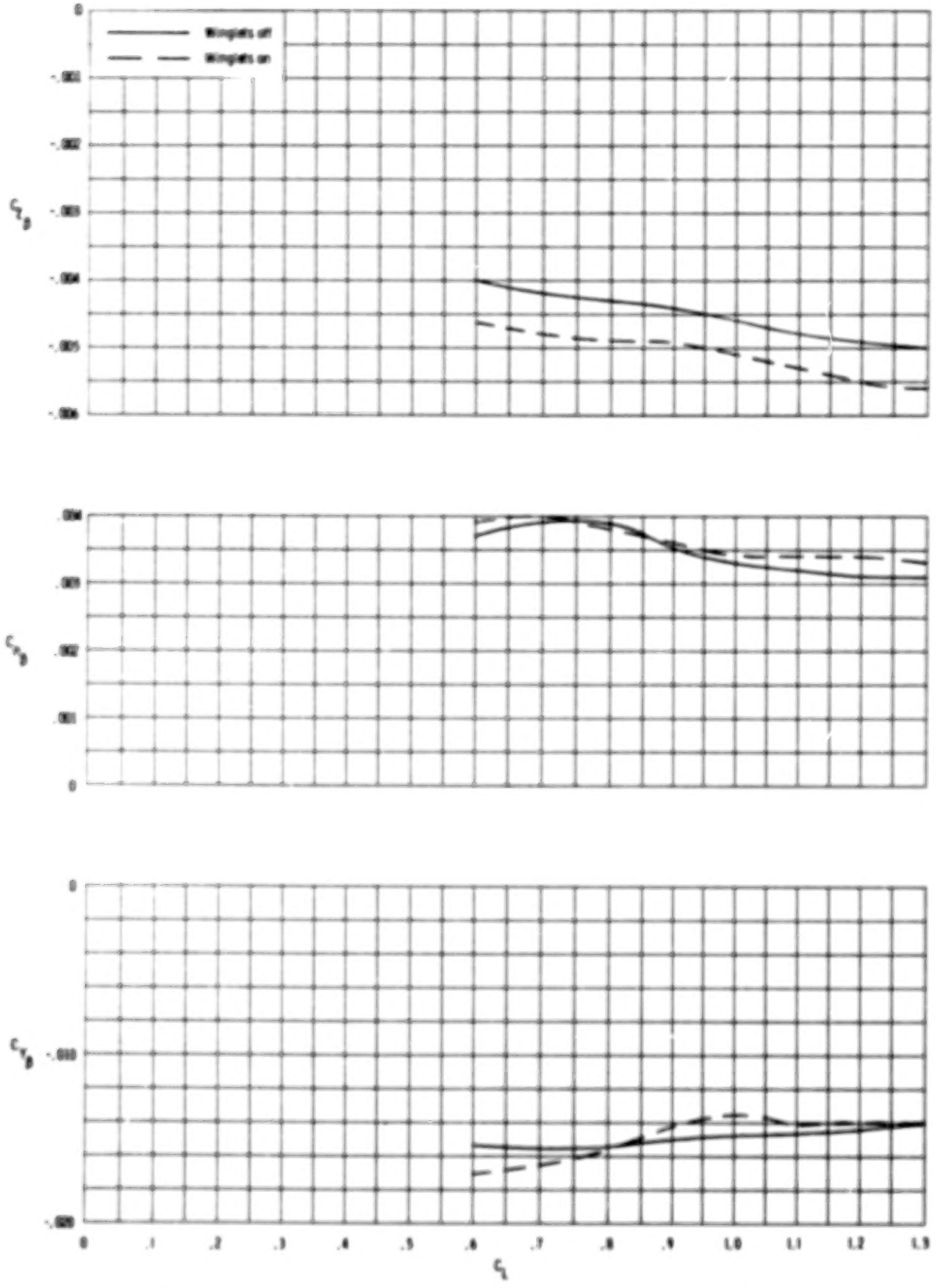

Figure 25.- Effect of winglets on lateral-directional stability derivatives. $\delta_h = -10^\circ$; $\delta_f = 50^\circ$; $\delta_{a,L} = -20^\circ$; $\delta_{a,R} = 20^\circ$.

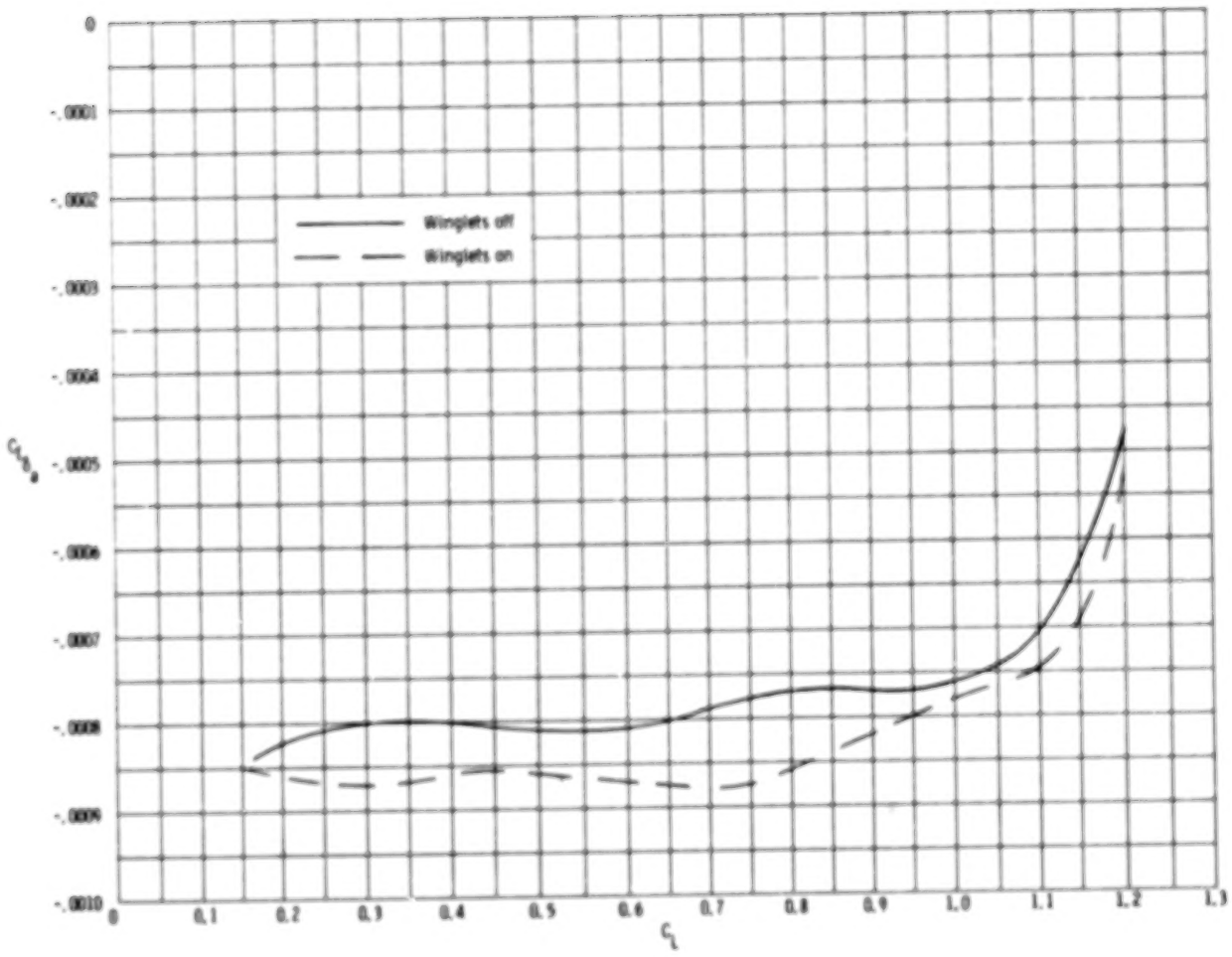

Figure 26.- Effect of winglets on aileron effectiveness. $\delta_h = -10^\circ$; $\delta_f = 30^\circ$; $\beta = 0^\circ$.

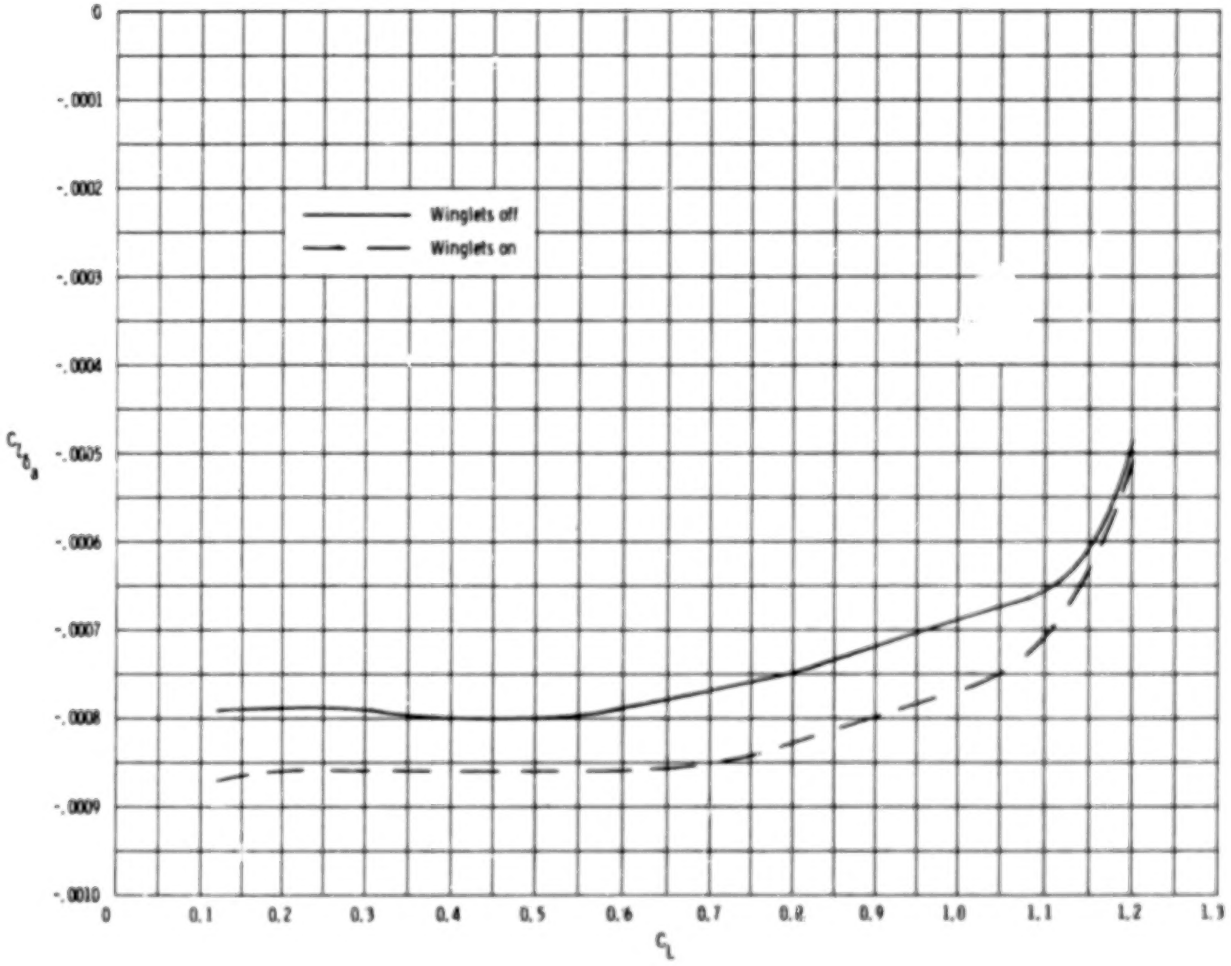

Figure 27.- Effect of winglets on aileron effectiveness. $\delta_h = -10^\circ$; $\delta_f = 30^\circ$; $\beta = 5^\circ$.

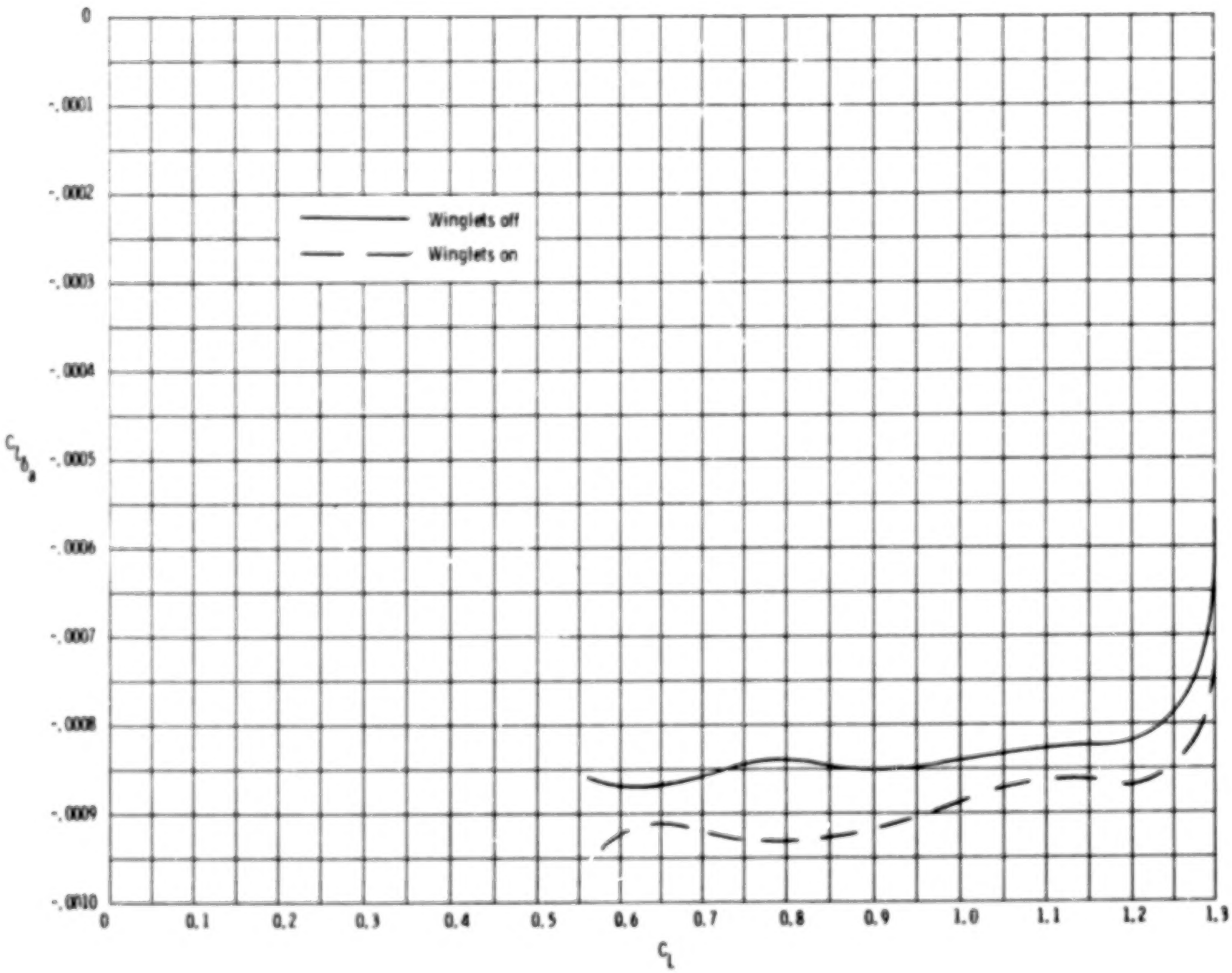

Figure 28.- Effect of winglets on aileron effectiveness. $\delta_h = -10^o$; $\delta_f = 50^o$; $\beta = 0^o$.

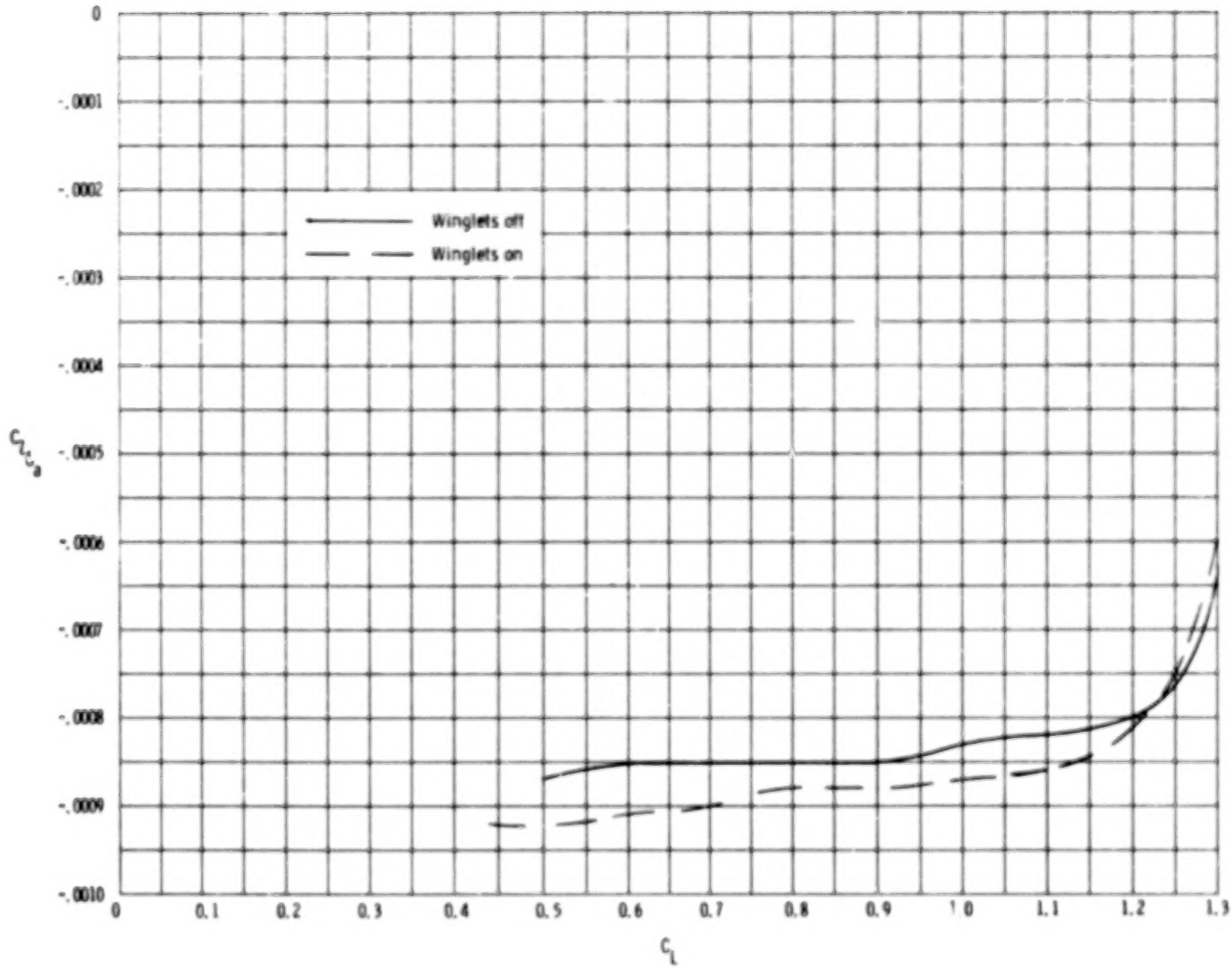

Figure 29.- Effect of winglets on aileron effectiveness. $\delta_h = -10^\circ$; $\delta_f = 50^\circ$; $\beta = 5^\circ$.

1. Report No.	2. Government Accession No.	3. Recipient's Catalog No.
NASA TP-1119		

4. Title and Subtitle	5. Report Date
EFFECT OF WINGLETS ON A FIRST-GENERATION JET TRANSPORT WING. IV - STABILITY CHARACTERISTICS FOR A FULL-SPAN MODEL AT MACH 0.30	February 1978
	6. Performing Organization Code

7. Author(s)	8. Performing Organization Report No.
Robert R. Meyer, Jr.	L-11705
	10. Work Unit No. 505-11-16-08

9. Performing Organization Name and Address	11. Contract or Grant No.
NASA Langley Research Center Hampton, VA 23665	
	13. Type of Report and Period Covered Technical Paper

12. Sponsoring Agency Name and Address	14. Sponsoring Agency Code
National Aeronautics and Space Administration Washington, DC 20546	

15. Supplementary Notes

Robert R. Meyer, Jr.: on special assignment from Dryden Flight Research Center, Edwards, California.

16. Abstract

The static longitudinal and lateral-directional characteristics of a 0.035-scale model of a first-generation jet transport were obtained with and without upper winglets. The data were obtained for take-off and landing configurations at a free-stream Mach number of 0.30. The results generally indicated that upper winglets had favorable effects on the stability characteristics of the aircraft.

17. Key Words (Suggested by Author(s))	18. Distribution Statement
Winglets KC-135A Stability and control	Unclassified - Unlimited Subject Category 02

19. Security Classif. (of this report)	20. Security Classif. (of this page)	21. No. of Pages	22. Price*
Unclassified	Unclassified	71	$5.25

* For sale by the National Technical Information Service, Springfield, Virginia 22161

NASA-Langley, 1978